Control of Distributed Renewable Energy Generation Systems in Converter-Dominated Microgrid Applications

by

Andrés Peña Asensio

in partial fulfillment of the requirements for the degree of Doctor in

Electrical Engineering, Electronics and Automation

Universidad Carlos III de Madrid

Advisors:
Dr. Santiago Arnaltes Gómez
Dr. Jose Luis Rodríguez Amenedo

March 2019

Acknowledgments

This Thesis is the result of the effort of many people who have either contributed directly, inspired or suffered the work developed during the last three years.

First of all, I have an special gratitude to my supervisors, who gave me this opportunity and are a continuous source of inspiration. I would also like to thank my original supervisors, who despite not appearing in the cover have never ceased to support and inspire this Thesis.

This Thesis was financed by the Autonomous Community of Madrid under the PRICAM project. The opportunity to work in the PRICAM project made possible, not only this Thesis but my introduction in the academic research. I would like to thank all the people that made the PRICAM project possible, with an special gratitude to my colleagues at the IMDEA Energy Institute, who had the kindness of inviting me to a research stay and some very nice bowling afternoons, and at the GEISER group of the University of Alcalá, who introduced me to the world of Power Electronics.

Most of the work for this Thesis was developed in the Electrical Engineering department of University Carlos III de Madrid, in Spain. Working there, I had the opportunity to meet some of the greatest people that I have had the pleasure to work with. I would like to make an special note for *Lolo* and *Quino*, who introduced me in the department and helped me more than I could have ever hoped. It is a great experience when you work with someone that you can trust, and even better when you can call them friends.

Outside of the department, I would also like to thank Francisco Longatt and all the people that I met at Loughborough for the great time that I had there. It is difficult to work outside of your home country but they made it as easy as possible.

Por último, porque son lo más importante, gracias a mi familia. A mis padres por aguantar mis impertinencias y confiar en mi y a mis hermanos, porque siempre tienen el tiempo y las palabras adecuadas para animarme. Y a Kris, que mientras escribo estas lineas sigue sufriendo esta Tesis, que no existiría sin ella.

Thank you!

PUBLISHED AND SUBMITTED CONTENT

This document includes contents that have been either submitted or published by the same author in:

- A. P. Asensio, S. A. Gómez, J. L. Rodriguez-Amenedo, M.A. Cardiel-Alvarez, "Reactive Power Synchronization Method for Voltage Sourced Converters," IEEE Transactions On Sustainable Energy, 2019. *In review.*
  - Material from this source is included in chapters 3, 5, 6 and A.1.
  - The material from this source included in this thesis is not singled out with typographic means and references.
- A. P. Asensio, S. A. Gómez, J. L. Rodriguez-Amenedo, M.A. Cardiel-Alvarez, "Distributed Frequency Control for Black Start of Full-Converter Wind Turbines," IEEE Transactions On Power Systems, 2019. *In review.*
  - Material from this source is included in Chapter 6.
  - The material from this source included in this thesis is not singled out with typographic means and references.
- A. P. Asensio, S. A. Gómez, J. L. Rodriguez-Amenedo, M. G. Plaza, J. E. G. Carrasco, and J. M. A. M. De Las Morenas, "A voltage and frequency control strategy for stand-alone full converter wind energy conversion systems," Energies, vol. 11, no. 3, p. 474, 2018. DOI: 10.3390/en11030474.
  - Material from this source is included in chapters 6 and A.2.
  - The material from this source included in this thesis is not singled out with typographic means and references.
- A. P. Asensio, S. A. Gomez, J. L. Rodriguez Amenedo, M. G. Plaza and M. Prodanovic, "Real-time operation of a centralized Energy Management System for an islanded Microgrid," The Renewable Energy & Power Quality Journal, vol. 1, no. 16, 2018. DOI: 10.24084/repqj16.293.
  - Material from this source is included in Chapter 2.
  - The material from this source included in this thesis is not singled out with typographic means and references.
- A. P. Asensio, M. G. Plaza, S. A. Gomez, J. L. Rodriguez Amenedo, J. E.-G. Carrasco and J. Alonso-Martinez, "Isolated operation of wind energy system in critical micro-grid," The Renewable Energy & Power Quality Journal, vol. 1, no. 15, 2017. DOI: 10.24084/repqj15.475.

  - Material from this source is included in chapters 6 and A.2.
  - The material from this source included in this thesis is not singled out with typographic means and references.

- A. P. Asensio, S. A. Gomez, J. L. Rodriguez Amenedo, J. Alonso-Martinez, M. G. Plaza, and J. E.-G. Carrasco, "Master of power: A power plant controller and energy management system concept," in 2017 IEEE PES Innovative Smart Grid Technologies Conference - Latin America (ISGT Latin America), 2017, vol. 2017–Janua, pp. 1–6. DOI: 10.1109/ISGT-LA.2017.8126701.
  - Material from this source is included in Chapter 2.
  - The material from this source included in this thesis is not singled out with typographic means and references.

Abstract

There is a growing interest in the use of renewable Distributed Energy Resources (DERs) that increase the efficiency of the transmission system and reduce the ecological impact of renewable energy infrastructures. At the same time, they reduce the associated capital requirements, thus increasing the potential installation of renewable energy.

Microgrids have been proposed as a solution to improve the integration of renewable DERs. By the use of advanced control techniques, they provide a reliable frame for DERs to support the power system operation. As such, Microgrids can be a promising solution to increase renewable energy penetration. However, since renewable DERs are usually interfaced by Power Electronic Converters (PECs), they do not provide the common stabilization characteristics of traditional generation interfaced by Synchronous Generators (SGs). Therefore, there are concerns about the stability of converter-dominated Microgrids.

This Thesis focus on the specific requirements of PEC-interfaced renewable DERs operating in Microgrids. An overview of available solutions show that, for PECs to support the Microgrid operation in both grid-connected and islanded modes, they require a synchronizing mechanism that does not rely on the measurement of an external frequency. A promising alternative is to emulate the behavior of traditional SGs in the PEC control system with the so-called Virtual Synchronous Machine (VSM) solutions. The synchronization system underlying to these proposals is analyzed. A comparison with the use of traditional frequency measurement systems, namely Phase-Locked Loops (PLLs), in the support of the Microgrid power balance is addressed, showing that the PEC synchronization system has a direct effect on the Microgrid stability.

The Thesis includes a new proposal to ensure synchronous operation based on the use reactive power, instead of active power as in VSMs, that does not require frequency measurements. A dynamic model of a grid-connected PEC is used to demonstrate that reactive power can be used to ensure synchronism. This Reactive Power Synchronization system is used to propose a solution for the black-start of Wind Energy Conversion Systems (WECSs), so that they can contribute to the restoration of the power system following a blackout. The proposed control systems are validated with experimental results of a grid connected PEC and an isolated WECS.

Acronyms

AC Alternating Current.

BESS Battery Energy Storage System.

CSC Current-Sourced Converter.

DB Database.

DC Direct Current.

DER Distributed Energy Resource.

DFIG Doubly-Fed Induction Generator.

DSM Demand Management System.

EMS Energy Management System.

ESS Energy Storage System.

FC Full-Converter.

GSC Generator Side Converter.

HMI Human-Machine Interface.

HPF High-Pass Filter.

HVDC High Voltage Direct Current.

IoT Internet of Things.

IT Information Technologies.

LSC Line Side Converter.

MGCC Microgrid Centralized Controller.

MLR Minimum Load Ratio.

MPPT Maximum Power Point Tracking.

PCC Point of Common Coupling.

PEC Power Electronic Converter.

PLL Phase-Locked Loop.

PMSG Permanent Magnet Synchronous Generator.

PPC Power Plant Controller.

PSC Power Synchronization Control.

PSR Power System Restoration.

PWM Pulse-Width Modulation.

RES Renewable Energy System.

RoCoF Rate of Change of Frequency.

RPS Reactive Power Synchronization.

SCADA Supervision Control and Data Acquisition.

SCIG Squirrel-Cage Induction Generator.

SCR Short-Circuit Ratio.

SG Synchronous Generator.

SOC State of Charge.

UPS Uninterruptible Power Supply.

US United States.

VCR Voltage and Current Regulators.

VFC Voltage and Frequency Controller.

VI Virtual Inertia.

VOC Voltage Oriented Control.

VPP Virtual Power Plant.

VSC Voltage-Sourced Converter.

VSM Virtual Synchronous Machine.

WECS Wind Energy Conversion System.

WT Wind Turbine.

Contents

Acknowledgments iii

Published and submitted content v

Abstract vii

Acronyms xi

Contents xiii

List of Tables xvii

List of Figures xix

1 Introduction 1

1.1 Problem definition and motivation 1

1.2 Objectives of the thesis 4

1.3 Structure of the thesis 4

2 Microgrids 7

2.1 Microgrid concept and structure 7

2.1.1 Microgrid definition and characteristics 7

2.1.2 Microgrid control structure 11

2.2 Global Control Level: Microgid Centralized Controller 13

2.2.1 Functions of a Microgrid Centralized Controller 13

2.3 Local Control Level: Voltage Sourced Converters 17

2.3.1 VSC in MG applications. 17

2.3.2 Control topologies review 18

3 Virtual Synchronous Machine **23**

3.1 Introduction . . . 23

3.2 Review of VSM implementations . . . 24

3.2.1 VSM applications . . . 24

3.2.2 VSM implementations . . . 25

3.3 Synchronization of Grid-Supporting VSMs . . . 28

3.3.1 Synchronizing torque . . . 28

3.3.2 Application to VSCs . . . 30

4 Inertia Emulation **35**

4.1 Introduction . . . 35

4.2 Implementation of Inertia Emulation solutions . . . 36

4.2.1 Voltage Oriented Control (VOC) . . . 36

4.2.2 Grid-Supporting VSM . . . 38

4.2.3 Grid-Tied VSM . . . 40

4.3 Application in an isolated Microgrid case study . . . 42

4.3.1 Simulation case study . . . 42

4.3.2 VSM control systems comparison . . . 44

4.3.3 Final discussions . . . 47

5 Reactive Power Synchronization **51**

5.1 Introduction . . . 51

5.2 Proposed control . . . 52

5.2.1 Reactive Power Synchronization concept . . . 54

5.2.2 Description of the Reactive Power Synchronization control . . . 57

5.2.3 Characteristic swing equation . . . 58

5.3 Modeling and analysis . . . 59

5.3.1 State-space model . . . 60

5.3.2 Stability analysis . . . 61

5.3.3 Damping of oscillations . . . 62

5.4 Results and discussions . . . 64

5.4.1 Simulations . . . 64

5.4.2 Experimental results . . . 65

6 Black start of Full Converter Wind Energy Conversion Systems 69

6.1 Introduction 69

6.2 Isolated operation of FC WECSs 71

6.2.1 System model 72

6.2.2 Proposed control 76

6.2.3 Stability analysis 81

6.2.4 Results and discussions 83

6.3 Control system for parallel operation 87

6.3.1 LSC control for parallel operation 88

6.3.2 Results and discussions 89

7 Conclusions 93

7.1 General conclusions 93

7.2 Original contributions 95

7.3 Publications 96

7.4 Funding 97

A Description of the set-up used to obtain experimental results. 99

A.1 Grid-connected Voltage Sourced Converter. 99

A.2 Isolated wind turbine system. 101

Bibliography 107

List of Tables

4.1 Inertia Emulation case study: Base case Voltage Oriented Control (VOC) parameters. . . 38
4.2 Inertia Emulation case study: Base case grid-supporting Virtual Synchronous Machine (VSM) parameters. 39
4.3 Inertia Emulation case study: Base case grid-tied VSM parameters. 42
4.4 Inertia Emulation case study: Microgrid parameters. 43
4.5 Inertia Emulation case study: Synchronous Generator (SG) parameters. 44
4.6 Inertia Emulation case study: Comparison of control systems performance indicators. . . 45

5.1 Reactive Power Synchronization: Base values for per unit transformations 53
5.2 Reactive Power Synchronization: Base case operating point in pu 56
5.3 Reactive Power Synchronization: Base case system parameters in pu 58
5.4 Reactive Power Synchronization: Base-case eigenvalue analysis. 61

6.1 Isolated FC WECS: Base values for per unit transformations 76
6.2 Isolated FC WECS: Base case system parameters in pu. 81
6.3 Isolated FC WECS: Base case operating point in p.u. 82
6.4 Isolated FC WECS: Base-case eigenvalue analysis. 82
6.5 Isolated FC WECS: Simulation parameters. WT: wind turbine. 83

List of Figures

2.1 Graphical representation of the defining characteristics of a Microgrid. 9

2.2 Hierarchical structure of a MG control system. 11

2.3 Hierarchical structure of a MG control system and communications with a Microgrid Centralized Controller (MGCC). 14

2.4 Classification of VSC control systems for MG applications according to their interaction with the grid including (a) Grid-Tied, (b) Grid-Forming y (c) Grid-Supporting systems. . 19

3.1 Comparison of (a) Grid-Tied and (b) Grid-Supporting VSM control systems. 25

3.2 Contrast between the droop or power-speed characteristic implemented in (a) Grid-Supporting systems and synchronous generator governors and (b) Grid-Tied systems. . . 27

3.3 Schematic diagram of a grid-connected synchronous generator. 28

3.4 Block diagram of a synchronous generator swing equation. 30

3.5 Comparison of (a) Synchronverter, (b) Power Synchronization Control and (c) P-f droop control systems. Original notation has been modified for coherence between implementations. Lowercase variables indicate per unit notation. 31

4.1 Voltage Oriented Control implementation scheme. 37

4.2 Phase-Locked-Loop (PLL) based on the regulation of the grid voltage quadrature component (v_q). 37

4.3 Current controller implementation scheme. 37

4.4 Grid-supporting VSM implementation. 38

4.5 VSM active (a) and reactive (b) power control. 39

4.6 Grid-tied VSM implementation. 40

4.7 PLL small signal model. ω_g: grid frequency. θ_g: grid voltage phase 41

4.8 Microgrid case study for inertia emulation simulations. 42

4.9 Synchronous generator speed variation on load change for VOC (black, solid line), VSM (red, * marked), VI (green, circle marked) and Droop (blue, + marked) control systems and no BESS connection (magenta, x marked). 45

4.10 BESS active power variation on load change for VOC (black, solid line), VSM (red, * marked), VI (green, circle marked) and Droop (blue, + marked) control systems and no BESS connection (magenta, x marked). 46

4.11 $RoCoF_{tp}$ variation on load change for VOC (black, solid line), VSM (red, * marked), VI (green, circle marked) and Droop (blue, + marked) control systems and no BESS connection (magenta, x marked). 46

4.12 Synchronous generator (a) speed variation and (b) $RoCoF_{tp}$ on load change for VSM (red, * marked), VI (green, circle marked) and Droop (blue, + marked) control systems if the BESS assumes 100% of the load variation versus 50% with droop (black, x marked) and VSM (magenta, square marked) control systems. 48

5.1 General scheme of the proposed control and system under study. VCR: Voltage and Current Regulation. 53

5.2 Internal Voltage and Current Regulation (VCR) system for the Reactive Power Synchronization (RPS) control. HPF: High-pass filter. 54

5.3 Case study scheme. VSC: Voltage Sourced Converter. 54

5.4 Vector diagram of the system under study. δ: power angle. e: grid voltage vector. v: converter voltage vector. ω: dq frame angular frequency. ω_g: grid frequency. 55

5.5 Reactive power synchronization loop. 57

5.6 Block diagram of the complete system. RPS: Reactive Power Synchronization. 57

5.7 Bode diagram of the open-loop transfer function for the reactive power synchronization model. Ω_{co}: Cross-over frequency. 59

5.8 Base case eigenvalues and related states according to their participation factors. 62

5.9 System response against variations on (a) the grid impedance z_e, (b) the grid inductive to resistive ratio X/R_e, (c) the synchronization loop gain K_s and (d) the damping gain K_D. 63

5.10 Simulation results against frequency, active power reference and reactive power reference variations. 65

5.11 Simulated system response against a grid fault. 66

5.12 Experimental results for (a) an active power reference step variation and (b) a reactive power reference step variation. 67

6.1 Scheme of an isolated Full-Converter Wind Energy Conversion System. PMSG: permanent magnet synchronous generator; LSC: line side converter; GSC: generator side converter. . . . 71

6.2 Graphical representation of wind turbine (WT) equations: (**a**) C_p versus λ for different β values; (**b**) WT power (p_m) for different wind speeds and maximum power loci (curve BC). . . . 73

6.3 Scheme of the Line-Side Converter (LSC) operating in isolated mode. . . . 75

6.4 Control scheme for the WT Rotational speed . . . 77

6.5 Control scheme for the Generator Side Converter (GSC) . . . 78

6.6 VFC scheme for the LSC . . . 79

6.7 Model sensitivity to: . . . 83

6.8 Load step response in simulation . . . 84

6.9 Load step response in real-time system including (**a**) an active power step variation and (**b**) a reactive power step variation. . . . 85

6.10 Real-time system response to wind variations. . . . 86

6.11 General scheme of the system under study with 2 wind energy conversion systems connected in parallel. . . . 88

6.12 Line Side Converter (LSC) control for the parallel operation solution. RPS: Reactive Power Synchronization, APS: Active Power Sharing, VCR: Voltage and Current Regulator. 88

6.13 Active Power Sharing control. . . . 89

6.14 Results for: the black-start connection of WT_1 (t=0.01 s), the subsequent connection of WT_2 (t=0.1 s), a variation in the wind power available in WT_1 (t=0.2 s) and the connection to the main grid (t=0.3 s). . . . 90

A.1 Schematic diagram of the set-up configuration used in the real-time experiments . . . 100

A.2 Overview of the set-up used in the real-time experiments. . . . 100

A.3 Picture of the diode rectifier and transformer used in the real-time experiments. . . . 101

A.4 Capture of the Human Machine Interface (HMI) used in the real-time experiments for an active power step. . . . 102

A.5 Capture of the Human Machine Interface (HMI) used in the real-time experiments with instantaneous values. . . . 102

A.6 Test bench used for real-time experiments of the isolated Full-Converter system. PWM: pulse-width modulation. . . . 103

A.7 Pictures of the elements used for the Wind Turbine emulator including (a) the DC motor driver, (b) the back-to-back converter, (c) the DC motor and (d) the Permanent Magnet Synchronous Generator (PMSG). 104
A.8 Capture of the Human-Machine Interface (HMI) of the LabVIEW software used for the Wind Turbine emulator. 105
A.9 Power Analyzer used for electrical measurements of the Wind Turbine emulator including (a) a picture of the Power Analyzer and (b) results of the voltage measured during the tests. 105

Chapter 1

Introduction

Contents

1.1 Problem definition and motivation 1
1.2 Objectives of the thesis 4
1.3 Structure of the thesis 4

1.1 Problem definition and motivation

The increasing levels of renewable energy penetration are changing power systems operation. Since the first electric power systems in the late 19th century, power generators have been mainly interfaced to the electrical system through the use of rotating machines such as Synchronous Generators (SGs). Moreover, the energy for this generation was obtained from controllable sources like combustion engines. The electrical industry and the associated policies were built according to the specific characteristics of these systems [1], while the use of non-controllable sources like wind energy was not very extended due to their reduced controllability and higher costs [2].

With the development of power electronics, new ways of interfacing generation systems, known as Power Electronic Converters (PECs), were introduced in power systems. Among other applications, PECs allow a greater controllability in the extraction of power from non-controllable sources, such as wind energy an photovoltaic systems [3]. Control of PECs has been traditionally designed considering a reduced penetration, so the power system could still be operated considering a strong contribution of traditional sources. However, penetration of PEC-interfaced systems is starting to represent significant levels and it is targeted to increase, with renewable energy penetration hitting targets of up to 100% in countries like Denmark [4]. This change in the operation paradigm requires a revision of the PECs control systems in order to ensure the stability of future power systems.

In the context of improved control possibilities through PECs and an interest in increasing the penetration of renewable energy, the use of Distributed Energy Resources (DERs) has emerged a as a promising solution. DERs are small generating units typically located near the place where the energy is used [5]. This allows a more efficient use of resources like the electrical transmission systems or the space required for photovoltaic and wind energy generation facilities while reducing the capital requirements associated to renewable energy installations [6].

Traditionally, the integration of DERs in power systems has been approached considering the contribution of only a few DER units to a wider conventional power system [7]. However, this implies a small penetration of DERs, reducing the possibilities for renewable energy integration. A solution to improve the contributions of DERs to power systems is to build clusters of units, such as loads, generators or energy storage systems, that coordinate to take advantage of the benefits of each other. These clusters can then be considered and operated as small power systems or Microgrids (MGs) [8]. With MGs, DERs could potentially have attributions comparable to those of conventional generation units, including the possibility of feeding a given set of loads on their own as an islanded system [5].

However, the operation of DERs in MG applications is still affected by technical problems. Moreover, MGs are expected to integrate a large share of distributed renewable energy while, as noted earlier, power systems have been traditionally built considering only a small penetration of PEC-interfaced systems. Therefore, distributed renewable energy systems operating in MG applications represent a critical case of a power system with a high penetration of PECs [9].

This Thesis deals with the control systems used in the PECs of distributed renewable energy systems for MG applications. Specifically, the work focus on three technical challenges:

1. **Synchronous operation in converter dominated systems:** Synchronization of PECs has been traditionally based on measuring the grid frequency by means of a Phase-Locked Loop (PLL). However, there are reports of stability problems in systems with a high penetration of PLL-based PECs [10–12]. On the other hand, SGs are able to operate in sycnrhonism with each other without measuring the grid frequency. Therefore, there is an interest in synchronization systems for PECs that replicate the advantages inherent to SGs in order to allow a high penetration of PECs.

2. **Lack of inertial response:** Due to their rotating nature, SGs inherently storage kinetic energy. In the event of a power unbalance in the system, they exchange this energy with the power grid, improving the system stability. This feature is known as inertial response since it is related to the inertia constant of the generators, that defines the amount of kinetic energy stored. PECs do not have this inherent energy exchange mechanism and thus any support of power unbalances depends on the PEC control system. Inertial response from PECs could be achieved by the use of appropriate control systems. The lack of inertial response form PECs could compromise the

stability of converter-dominated systems [13].

3. **Reduced contribution to the Power System Restoration (PSR):** PSR is the reconnection of a power system following a blackout. Nowadays, PSR is carried out by a few large generators. As their penetration increases, DERs are expected to become important for the PSR of future systems [14]. MGs with black-start capability are a possible solution for DERs to contribute to PSR. However, DERs are not prepared to perform a black-start since, as noted earlier, they are designed to operate connected to a larger power system. Black-start from renewable DERs is specially troublesome since it must take into account the availability of the primary resource. A solution for the black start of a MG with only Wind Energy Conversion Systems (WECSs) and loads is proposed in this thesis in order to improve the contribution of WECSs to the PSR.

As can be seen from the aforementioned problems, the operation of power systems with a high penetration of PECs presents problems that are already solved for traditional SG-based power systems. This is why there has been a lot of interest in replicating the behavior of SGs in the control system of PECs with the so-called Virtual Synchronous Machine (VSM) solutions. VSMs are very promising since they are expected to share some of the positive features of SGs such as inertial response and synchronous operation without frequency measurements.

On the other hand, VSMs might also share other SGs features that are not desirable for the operation of PECs. As will be seen in Chapter 3, the inertial response of VSMs and their synchronizing mechanism comes from the replication of the SG swing equation on the PEC control system, which implies that the active power of the PEC is directly controlled by the power angle. In contrast, Voltage Oriented Control (VOC) systems include internal current loops that regulate the active power by means of the PEC current. Controlling the PEC current has the advantage of being able to limit the current amplitude. On the other hand, VSMs solutions that do not regulate the PEC current have to switch to a non-VSM solution in order to limit the current amplitude [15, 16]. Moreover, using active power for synchronization affects the active power regulation of the PEC, which depends not only on the PEC but on the energy primary source (wind energy systems, photovolatic generators, hydraulic turbines, etc.). Another problem of replicating a SG swing equation is that it leads to the appearance of low-frequency oscillations.

In this thesis an alternative solution is proposed that synchronizes PECs using reactive power instead of active power and includes internal current loops for the regulation of the PEC currents. While VSM control systems use the static dependency between active power and power angle in power systems in order to ensure synchronism, in this Thesis a dynamic model of a grid connected PEC is used to demonstrate that reactive power is dynamically coupled to power angle and therefore that reactive power can be used to ensure synchronism. The proposal includes an oscillation damping mechanism based on this coupling between reactive power and power angle.

1.2 Objectives of the thesis

The objectives of the thesis are:

1. To propose a control system that ensures the synchronous operation of PECs based on reactive power variations without the use of PLLs, which are known to cause stability problems in converter-dominated grids. This control system addresses the problems of renewable generation in converter dominated Microgrids including all the aforementioned problems of synchronous operation in converter dominated systems, inertial response and contributions to Power System Restoration (PSR). Moreover, the proposal should overcome some of the drawbacks of existing solutions regarding the regulation of the PEC current and the damping of low frequency oscillations.

2. To propose a model that demonstrates that reactive power can be used as a synchronizing mechanism. The model of the synchronizing mechanism of existing VSM solutions and its effect on the Microgrid is analyzed as a reference. These models should allow for both a better understanding of the problems and to validate the contributions of the proposed solutions.

3. To implement the proposed control system in an experimental Microgrid dominated by distributed renewable energy systems. While analytical models and simulations are useful to understand the behavior of electrical systems, experimental implementations are more realistic due to considerations such as the execution of the control on a digital platform or the noise inherent to every real system that are hard to model or simulate. The experimental implementation therefore validates that the proposed solutions can be used in a real power system.

1.3 Structure of the thesis

This Thesis is divided in seven chapters and one appendix. This first chapter introduces the motivation of the work and presents the objectives and structure of the Thesis.

In Chapter 2, the MG concept is analyzed, exploring the technical problems associated to MG operation and giving an overview of existing control solutions. The focus is placed on the control of Voltage Sourced Converters (VSCs), a specific PEC technology. Chapter 3 studies VSM solutions, including a dynamic model that analyzes the synchronizing mechanism and emulated inertial response of VSMs. In Chapter 4, the effect of the PEC synchronizing system on the resulting emulated inertial response is addressed by comparing implementations with and without the use of PLLs in a dynamic simulation of an isolated Microgrid.

A novel proposal for the synchronization of VSCs without frequency measurements is presented in Chapter 5. An application of this solution for the black-start of WECSs is analyzed in Chapter 6. Real-time results are presented to validate the proposals.

Finally, Chapter 7 summarizes the main conclusions extracted for the Thesis and acknowledges the associated publications and fundigs.

An appendix is included in order to give a more detailed description of the experimental test-benchs that were used to obtain the real-time results.

Chapter 2

Microgrids

Contents

2.1 Microgrid concept and structure 7

2.1.1 Microgrid definition and characteristics 7

2.1.2 Microgrid control structure 11

2.2 Global Control Level: Microgid Centralized Controller 13

2.2.1 Functions of a Microgrid Centralized Controller 13

2.3 Local Control Level: Voltage Sourced Converters 17

2.3.1 VSC in MG applications. 17

2.3.2 Control topologies review 18

2.1 Microgrid concept and structure

2.1.1 Microgrid definition and characteristics

The concept of "Microgrid" (MG) has been extensively studied in the past decade. It is a wide concept that is studied by multiple areas such as power systems analysis, energy sources, control theory, economic optimization or telecommunications. However, there is yet no consensus on the actual definition or specific characteristics of a MG. In fact, it is easy to find multiple definitions in the literature. One of the most cited comes from the United States (US) Department of Energy:

> [A microgrid is] a group of interconnected loads and distributed energy resources within clearly defined electrical boundaries that acts as a single controllable entity with respect to

> the grid. A microgrid can connect and disconnect from the grid to enable it to operate in both grid-connected or island mode [8]

This definition is clearly defined from the point of view of the electrical system and also imposes the restriction of being able to operate both connected or disconnected (island mode) from the grid.

Possibility of islanded operation is often regarded as the most compelling feature of MGs [17, 18]. Most standards require distributed energy resources (DERs) to shutdown following a grid outage, like the IEC 62116 international standard for utility-interconnected photovoltaic inverters [19]. However, new standards are beginning to include the possibility of islanded operation, provided that the generation system can control the local voltage and frequency and not feed power back to the larger utility grid [20]. Microgrids, by integrating multiple systems, can provide a reliable solution for intentional islanding.

However, the US Department of Energy definition gives little insight into the internal composition of the microgrid. Another popular definition was published by Lasseter in [21]:

> The MicroGrid concept assumes a cluster of loads and microsources [($<$100kW)] operating as a single controllable system that provides both power and heat to its local area [21].

This definition imposes a combination of heat and power that is largely not included as a requirement for MGs but as a solution to improve the overall system efficiency [22].

The Lasseter definition also imposes a limit on the maximum power of the connected elements, although there is no consensus on this limit and later authors have made the MG concept independent of the system size [9].

However, it agrees with the previous definition in the notion of a "single controllable system". This notion is not limited to MGs but included in the broader term of Virtual Power Plant (VPP) [23]. Although both terms are sometimes used interchangeably, the VPP concept is also used for the coordination of multiple generation units as a bulk power system [24]. Moreover, VPPs migh not even include generation systems and rely solely on Demand Side Management (DSM) [17], making some MG characteristics, such as the isolated operation, completely impossible.

The Lasseter definition also highlights one of the most important aspects of MGs, which is the integration of what it names as "microsources" and is more usually known as "Distributed Energy Resources" (DERs) [22].

This is especially interesting for DERs based on Renewable Energy and further studies have given special attention to the feature of integrating Renewable Energy Systems (RESs) [9, 18, 25, 26]. Traditionally, the more reliable operation Conventional Generation System (CGS) and economy of scale has driven RESs to central energy production. However, connecting RESs to the distribution level could provide technical advantages such as reliability improvement and reduction of transmission network

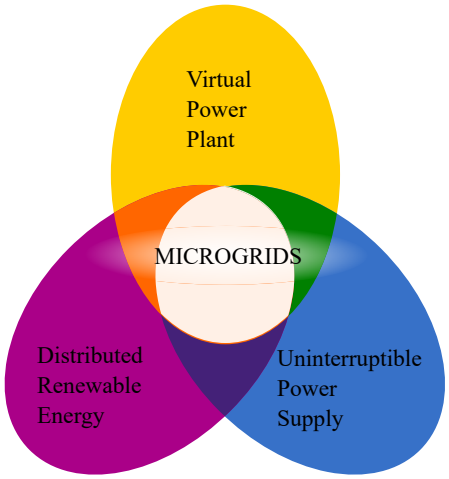

Figure 2.1: Graphical representation of the defining characteristics of a Microgrid.

infrastructure costs [27]. Also, distributed connection of WECSs and PV systems could potentially avoid the use of large terrains and the associated environmental problems such as destruction of natural habitats [6].

Based on this review, in this work the MGs characteristics are summarized as:

1. **Operation as a single controllable system from the point of view of the utility:** Implies that an external agent, such as the grid operator, can operate the microgrid as a single system, irrespective of its internal composition. Thus, the MG as a whole can be commanded to provide ancilliary services or to follow a given power set-point.

2. **Capacity to operate both connected and disconnected from a wider power system (such as the utility grid):** A MG can operate as an islanded system, using the internal generation and storage system to supply its loads.

3. **Capacity of integration of distributed RESs:** The integration of RESs is included as a defining characteristic due to the importance given by most of the published literature to this application of MGs. Note that even under this condition it is possible for a non-RESs-based system to actuate as a MG provided that the structure and control systems allows for an easy or *plug and play* future integration [25].

Therefore, MGs can be understood as an unique solution that combines multiple services as shown in Fig. 2.1.

Under this definition, a MG could provide services such as:

1. **Uninterruptible Power Supply (UPS) for critical loads:** By being able to operate both connected and disconnected from the grid, MGs can be used in systems were critical loads must be kept online following a grid outage. Traditionaly, this funcion has been performed by fuel-based generators. Using MGs, a more diverse system included RESs and ESSs could be used instead.

2. **Providing ancillary services:** Just like in VPPs, MGs can be controlled as a single entity. Therefore, the capacities of the different systems that compose the MG can be combined in order to provide services to the grid by controlling the bulk active and reactive power. This allows systems such as RESs, ESS and even loads to collaborate in these services as a mix.

3. **Information for Smart Grid services:** With the development of information technologies (IT), there is a growing interest in obtaining information from electrical systems that could allow a more efficient and transparent operation. A MG structure simplifies the management of information. Moreover, MGs are usually based on Smart Grid concepts and thus are more easily integrated in these structures.

4. **Economical redistribution:** MGs can promote a paradigm change from an electricity market based on a few central providers to a more distributed system where MG users can operate as an active agent both purchasing and selling energy in a common market with traditional suppliers.

Due to these promising applications, stakeholders of electrical systems such as policy makers, producers and consumers are actively promoting MG development. However, there are several limitations in the development of MGs. Besides the technical barriers, that will be further discussed in the following sections, there are also economical and legal limitations. Defining clear responsibilities on the system operation in this new paradigm, such as the sharing of O&M costs, is one of the main reasons for some of the most relevant energy producers to be skeptical of the concept [9].

Nevertheless, nowadays there already some examples of installed MGs. One of the most succesful examples is the Santa Rita Jail test site in California [28], a proof of concept of the US Consortium for Electric Reliability Technology Solutions (CERTS) MG [29] that is focused on reliability improvement through islanded operation [9]. A review on experimental MG installations in Europe, US and Asia was recently presented in [30]. Most of them have been developed as pilot projects.

In this chapter, the focus will be on analyzing MGs from the perspective of renewable energy integration and the associated control problems. Related areas such as MGs communication systems will be briefly discussed as well.

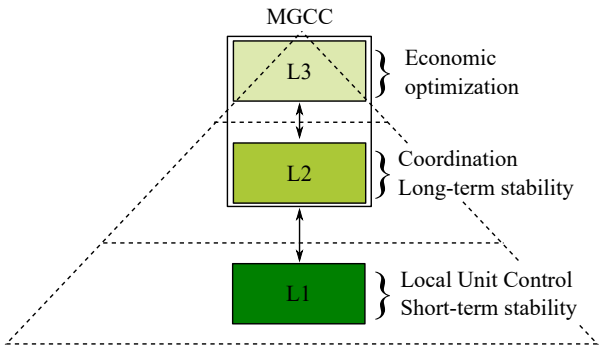

Figure 2.2: Hierarchical structure of a MG control system.

2.1.2 Microgrid control structure

MGs are composed of multiple systems and thus it must be ensured that they operate in a coordinated manner. The most common solution is to implement a hierarchical control system [9]. This control system is usually divided in three layers as depicted in Fig. 2.2.

The hierarchy goes from the low level control of the different units to the top-lovel optimization of the MG. Usually the control of levels 2 and 3 is performed in a centralized controller, known as the Microgrid Centralized Controller (MGCC) [27], that communicates with the different elements where the level 1 control is running.

This structure presents a lot of similarities with the primary, secondary and tertiary control levels of traditional power systems, which regulates active and reactive power between multiple synchronous generating units [1]. However, MGs are based on DERs that might not be based on synchronous generation, such as WECSs and PV systems. This change in the base system introduces changes in the architecture that makes MG operation significantly different from the operation on traditional power systems. Morever, a MG control architecture includes objectives outside of those of traditional power systems, such as internal economic optimization.

These control levels are explained in more detail in the following paragraphs. Note that this chapter is focused on the architecture from the point of view of the control system, but it could also define economical and legal hierarchies [31].

The different MG control levels are briefly discussed following. A more in-depth description is given in the next sections.

Level 1: Local unit control

Level 1 is related to the internal control of the DERs, ESSs and loads. Level 1 control systems must ensure that all units are stable and that they follow the instructions given by levels 2 and 3.

It is a complex field of study due to the variety of systems and also to the internal sub-levels of control. These internal sub-levels are sometimes included in a different "zero" level [32].

In traditional power systems, this level is related to the governor units of the generators, that introduce a droop relation between the generator power output and its speed, allowing for the parallel connection of multiple units [1]. In fact, this control system can also be implemented for DERs of the MG that are based on synchronous generation [27].

Level 1 control is implemented in a time frame that ranges from microseconds, for the internal sample time of inverter controllers, to seconds for the governor control systems of synchronous generators.

Control of distributed RESs in this level presents specific requirements for MG applications since in conventional power system, the local control of RESs assumes the connection to a wider power system based on synchronous generation. Providing solutions for this level is the main focus of this thesis and thus will be largely discussed in following chapters. Section 2.3 provides a summary of the most relevant problems and the available solutions.

Level 2: Coordination

As stated earlier, one of the most relevant aspects of MGs is their ability to operate as a single controllable system from the point of view of the utility grid. The level 2 is in charge of coordinating the different elements in order to follow the utility grid and system operator requirements, providing the references for the Level 1 control.

Therefore, this level manages the interaction between the different systems to ensure that the MG global operation is inside the desired restrictions. This regulation is performed in a wider time frame than the Level 1 control (tens of seconds to minutes).

It is directly comparable to the secondary control of traditional power systems, that restores the grid frequency and voltage and regulates the power exchanges between areas [1].

Level 2 also regulates the connection and disconnection to the main grid, providing the necessary information to the MG units to perform this process seamlessly.

This control level can be decentralized, implemented in the local control of the units, or in a centralized controller [33]. Nevertheless, since the control objectives are global, that is for the MG as a whole, in this work it is always considered a central control.

Level 3: Optimization

From the control perspective, one of the most compelling features is to ensure that the MG operation is economically optimal. This optimizing process is usually divided in different time frames or *horizons* that range from several days to minutes [34].

Therefore, while levels 1 and 2 regulate the MG to operate inside the defined paremeters, level 3 decides the operation of the MG as a whole, providing references of active and reactive power depending on both technical and economical considerations.

While Levels 2 and 3 comprise different functions, both require the coordination of multiple systems and thus are usually implemented in the MGCC [27]. This MGCC can be considered as an application of an of Energy Management System (EMS) [35]. Although both terms are sometimes used indistinctly, EMSs are also used for other applications outside of the MG concept. This concept is explored in more detailed in the next section.

2.2 Global Control Level: Microgid Centralized Controller

2.2.1 Functions of a Microgrid Centralized Controller

This section discusses the control of a MGCC, including Levels 2 and 3 of the hierarchical structure presented in section 2.1. As for MGs, there are multiples definitions of the functions associated to a MGCC. Again, we begin with the definition given by the US Department of Energy:

> A microgrid controller refers to an advanced control system, potentially consisting of multiple components and subsystems, capable of sensing grid conditions, and monitoring and controlling the operation of a microgrid to maintain electricity delivery to critical loads during all microgrid operating modes (grid-connected, islanded, and transition between the two). The EMS is the control system included in the MG controller. [8].

As with the MG definition from the same source, this MGCC definition is focused on the function of the MG coordination for islanded operation. Besides, control and monitoring of the MG components, functions usually related to Supervisory, Control and Data Aquisition (SCADA) and Power Plant Controller (PPC) systems, are also included in th MGCC. The EMS is regarded as an internal subsystem of the MGCC.

These characteristics are shared with other MGCC definitions such as [36], which distinguish between the dispatch function, which computes the set point of the DER units and the status of the controllable loads in grid connected and islanded modes, and the transition function, which defines the controller operation in the transition between grid-connected and islanded modes and in the reconnection process. Thus, the MGCC can be understood as an integration of different functions or subsystems, as described following. A general scheme of the MGCC inside the MG hierarchical structure is depicted in Fig. 2.3

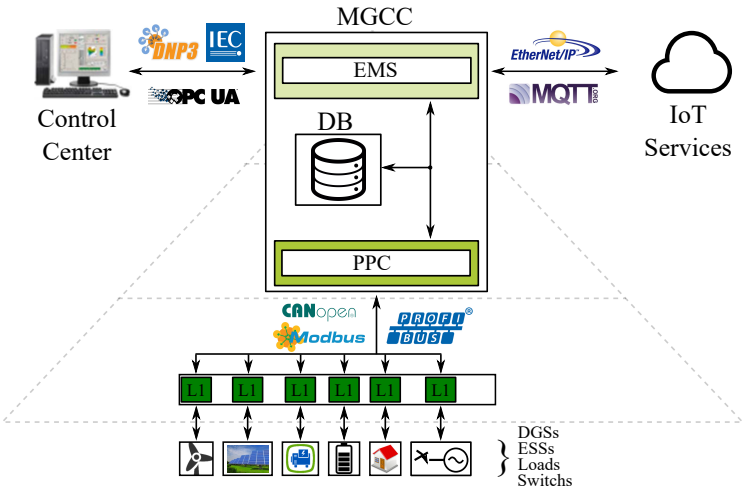

Figure 2.3: Hierarchical structure of a MG control system and communications with a Microgrid Centralized Controller (MGCC).

Energy Management System

EMSs have been widely studied in the literature as high level coordinating elements, mainly in MG applications [37, 38], but also in other distributed generation systems such as hybrid systems [38] and combined heat and power systems [23] and even on electric vehicles applications [39].

The main objective of an EMS is to ensure the economical optimization of the MG operation [27]. This problem is called Unit Commitment and is not only applied to MGs but to any electrical system. However, unit commitment in a MG is especially relevant [40] and can determine:

- **Grid exchange**: In grid-connected mode, a MG can decide to export or import energy depending on the internal cost and expected revenue.
- **Planned disconnections:** Some units, such as combustion-based DERs, require a certain amount of time and energy to start [41]. Also, combustion-based generators are normally not recommended to operate below a defined load or Minimum Load Ratio (MLR). Therefore, having these generators in operation implies a fixed cost. The connection and disconnection of these systems can be planned in order to optimize these costs.
- **Energy storage**: If the MG includes ESSs, they can be used to store energy. Again, this will depend on the expected cost and revenue of energy production, but also on the cost of energy storage, which might vary depending on the ESSs operating point [42]. This cost also varies between technologies, so the optimization might come from the operation of a hybrid of multiple ESS technologies [43].

- **Demand Side Management (DMS)**: Depending on the cost, it might be preferable act on the loads instead of the generation or storage of energy.

This optimization problem is usually solved using linear programming methods that determine the MG units operating points depending on the predicted behaviour of the system [44]. This optimization can be applied to multiple time frames or horizons so the short-term planification, for the next few minutes, is done depending on a wider long-term horizon that ranges from hours to several days [45,46].

These studies are based on the availability of information from forecast systems and from the MG elements. However, precision of forecast, both for load and renewable energy systems, is still a developing topic [47]. Moreover, despite the deployment of smart metering systems, real-time information from load demand is still unavailable in most systems [48].

Power Plant Control

The EMS optimization solution gives the different MG units operating points. As noted in the previous section, these operating points might also come from the utility grid or system operator. The MGCC must then ensure that these operating points are followed while complying with the applicable grid code or system operator requirements. Therefore, the MGCC must operate as the PPC of the MG.

PPCs are systems with a long industry experience. They are usually designed to automatically operate power plant generation facilities active and reactive power according to different criteria or functions:

- **Power Factor:** Power plants can be required to operate at a given power factor. Therefore, the PPC must continuously adapt the different units reactive power to the total active power of the plant. This is especially relevant for non-controllable RESs that continuously vary their power generation depending on the available resource.

- **Active power curtailment:** Depending on the requirements of the electrical system, a power plant might be required to curtail its active power generation. The PPC must coordinate the curtailment on the different units depending on the external commands from the electrical system operator.

- **Voltage control:** A plant might be required to support the control of the system voltage by injecting different levels of reactive power depending on the measurement of the voltage at the point of common coupling.

- **Frequency control:** As with voltage, power plants are usually required to adapt the generated active power to the frequency of the electrical system. This control is included in the governor of CGSs but is usually performed by a centralized controller for RESs.

- **Power ramp-rate:** There is a growing interest in reducing the maximum allowed variation of RESs. It is expected that future standards will impose a limit to this variation [49, 50]. The ramp-rate of the complete power-plant can be controlled by the PPC, thus using the advantages of the aggregation of multiple units such as spatial smoothing of WECS [51].

To fulfill these functions a PPC requires to communicate both internally within the plant and with systems external to the MG.

Internal communication: The internal communication system is one of the main considerations for the implementation of a MGCC since communication delays impose a limit in the EMS actuation time.

In this level are applicable, in general, all the communication protocols that are commonly used at the plant level of industrial application such as CAN, PROFIBUS or Modbus. Modbus is the most extended due to its open specification and ease of use. It is an application level protocol in the OSI model. Originally it was implemented over RS232 and RS485 but it can also be implemented over Ethernet/IP networks. However, it can lead to an inefficient use of the computation and network capacity due to the inherent polling scheme. Also, it does not include specific cybersecurity functions [52].

The development of Smart Grids is also extending the communication capabilities of power plants with intelligent electronic devices such as remote sensors that use low-consumption wireless communication protocols such as ZigBee or Bluetooth [53].

There have been different efforts to standardize these communications. In Europe, the IEC61850 standard includes a data model that can be implemented over different application level protocols. In the US, a similar approach has been made in the NERC-CIP (North American Electric Reliability Corporation - Critical Infrastructure Protection) standard. These standards are not specific for MGs, but applicable to any electrical system with requirements of internal communication.

External communication: The PPC set-points are usually determined by the grid operator remotely through telecontrol. Telecontrol protocols are designed for the secure transmission of information of power plants over long distances. DNP3 is usually implemented in the US while IEC 60870-5/104 is used in Europe.

As for the internal communication, there are efforts to implement specific data model to standarize communication with PPCs of different plants. For EMS systems, standards IEC 61968 and IEC 61970 are applicable.

Supervision and Data Acquisition

Although not directly related to the control system, MGCCs are also in charge of the supervision and data aquisition of the MG. This function is gaining more relevance due to the development of Smart

Grids, that require the storage and remote tranmission of large amounts of data. However, there are concerns regarding the security of this information [54, 55].

2.3 Local Control Level: Voltage Sourced Converters

Once the active and reactive power set-points of the different units is established by the MGCC, each unit must be controlled to follow these set-points. As noted earlier, this is a very wide field of study due to the different elements that might comprise the MG. However, it is expected that power electronic converters will play a major role in future electrical systems, and specifically in the control of DERs [9]. Nowadays, most renewable and energy storage systems are already interfaced through power electronic converters in order to improve their controllability and to be able to interface DC and AC systems [3].

Among the local or Level 1 control possibilities in MG, this thesis is focused in the control of power electronic converters and, specifically, in the control of Voltage Sourced Converters (VSCs) for MG applications.

2.3.1 VSC in MG applications.

VSCs are a type of power electronics converters that are very extended due to the good relation between controlability and power ratings [3]. VSCs are forced-conmutated DC/AC converters that are characterized by having a constant DC voltage polarity. The power flow direction is thus determined by the current polarity, as opposed to Current-Sourced Converters (CSCs).

The basic component of the VSC is the switching element, which is commercially available as IGBTs or power MOSFETs, among others. Depending on the desired power rating, it is possible to include more than one switch in series to increase the voltage rating in the so-called multilevel configurations. Multilevel configurations present especial control requirements that are outside of the focus of this chapter.

This thesis is focused on the control systems that generate the switching signals. These signals are usually generated by a modulation technique. In power system applications, modulation techniques are usually based on controlling the AC voltage on the converter terminals, v_c. In the rest of the work a Sinusoidal Pulse-Width Modulation (S-PWM) is assumed and thus the output of the control systems are not directly the switching signals but the desired AC terminal voltage components $v_{c,abc}$.

Control of VSCs have been extensively studied for integration of RESs in traditional power systems. Therefore, there are problems that are currently not addressed by most VSC control systems, including.

- **Load Following:** When a MG operates in islanded mode, RESs must be able to supply the power demanded by the load, while keeping voltage and frequency betweend admissible levels. However,

in grid-connected operation, RESs are designed to generate as much energy as possible. This represents a change in the VSC control objectives.

- **Synchronous operation in converter-dominated systems:** Traditionally, VSC control has been designed using measurements from the grid phase and frequency as the reference for the orientation of the internal signals. However, in a MG scenario, where VSC-based generation might have a high penetration, there is no stiff grid to be oriented to. The critical scenario would be an isolated system without grid connection. This implies that new synchronization systems that do not rely on a stiff grid must be implemented.

- **Parallel operation:** When operating in parallel, multiple VSCs have to share the load active and reactive power while remaining in synchronism with each other and possibly with other non-VSC interfaced systems. It is not an additional problem but a complication of load following and synchronization problems since some of the available solutions are only applicable when there is only one VSC.

- **Inertia support:** In traditional power systems, any mismatch between generation and demand is automatically extracted from the energy stored in rotating elements. This is known as inertial response. VSC-interfaced untis do not have this intrinsic behavior so the control must be able to help the MG in these situations. In a MG with a high penetration of VSCs, this help can be decisive for the system stability.

Solutions for these problems are yet being investigated. This section presents a classification of the most representative control systems that have been proposed and their effect on the MG. Each system has a different objectives so a MG might include one or several of these control systems at the same time depending on the DER purpose.

These solutions are not exclusive to MGs and could be used for other applications. For instance, inertia support through VSC-interfaces systems is a growing issue for traditional power systems operators like the United Kingdom National Grid [56].

2.3.2 Control topologies review

The presented problems highlight the importance of the interaction between the VSC and the rest of the MG. Solutions for controlling VSCs in MGs can be classified according to their interaction with the MG in Grid-Tied, Grid-Supporting and Grid-Forming solutions [57]. A simplified scheme of each category is depicted in Fig. 2.4. This section includes a description of these control systems according to their most common implementations. Although there are multiple proposal the focus is not on giving

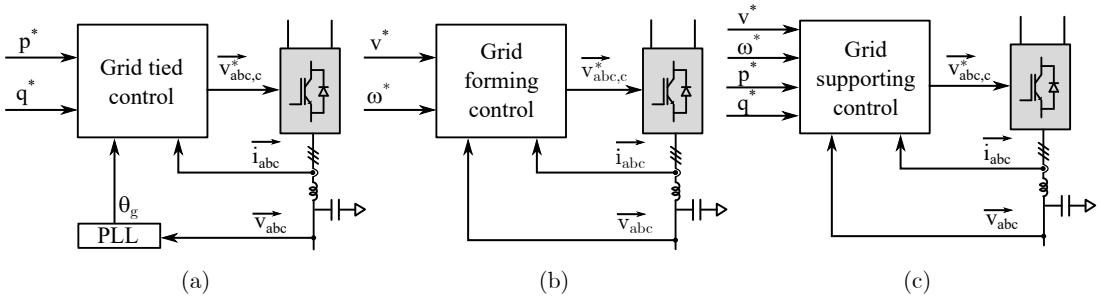

Figure 2.4: Classification of VSC control systems for MG applications according to their interaction with the grid including (a) Grid-Tied, (b) Grid-Forming y (c) Grid-Supporting systems.

an exhaustive review of all the possibilities but to give a categorization in which to frame the rest of the thesis work, which is specifically related to Grid-Supporting solutions.

Grid-Tied

Grid-Tied solutions are the most common control system for VSCs, not only for renewable energy systems but also for a lot of ESSs applications.

As seen in Fig. 2.4.a, the objective of Grid-Tied solutions is to regulate the VSC active and reactive power based on the references given to the control system. Sometimes current is controlled instead of power or as an intermediate step in order to keep the VSC current between admisible limits [3].

This power regulation is possible due to the measurement of the grid frequency and angle through a Phase-Locked Loop (PLL). In a PLL, the grid phase angle is obtained through the measurement of the grid voltage. The control system adapts the generated voltage to this measured phase angle in order to control the generated active and reactive power.

With this system, VSCs are seen from the grid as current sources or PQ nodes. Accordingly, they are not intrinsically prepared to respond to changes in the grid power balance, such as load variations.

Nevertheless, it is possible for Grid-Tied systems to support the grid power balance by acting on the active power reference. In traditional power systems, based on SGs, active power balance is related to frequency. SGs have power sharing methods based on the measurement of the SG rotational speed, which is related to the grid frequency. Therefore, frequency can be used as an indicator of the power unbalances in the grid. Therefore, the control could act following a variation on the grid frequency in order to support a power mismatch on the MG. This is possible even for RESs, provided that they have enough power available.

Some authors call systems that use this solution for supporting the grid Current-Source based Grid-Supporting systems, although noting that, as opposed to Voltage-Source based Grid-Supporting systems,

they cannot operate on islanded mode [57]. Due to their relation with the operation of traditional SGs, they are also known as Virtual Synchronous Machines (VSMs). As will be seen later, there are also Grid-Supporting systems that are based on the operation of SGs. The differences between Grid-Tied and Grid-Supporting VSMs are explained in more detail in Chapter 3.

Grid-Tied systems have proven very effective in the connection of RESs, such as WECSs and PV systems, to the grid. However, due to the synchronization system based on grid measurements they are not suited for islanded operation, which could appear in a MG system. Moreover, a high penetration of VSCs under PLL synchronization systems could be troublesome even in non-isolated systems [10].

Grid-Forming

When a VSC operates in islanded mode, it must guarantee the stable operation of the MG. This implies that it must be able to feed the MG loads while keeping voltage and frequency between admissible levels. Thus, the control objectives change with respect to Grid-Tied operation since the VSC cannot decide the active and reactive power generation on its own.

As shown in Fig. 2.4.b this is achieved by directly controlling the MG voltage and frequency. This implies that the MG frequency is fixed by the VSC control and not obtained from grid measurements. From the point of view of the grid, a VSC operating as a Grid-Forming unit is the equivalent of a voltage source or slack node.

This operation mode is also equivalent to an isochronous generator, which is a synchronous generator operating under a constant speed governor [1]. As with isochronous generators, it is not possible to connect multiple VSCs operating in this mode in parallel since the different control systems will conflict. A master-slave approach could be used, where one master VSC operates as a Grid-Forming unit and the rest as Grid-Tied slaves synchronized to the master [58]. Consequently, it also not possible to operate in grid-connected mode so a change to a Grid-Tied or Grid-Supporting control system would be required.

The most common application for this control system are Uninterruptible Power Supply (UPS) systems based on battery ESSs [57]. There are also authors that implement Grid-Forming systems with non-controllable RESs [59, 60]. In this case, the additional problem is to guarantee that the power extracted from the non-controllable source equals the MG demand so some authors propose the integration of additional systems such as battery ESSs [61], hydraulic generation [62] or controllable loads [63]. This is further discussed in section 6.2.

Grid-Supporting

In a MG, DERs are the main source of generation and thus should be able to support the system operation. Therefore, their purpose cannot be limited to deliver a fixed amount of power but also to

be responsive to the MG state. At the same time, they should be able to operate both in isolated and grid-connected mode.

It can be deduced that the previously presented control systems are not prepared to comply with these objectives. On one hand, Grid-Forming systems cannot be used to operate in grid-connected mode or share the MG requirements among multiple systems. On the other hand, Grid-Tied systems rely on a stiff power system so they are not prepared to operate in islanded or weak-grid scenarios.

Grid-Supporting systems try to handle these problems. As shown in Fig. 2.4.c, they try to regulate a certain power set-point but at the same time to maintain the MG voltage and frequency. In contrast with Grid-Tied systems, a PLL is not required for operation.

By combining the objectives of supporting the MG voltage and frequency with their own power reference, multiple VSC-based systems can support the MG operation at the same time while complying with their own requirements.

In order to allow both grid-connected and isolated operation modes, Grid-Supporting systems do not rely on grid frequency measurements for synchronization. However, they must operate in synchronism with the rest of the DERs and with the grid, in case of grid-connected operation. Therefore, in contrast with Grid-Forming systems that only synchronize to their internal frequency reference, a synchronizing system between multiple untis is needed.

These control objectives are analogous to those of traditional SGs. SGs can be modelled as voltage sources that inherently synchronize to the grid [64]. This synchronization mechanism can be replicated by the VSC control system, as will be seen in Section 3.3.

The active power generation of SG systems is controlled by the governor, which regulates the generator rotational speed by acting on the applied mechanical torque, for instance varying the gate opening of hydraulic turbines. Since the rotational speed is related to the electrical frequency, this regulation indirectly supports the grid power balance. In order to allow the parallel operation of multiple generating units that share the load, the speed regulation on the governor of SGs includes a droop relation, also called power-speed characteristic, that reduces the speed reference proportionally to the governor actuation [1]. This droop relation determines the amount of load assumed by each generator.

An analogous droop relation can be replicated in the control system of a VSC, generating the VSC frequency according to its active power generation, as in the so-called droop control systems [65]. Droop control systems were proposed in order to share the load between multiple UPSs operating in parallel [66]. It has been demonstrated how it is possible to synchronize multiple VSCs when they operate using droop [67], and also that it is possible to synchronize a VSC to the grid [15].

As noted earlier, in Grid-Tied systems there are also solutions based on introducing a relation between active power and frequency. Since Grid-Tied systems are based on regulating the VSC active

power generation instead of its frequency, the droop relation is implemented in an opposite way than in SG governors, acting on the active power reference depending on the frequency measurement provided by the PLL. The effect of this difference on the resulting support of the MG is discussed in chapter 4.

A more explicit replication of synchronous generators behavior is proposed by Grid-Supporting Virtual Synchronous Machine (VSM) and Droop control systems. Although there are multiple implementations, as will be discussed in Chapter 3, it can be demonstrated that Droop and Grid-Supporting VSM control system are equivalent [68]. Therefore, in this work the term VSM is used to refer to them indistinctly.

Grid-Supporting VSM control systems can operate in both grid-connected and islanded operation modes and allow multiple VSCs to support the MG. However, there are still concerns about stability issues related to the selection of the droop control gains, that affect both the steady-state power and frequency values and the dynamic behavior of the system [69]. Moreover, all of these implementations have in common the use of a dependency between active power and frequency as synchronizing mechanism [68, 70].

In this thesis, a different approach is proposed where reactive power is used instead of active power for the synchronous operation of VSCs, thus decoupling the synchronization mechanism from the VSC active power, while no PLL is required for frequency measurement. It will be referred as Reactive Power Synchronization (RPS). It will be seen how this allows the use of Grid-Supporting systems even in non-controllable sources such as WECSs.

It can be seen that Grid-Supporting systems are very promising for MG applications and will be the main focus of this thesis. However, as noted earlier, depending on the control objectives a Grid-Tied or Grid-Forming system might be more interesting and the appropriate system should be selected depending on the application. Nevertheless, some authors expect Grid-Supporting systems such as VSM to replace the rest of the systems and become the *unified* solution for grid integration [71].

Chapter 3

Virtual Synchronous Machine

Contents

3.1 Introduction 23

3.2 Review of VSM implementations 24

3.2.1 VSM applications 24

3.2.2 VSM implementations 25

3.3 Synchronization of Grid-Supporting VSMs 28

3.3.1 Synchronizing torque 28

3.3.2 Application to VSCs 30

3.1 Introduction

As presented in the previous chapter, VSMs are control systems for power electronic converters that are based on emulating the behavior of traditional SGs in order to improve the support of grid stability through converter-interfaced systems. VSMs have attracted a lot of attention in recent years in multiple applications such as WECS [72], electrical vehicles [73], stationary energy storage systems [43] and HVDC systems [74].

In this chapter, VSMs will be analyzed as a solution for the control of VSCs in MG applications. In section 3.2, a brief review on VSM implementations is presented. The purpose is not to present an exhaustive review but to overview VSMs most interesting features for MG applications. VSM implementations will be categorized with respect their interaction with the MG according to the control topologies review presented in 2.3.

In section 3.3, one of VSM most interesting features, synchronization to weak grids, is analyzed in

an analogy to the operation of traditional SGs. This analogy with SGs will also be used to introduce the RPS control in Chapter 5.

3.2 Review of VSM implementations

There are multiple implementations available in the literature under the name of VSM or similar or that are based on the operation of SGs. In this thesis the focus is on VSM implementations that can be useful from MG applications. First the interest in VSMs for MG applications is analyzed by exploring the most interesting VSM applications. The next section presents a review of VSM implementations that comply with these applications.

3.2.1 VSM applications

The interest in control systems that imitate the behavior of SGs in MG applications comes from two interesting features of SGs: inertial response and synchronizing torque.

Inertial response

The VSM concept was originally proposed in [75] to provide converter-interfaced systems, especially DERs, with the capability of emulating the inertial response of SGs. Like conventional SGs, a VSM reacts to variations in the power balance by exchanging energy that supports the system operation. Thus, a converter-interfaced unit with enough energy available can provide an inertial response equivalent to that of a SG [73].

This feature has attracted a lot of interest, even in conventional power grids where converter-interfaced systems penetration is increasing [56]. This application of power electronic converters is usually known as inertia emulation [76].

It is a critical application for converter-dominated MGs since a reduced inertia can compromise a power system stability [13]. The use of VSMs for inertia emulation is further discussed in Chapter 4.

Synchronizing torque

One of the main features of VSCs is the possibility to independently control their active and reactive power. To perform this control, the generated voltage must be synchronized with the system they are connected to [3]. In a MG, this outer system could be an isolated load, a main grid or even other VSCs.

A common approach, used in Grid-Tied systems as presented in section 2.3, is measuring the frequency by means of PLL [77,78]. This ensures that the generated internal voltage has the same frequency

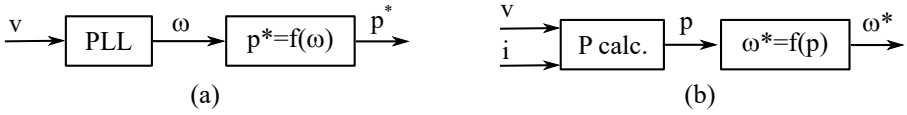

Figure 3.1: Comparison of (a) Grid-Tied and (b) Grid-Supporting VSM control systems.

as the grid voltage and the angle required for the power injection. However, PLLs are known to present problems when applied to islanded systems [10, 11].

On the other hand, SGs do not rely on frequency measurements for grid synchronization and are commonly used in isolated and weak-grids without synchronization problems. This due to the synchronizing torque, which introduces a negative feedback of the phase displacement, ensuring that mechanical forces will be set up to restore the rotor angle of the machine following an arbitrarily small displacement of this angle [64]. This is why VSMs are being proposed for the connection of converter-interfaced systems to weak grids [79]. It has been demonstrated how it is possible to synchronize multiple VSCs when they operate using this strategy [67].

As explained in [15], synchronization in VSMs is based on introducing a coupling between the VSC active power and its frequency. This coupling is common among the different VSM implementations [68, 70]. Moreover, it is also the basis of the power-frequency droop control systems [65, 66, 80–82].

As noted in section 2.3, this application allows VSMs to operate as Grid-Supporting units, which provides several advantages. In order to provide a better understanding of this feature, the synchronization mechanism of VSMs is studied in Section 3.3.

3.2.2 VSM implementations

There is yet no consensus on the implementation of a VSM to fulfill the aforementioned applications. Moreover, among the different control systems that are based on the operation of SGs, not every implementation comply with both inertia emulation and synchronous operation without PLLs.

It should be noted that, although most publications have focused on SGs, there are also works on the replication of induction generators, also known as “Inducverters” [83]. However, with regard to synchronous operation and inertial response, the operation principle is analogous to SG-based systems.

Going back to the classification made in section 2.3, there are both Grid-Tied and Grid-Supporting VSM solutions. As presented in Section 2.3, Grid-Supporting solutions are able to operate in synchronism in both grid-connected and islanded modes while Grid-Tied solutions require an external frequency measurement unit and can lead to instabilities when used in an converter-dominated systems. The difference in the relation between frequency and power in Grid-Tied and Grid-Supporting VSM control systems is depicted in Fig. 3.1.

Grid-Supporting solutions

The first Grid-Supporting VSMs were based on the digital implementation of complete SG numerical models on the converter control system. This is the case of the VISMA, which implements a 7th order model [75]. This is also the basis of Synchronverter concept, which implements a reduced second-order model [84, 85]. These implementations have the advantage of using well-known parameters from SG operation for the control tuning. The use of higher order models, while incresing the control complexity, has not been reported to provide enhanced properties [86].

However, for synchronizing and inertia emulating purposes, it is not necessary to emulate the complete behavior of a SG. As stated earlier, the inertial response comes from the SG intrinsic swing equation. A more specific implementation of the SG swing equation can be found in the Power Synchronization Control [15], which avoids the use of a numerical model of the machine.

Moreover, [68] demonstrates that the power/frequency (p/f) droop control that is commonly used in UPS applications to share the load between converters [65, 82], also implements an analogous swing equation where the inertia is represented by the power measurement filter time constant. This is further developed by the Virtual Synchronous Machine with Zero Inertia (VSMH0) concept [16], that modifies the filter so the system can keep the VSM synchronizing capabilities but without providing inertia. Therefore, although p/f droop control systems were proposed prior to the extension of the term of VSM [66] in this work they is considered as an implementation of a Grid-Supporting VSM.

Grid-Tied solutions

In a power system including SGs, the electric frequency changes following variations in generation and demand. Therefore, frequency can be used as an indicator of power unbalances. A possible implementation of inertia emulation is to vary active power generation according to frequency variations [87]. Most converter-based generation is prepared to regulate its power output and perform a frequency estimation through a PLL, so the implementation in already operating systems is quite straightforward. This mechanism is usually referred to as “Virtual Inertia” (VI) [76].

VI control systems were reported before the extension of the VSM concept [87]. However, since they operate based on the behavior of SGs they are now usually included in VSMs [86]. The VSM implementation proposed in the VSYNC project, of the 6th European Research Framework program, is based on a Grid-Tied VSM control system [88].

Virtual Inertia is usually a combined effect of a “derivative control” component and a “proportional control” or “droop” component [89]. The derivative term is designed to emulate the extraction of mechanical energy from the SG inertia while the proportional term emulates the SG governor “droop” action. This difference is used by some authors to differentiate between the proportional and derivative

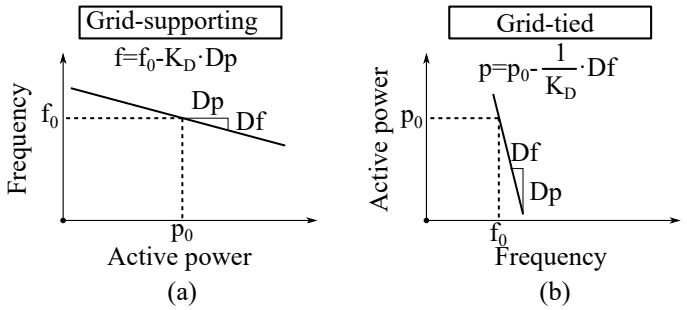

Figure 3.2: Contrast between the droop or power-speed characteristic implemented in (a) Grid-Supporting systems and synchronous generator governors and (b) Grid-Tied systems.

terms as different applications [90].

It should be noted that the "droop" action in VI systems is implemented in an opposite way than in a SG governor. While in the SG governor the speed reference is varied depending on the controller actuation, for VI this is emulated in an opposite way, measuring the frequency (speed) and varying the power output (actuation). Both implementations are compared graphically in Fig. 3.2.

Another solution is to introduce a fixed power value in the event of a threshold frequency variation. Some examples can be found in [91–93]. They can act very fast because their dynamic is not dependent on a frequency or power regulation. The active power variation is usually determined by the system capacity (SOC, wind availability...) instead of the grid requirements and thus it is hard to adapt to different situations. Implementation strategies differ between manufacturers and academic studies; however, in general, such controls cause the power output to temporarily vary in the range of 5% to 10% of the rated power, following a significant frequency excursion, for a period of several seconds [94].

Grid-Tied VSM control systems depend on a frequency variation to actuate, which is usually the case only when there is synchronous generation on the system and it has already been decelerated (or accelerated). Therefore, these systems have little effect on the initial Rate of Change of Frequency (RoCoF) but a great influence on the frequency nadir [95]. On the other hand, they are known to have adverse effects on the small-signal stability of weakly interconnected systems [96]. For the same reason, they require the presence of an external voltage with physical inertia and therefore are not suitable for islanded operation [84].

As other Grid-Tied solutions, these systems are not able to operate without a frequency measurement unit (PLL). Therefore, although both Grid-Supporting and Grid-Tied VSM systems are reported to emulate inertia, there is a difference in the synchronization mechanism. The effect of this difference on the resulting inertial response is discussed in chapter 4.

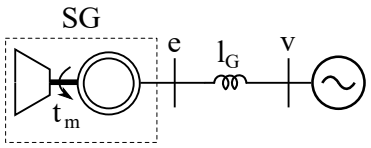

Figure 3.3: Schematic diagram of a grid-connected synchronous generator.

3.3 Synchronization of Grid-Supporting VSMs

In this section, the synchronization mechanism used by Grid-Supporting VSMs will be studied based on the operation of a SG. This will be contrasted with the proposed Reactive Power Synchronization method in chapter 5.

3.3.1 Synchronizing torque

SGs are able to operate in synchronism without a dedicated frequency measurement unit. As presented earlier, this synchronism is possible because of the SGs synchronizing torque. In this section the origin of this synchronizing torque is explored in order to understand the operation and resulting limitations of VSMs.

The rotational speed of a SG is defined by the mechanical equation

$$2H\frac{d\omega_r}{dt} = t_m - t_e \tag{3.1}$$

where

$\omega_r =$ rotor angular velocity

$t_m =$ mechanical torque developed by turbine connected to the SG

$t_e =$ electromagnetic torque developed by the SG

$H =$ Inertia constant [s]

and all the values are expressed in per unit with respect to the synchronous generator rated power (P_b) and frequency (Ω_b). This equation defines the relationship between the SG rotational speed and the difference in the torque developed by the SG and the external electrical system.

To explore the synchronization to another power system we study the connection of a SG to the grid through a power line as seen in Fig. 3.3.

As we have seen, the SG frequency, related to its rotational speed, is determined by its mechanical equation, (3.1), while the grid frequency is fixed at ω_g. The difference between both frequencies can be defined as

$$\frac{1}{\Omega_b}\frac{d\delta}{dt} = \omega_r - \omega_g \tag{3.2}$$

Synchronization is ensured if $\frac{d\delta}{dt} = 0$, that is if δ has a fixed value.The differential equations (3.1) and (3.2) form a dynamic non-linear system with two states. In order to study the small-signal stability around the operating point defined by δ_0 and ω_0, the mechanical equation, (3.1), can be rewritten in terms of δ as

$$\frac{2H}{\Omega_b}\frac{d^2\Delta\delta}{dt} = \Delta t_m - \Delta t_e \tag{3.3}$$

Equation (3.3) represents an ideal oscillator. There are different effects that introduce a damping in this oscillation, including power losses on the SG mechanical system, which are usually neglected, variations in load demand proportional to frequency, which are not considered in this case since the SG is connected to a stiff grid, and, more importantly, damping mechanisms introduced through the SG excitation. This damping can be implemented by introducing voltage variations in phase with the SG rotation [1]. This will be the basis of the damping mechanism proposed in Chapter 5. Without a damping torque, the operation of a SG would be unstable [64].

The resulting equation when considering the effect of the damping gives

$$\frac{2H}{\Omega_b}\frac{d^2\Delta\delta}{dt} = \Delta t_m - \Delta t_e - \underbrace{\frac{D}{\Omega_b}\frac{d\Delta\delta}{dt}}_{\text{Damping torque}} \tag{3.4}$$

which leads to the so-called SG swing equation.

Still, this equation does not show that the operation of a SG is stable and therefore that synchronism is ensured. However, the electromagnetic torque t_e is not an independent variable since it depends on the electrical power exchanged with the grid.

From the notation in Fig. 3.3, the power exchanged between the SG and the grid is defined by the current between e and v as

$$\frac{l_g}{\Omega_b}\frac{d\vec{i}}{dt} = \vec{v} - \vec{e} - r_g\vec{i} - j\omega l_g\vec{i}, \tag{3.5}$$

Assuming that the electromagnetic transients in l_g are significantly faster than the mechanic transients of the SG swing equation, it can be written that

$$p_e = \frac{2}{3}\Re(\vec{e}\cdot\vec{i}^*) = \frac{ev}{\omega_r l_g}\sin\delta \tag{3.6}$$

Considering this equation in the operating point defined by δ_0 and ω_0

$$\Delta p_e = \underbrace{\frac{e_0 v_0}{\omega_0 l_g}\cos\delta_0}_{K_s}\Delta\delta \tag{3.7}$$

Voltage magnitude e depends on the SG excitation and on the rotational speed. For simplicity, it has been considered as independent from δ. The effect of variations of frequency on the electromagnetic

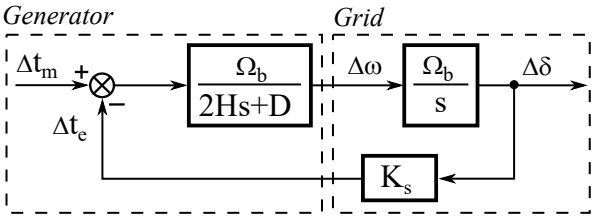

Figure 3.4: Block diagram of a synchronous generator swing equation.

power are small and therefore are also neglected so $t_e = p_e$ in pu. These assumptions are common in small-signal stability studies of power systems [1]. Note that the effect of frequency variations on active power is already considered through the damping term D of equation (3.4).

For this exposition, the importance is on the relation between active power and δ. As shown in (3.7), both are proportional. This is why δ is usually known as the power angle. Merging equations (3.4) and (3.7),

$$\frac{2H}{\Omega_b}\frac{d^2\Delta\delta}{dt} + \frac{D}{\Omega_b}\frac{d\Delta\delta}{dt} + K_s\Delta\delta = \Delta t_m \tag{3.8}$$

The proportional relation between p_e and δ introduces a negative feedback of the phase displacement on the swing equation, leading to a stable behavior for positive values of K_s. This is why $K_s\Delta\delta$ is known as the synchronizing torque. This is graphically represented in Fig. 3.4.

Therefore, SGs take advantage of the relation between active power and power angle that appears on power systems in order to ensure synchronous operation. Since internally the SGs speed is related to active power because of the mechanical system, there is a natural negative feedback that relates the speed back to an active power variation through the synchronizing torque, ensuring the system stability.

3.3.2 Application to VSCs

As presented in chapter 2, VSCs are one of the main solutions for interfacing RESs and ESSs in MGs. Using the appropriate modulation techniques, they can be regulated as a controllable AC voltage source [3]. In this section, the principles studied in the previous section for SGs are applied to the synchronization of a VSC to the grid, so the generated voltage frequency is equal to the grid frequency and the voltage angle has the value required for power injection.

Based on the literature review of section 3.2, three different grid-supporting VSM implementations are considered. For each of them, an analysis analogous to the one applied to SGs in the previous section is performed in order to study the synchronizing mechanism.

The selected solutions are the Synchronverter implementation in [86], the Power Synchronization Control (PSC) of [15] and the Power-Frequency Droop (P/f droop) control presented in [66].

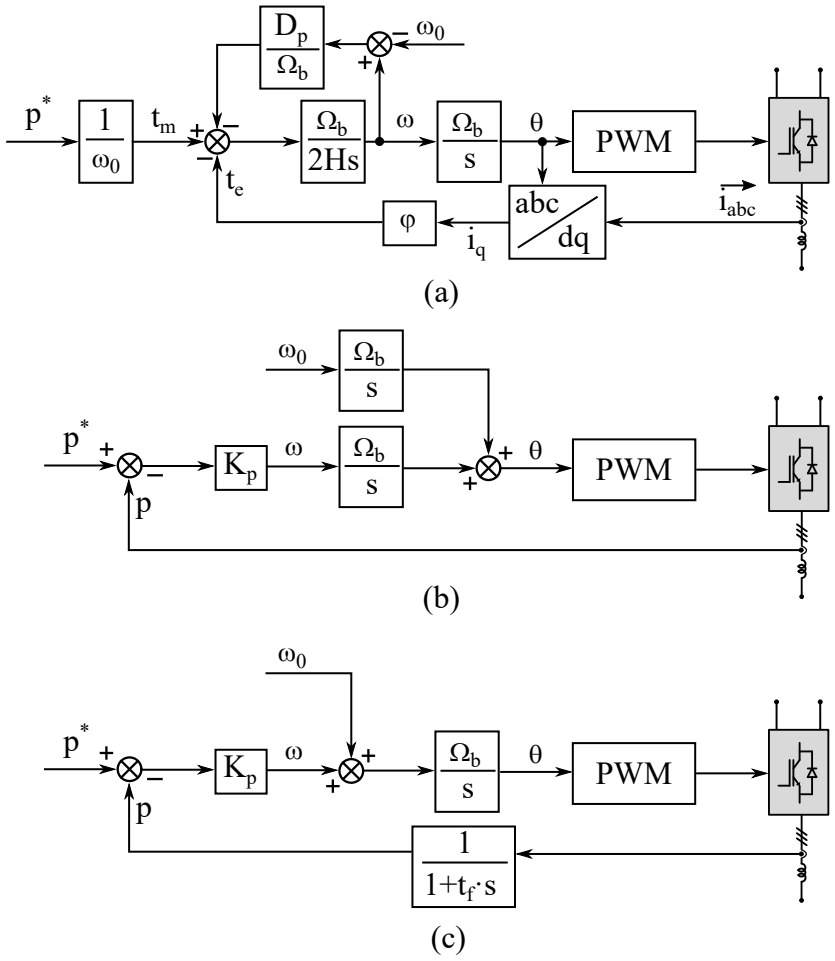

Figure 3.5: Comparison of (a) Synchronverter, (b) Power Synchronization Control and (c) P-f droop control systems. Original notation has been modified for coherence between implementations. Lowercase variables indicate per unit notation.

Schemes of these systems are depicted in Fig. 3.5. The notation of the parameters have been selected so that they resemble the common parameters of a SG. Only the active power part of the algorithms is considered since the focus is on the synchronization mechanism. All the implementations include also a voltage or reactive power control loop that is outside of the focus of this section.

From Fig. 3.5, it can be seen that the Synchronverter implementation is the one that more closely resembles the SG model of section 3.3.1. Also, the similarities between the PSC and P/f droop controls are noticeable. The P/f droop includes a low-pass filter of the active power measurement that is not present in PSC [15]. Low-pass filters of active power are usually included in order to reduce the effect of measurement noise and high-order harmonic components [65].

For the Synchronverter, the reasoning is similar to that of a SG. By emulating the behavior of the

mechanical system, the same relations as for a SG can be obtained. However, in this case, there is no real rotating system. Therefore, the power and energy required by the resulting swing equation must be available on the system to ensure stability. This is why these implementations are usually associated with ESSs [97].

For the PSC and P/f droop systems, a similar relation can also be obtained. In order to illustrate the effect of the active power filter, the P/f droop system is considered as a reference.

As with the SG, discarding the electromagnetic transients on the network, it is a system with two states so we study the small-signal model around the operating point defined by δ_0 and ω_0. δ is defined as in equation (3.2) but now considering the control system internal frequency ω in spite of ω_r. Therefore, the relation between the control internal angular position θ and δ can be defined as

$$\frac{1}{\Omega_b}\frac{d\delta}{dt} = \omega - \omega_g = \frac{1}{\Omega_b}\frac{d\theta}{dt} - \omega_g. \tag{3.9}$$

For small-signal variations around the operating point, asuming ω_g as independent

$$\frac{1}{\Omega_b}\frac{d\Delta\delta}{dt} = \frac{1}{\Omega_b}\frac{d\Delta\theta}{dt}. \tag{3.10}$$

From the diagram in Fig. 3.5.c, the control system is defined by the equation

$$\frac{1}{\Omega_b}\frac{d\theta}{dt} = (p^* - p)K_p + \omega_0. \tag{3.11}$$

so for the given operating point

$$\frac{1}{\Omega_b}\frac{d\Delta\delta}{dt} = (\Delta p^* - \Delta p)K_p. \tag{3.12}$$

The measured active power p represents a filtered estimation of the power exchange with the grid so, considering the relation with the power angle δ given by equation (3.7), it can be written that

$$\Delta p = \frac{1}{1+t_f s}\Delta p_e = \frac{1}{1+t_f s}K_s\Delta\delta \tag{3.13}$$

Using equation (3.13) into (3.12) leads to

$$\frac{t_f}{K_p\Omega_b}\frac{d^2\Delta\delta}{dt} + \frac{1}{K_p\Omega_b}\frac{d\Delta\delta}{dt} + K_s\Delta\delta = \Delta p^* \tag{3.14}$$

Note that (3.14) is analogous to the SG swing equation given in (3.8), where

$$H = \frac{t_f}{2K_p} \tag{3.15}$$

$$D = \frac{1}{K_p} \tag{3.16}$$

Therefore, in this case the inertia constant is related to the time constant on the active power filter t_f while the damping is related to the proportional gain between active power and frequency K_p and the synchronizing torque component is the same as in traditional SGs.

Note that a similar reasoning can be made for the PSC depicted in Fig. 3.5. If the filter is not considered, there is no resulting inertia, which could be interesting depending on the application. Usually, some kind of filter is necessary for noise rejection, although it can be tuned to reduce the resulting inertia effect [16].

Therefore, it can be seen that a synchronizing mechanism has been achieved by introducing a proportional relation between the VSC active power and its internal frequency. This allows Grid-Supporting VSMs to operate without the use of a PLL. However, at the same time, it imposes restrictions on their use since the synchronization is dependent on the capacity to supply the required active power set-point Δp^*. A solution for achieving synchronization without a requirement of active power is presented in chapter 5.

At the same time, it can be seen that this reasoning shows how VSMs can be used to provide inertia. As noted earlier, this feature is not limited to Grid-Supporting VSMs. This is further discussed in Chapter 4.

Chapter 4

Inertia Emulation

Contents

4.1 Introduction 35

4.2 Implementation of Inertia Emulation solutions 36

4.2.1 Voltage Oriented Control (VOC) 36

4.2.2 Grid-Supporting VSM 38

4.2.3 Grid-Tied VSM 40

4.3 Application in an isolated Microgrid case study 42

4.3.1 Simulation case study 42

4.3.2 VSM control systems comparison 44

4.3.3 Final discussions 47

4.1 Introduction

As opposed to traditional bulk power systems, MGs rely heavily on power converter-interfaced DERs. Therefore, converters are expected to provide services associated to the operation of traditional generation units such as emulated inertia. As presented in Section 3.2, this could be achieved by the VSC control system, provided that the VSC is connected to a system that has enough energy available.

Battery Energy Storage Systems (BESSs) are capable of storaging energy and are usually interfaced through Power Electronic Converters (PECs) that convert the DC voltage provided by the battery pack and injects it as a controllable AC source. Inertia emulation is a very promising application for systems that include BESSs. Sizing studies of BESS for inertia emulation show that it is becoming an economically feasible solution [98–100]. A successful study of the implementation of inertia emulation through

a Lithium-Ion BESS in a 2,686 MVA MG test system with a wind power penetration of the 33% can be found in [98]. Simulations results in [98] show that a 33MW (1,23% of the MG power) ESS was enough for providing the similar grid inertial response as in the grid without any wind power penetration.

As discussed in Chapter 3, both Grid-Tied and Grid-Supporting VSM control systems can provide an emulated inertial response. Inertia emulation in Grid-Tied systems is based on responding to frequency variations measured by the PLL. In contrast, Grid-Supporting systems rely on the emulation of the SG swing equation.

This chapter discuss the effect of the synchronization system on inertia support. Representative implementations of Grid-Tied and Grid-Supporting VSMs solutions are compared in a dynamic simulation of an isolated MG for a common set of inertia requirement. Section 4.2 describes the implemented models and discuss the selection of parameters to provide an equivalent inertial response through the different systems. Section 4.3 presents the isolated MG case study and the results obtained for the different systems.

4.2 Implementation of Inertia Emulation solutions

In order to compare the effect of the synchronizing system, the emulated inertial response from both Grid-Tied and Grid-Supporting VSMs, as defined in section 3.2, have been implemented in a discrete time simulation.

First, in order to study the effect of the PLL irrespective of the inertia control implementation, the BESS active power is controlled to a constant value through a PLL-based Voltage-Oriented Control (VOC) system. This control will later be used as the underlying control that regulates the active power reference provided by the Grid-Tied systems.

Then, the Grid-Supporting group will be represented by a VSM implementation focused on the relation between active power and frequency The Grid-Tied group is represented by a Virtual Inertia implementation that includes both proportional and derivative components. The effect of both systems is later studied separately in the results section.

4.2.1 Voltage Oriented Control (VOC)

VOC is a common control system for Grid-Tied VSCs. In VOC the VSC current is controlled through its dq-components. The dq frame rotates following the angle provided by a PLL. A general scheme is presented in Fig. 4.1.

The PLL is based on orientating the reference axis to the measured grid voltage, so that the quadrature component of the voltage becomes zero, as depicted in Fig. 4.2.

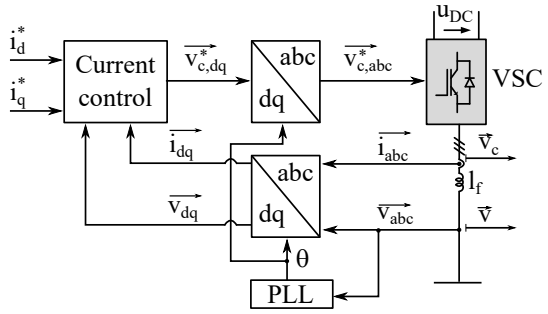

Figure 4.1: Voltage Oriented Control implementation scheme.

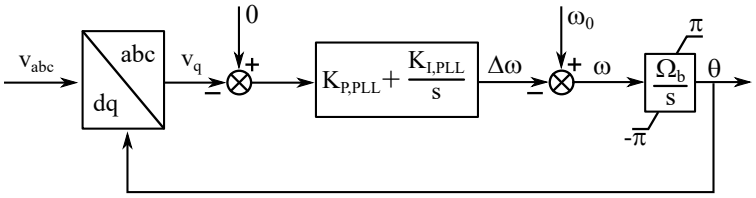

Figure 4.2: Phase-Locked-Loop (PLL) based on the regulation of the grid voltage quadrature component (v_q).

The control of current dq-components includes a decoupling between the d and q axes and a feed-forward of the voltage as depicted in Fig. 4.3.

In order to modulate the voltage on the VSC terminals, the dq components of the VSC reference voltage $v_c{}^*$ are transformed to abc components using the angle θ obtained from the PLL as seen in Fig. 4.1.

The main parameters related to the VOC are summarized in Table 4.1.

The PLL parameters have been selected according to the natural frequency $\omega_{n,PLL}$ and damping ξ_{PLL} of the resulting second-order closed-loop transfer function, as presented in [101]. The resulting gains

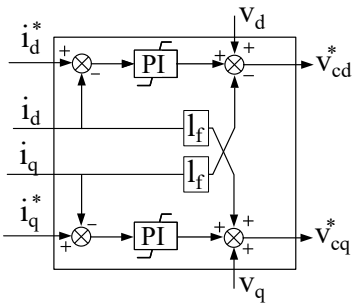

Figure 4.3: Current controller implementation scheme.

Table 4.1: Inertia Emulation case study: Base case Voltage Oriented Control (VOC) parameters.

Label	Value	Units	Description
T_s	100	μs	Controller sampling time.
$\omega_{n,PLL}$	$2\pi 100$	rad/s	PLL natural frequency.
ξ_{PLL}	$1/\sqrt{2}$	-	PLL damping coefficient.
τ_i	1	ms	Time constant of the current regulation loops.

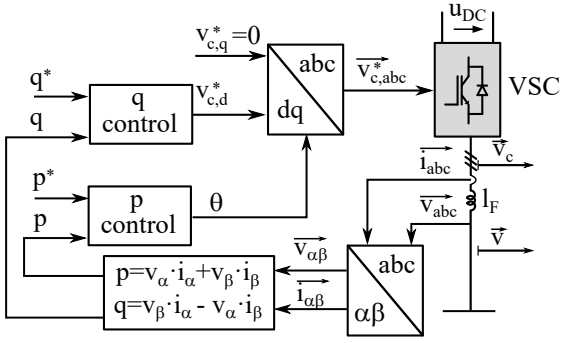

Figure 4.4: Grid-supporting VSM implementation.

can be calculated as

$$K_{p,PLL} = \frac{2(1-e^{-\xi\omega_n T_s}\cos(\omega_n T_s\sqrt{1-\xi^2})}{\Omega_b T_s} \tag{4.1}$$

$$K_{i,PLL} = \frac{1}{\Omega_b}\left(\frac{K_{p,PLL}}{T_s} - \frac{(1-e^{-2\xi\omega_n T_s})}{{T_s}^2}\right) \tag{4.2}$$

The current controllers PI gains have been selected according to the zero-pole cancellation method proposed in [3].

4.2.2 Grid-Supporting VSM

The Grid-Supporting VSM discrete time implementation is based on a simplified version of the Synchronverter concept similar to the one presented in [102]. The harmonic content elimination and the coupling between frequency and voltage amplitude introduced in [102] are omitted here since both power quality and reactive power control are out of the scope of the work. The resulting control system scheme is presented in Fig. 4.4. The p and q controller schemes are depicted in Fig. 4.5.

The parameters to be selected are the proportional gain of the active power controller, $K_{P,VSM}$, the damping gain D_{VSM}, and the gain of the reactive power controller $K_{Q,VSM}$. A summary of the selected VSM parameters is included in Table 4.2.

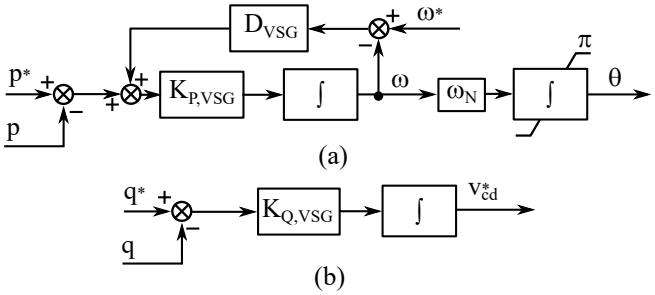

Figure 4.5: VSM active (a) and reactive (b) power control.

Table 4.2: Inertia Emulation case study: Base case grid-supporting Virtual Synchronous Machine (VSM) parameters.

Label	Value	Units	Description
$K_{P,VSM}$	5	s^{-1}	Active power controller gain.
D_{VSM}	7	-	Damping gain.
$\tau_{Q,VSM}$	10	ms	Reactive power time constant.

The damping gain D_{VSM} is referred in some works as analogous to the SG friction coefficient [68, 102] while in others it is interpreted as analogous to the droop coefficient of the SG governor [103] since it introduces a proportional relationship between frequency variations and active power reference as seen in section 3.3. It is selected depending on the desired contribution to load variations and is usually imposed by the grid-code [68].

According to standard EN 50438, it is required that the change of 100% of the generated active power corresponds to the change of 2% of the grid frequency. Since the case study comprises an isolated MG, it is expected that the frequency will present larger variations than traditional power systems. Thus, D_{VSM} has been selected experimentally so that the BESS provides near half of the load variation. The effect of choosing a different value is analyzed in the results section.

$K_{P,VSM}$ on the other hand, is related to the VSM inertia constant [68, 102]. To obtain a emulated inertia H_V, $K_{P,VSM}$ can be calculated as

$$K_{P,VSM} = \frac{1}{2H_V} \tag{4.3}$$

As noted in [103], H_V cannot be made arbitrarily big since as $K_{P,VSM}$ decreases, so does the frequency of the active power controller transfer function. This introduces a phase lag that reduces the phase margin (PM) of the system. From the open loop transfer function of the active power controller of Fig. 4.5 it can be obtained that, for a minimum PM of 45°

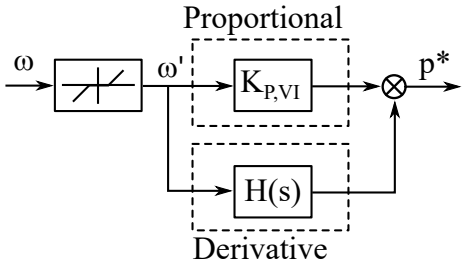

Figure 4.6: Grid-tied VSM implementation.

$$K_{P,VSM}{}^{min} = \frac{\omega_{cross-over}|_{PM=45^\circ}}{D_{VSM}} = 3 \tag{4.4}$$

Giving a maximum emulated inertia H_V of about $0.17s$. Here it is selected as $K_{P,VSM} = 5$ to allow for a greater phase margin and damping characteristics, so $H_V = 0.1s$. This inertia constant is similar to the one obtained in other similar VSM implementations [102, 103].

The value of $K_{Q,VSM}$ can be selected depending on the required closed loop time constant $\tau_{Q,VSM}$ as [102]

$$K_{Q,VSM} = \frac{3}{2\tau_{Q,VSM}} \tag{4.5}$$

4.2.3 Grid-Tied VSM

The Grid-Tied VSM has been implemented based on the model presented in [104], where the active current reference for the VOC is proportional to the MG frequency, as measured by the PLL, and to its derivative. A schematic representation can be seen in Fig. 4.6. The resulting active power reference (p*) is used as the input of the active current loop of Fig. 4.1.

The derivative term is designed to provide a fast response, while the proportional term allows the BESS to provide active power until the frequency is restored [104]. As presented in section 3.2, derivative and proportional terms are intended to emulate the behavior of a SG inertial and governor droop responses, respectively. The effect of the derivative term will be analyzed in the results section by comparing this scheme with a pure proportional (droop) system.

The frequency used for the control is passed through a dead-band which avoids the use of the BESS for small variations of the frequency around its normal operating point [105]. A filter might also be needed in order to reject high-frequency noise. The PLL can be designed to filter frequency variations in a compromise with its speed [106].

Calculation of the derivative of the frequency through $H(s)$ may lead to undesired variations so it is usually implemented together with a low-pass filter [107]. In [108] a second-order filter is implemented

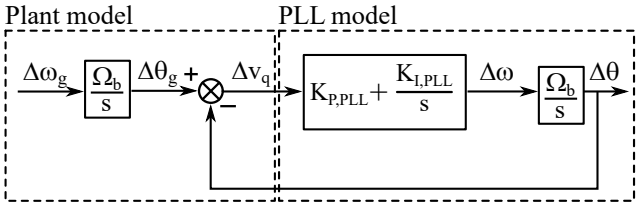

Figure 4.7: PLL small signal model. ω_g: grid frequency. θ_g: grid voltage phase

as

$$H(s) = \frac{K_{D_V I} s}{(s+\tau_1)(s+\tau_2)} \tag{4.6}$$

As reported in [108], it can be demonstrated that this transfer function is already included in the proposed PLL implementation. Based on the PLL of Fig. 4.2, a small signal model of the PLL, for small deviations around the operating point $v_{q,0} = 0$, is presented in Fig. 4.7. It can be deduced that

$$\Delta v_q = \frac{\Omega_b s}{s^2 + \Omega_b K_{P,PLL} s + \Omega_b K_{I,PLL}} \Delta\omega_g \tag{4.7}$$

Meaning that v_q is effectively a filtered estimation of the grid frequency derivative. It is a low pass filter so the estimation will be accurate for variations below the PLL bandwidth. Moreover, it can also be seen that

$$\Delta\omega = \frac{K_{P,PLL} s + K_{I,PLL}}{s} \Delta v_q \tag{4.8}$$

or, alternatively

$$\Delta v_q = \frac{s}{K_{P,PLL} s + K_{I,PLL}} \Delta\omega \tag{4.9}$$

Thus, calculating the derivative of the PLL output frequency ω together with a low-pass filter is analogous to using v_q.

In this work v_q will be used as an estimation of the grid frequency derivative. Since this estimation is only accurate for low frequency variations, a first-order low pass filter is also included.

References for the selection of VI parameters for grid-connected applications can be found in [104, 108]. However, these parameter selection methods are not directly applicable for the presented case study.

The parameters to be selected are the proportional gain, $K_{P,VI}$, the derivative gain $K_{D,VI}$ and the dead-band characteristics. A summary of the selected parameters is included in Table 4.3.

As noted in 3.2, the proportional gain $K_{P,VI}$ is equivalent to the inverse of the droop gain used in the governor of SG-based generation systems (see Fig. 3.2). Therefore, in order to make the controller comparable to the grid-supporting VSM implementation, $K_{P,VI}$ is selected as the inverse of D_{VSM}.

Table 4.3: Inertia Emulation case study: Base case grid-tied VSM parameters.

Label	Value	Units	Description
$K_{P,VI}$	0.15	–	Proportional gain.
$K_{D,VI}$	0.2	s	Derivative gain.

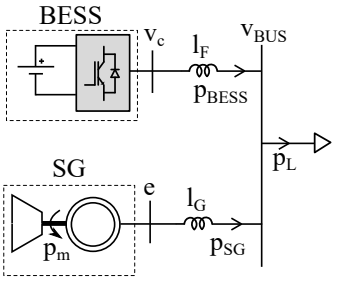

Figure 4.8: Microgrid case study for inertia emulation simulations.

The derivative gain is related to the emulated inertia constant H_V of the equivalent SG system as $K_{D,VI} = 2H_V$ [108]. Here it is selected to provide same inertia constant H_V as the Grid-Supporting VSM implementation.

The dead-band should comprise the variations of frequency that are considered acceptable in normal operation. Based on [104] they are selected as $\pm 0.2Hz$.

4.3 Application in an isolated Microgrid case study

This section is dedicated to estimate the effect of converter synchronising method on the emulated inertial response from BESSs in an isolated MG application. This effect is studied based on the implementations presented in Section 4.2.

Time-domain simulations on a test system are used to obtain numerical results and test the influence of the different control systems in the dynamics of frequency response of an isolated MG. Specifically, the focus of the assessment presented in this section is in the first moments following an active power variation or "inertial response", as defined in [1].

4.3.1 Simulation case study

For demonstration purposes, the isolated Microgrid of Fig. 4.8 is used as test system. The MG consist of one micro-source, one BESS and a local load.

The MG of Fig. 8 has been implemented in a dynamic simulation using the MATLB/Simulink Sim-

PowerSystem toolbox, in order to assess the system frequency response following a power imbalance. Due to the fast dynamics involved, dynamic simulations are required to analyze the time-domain behavior during the very short period of time involved in inertial response [1].

The main parameters of the MG are summarized in Table 4.4. Values in per unit (pu) are referred to the MG nominal power and voltage.

Table 4.4: Inertia Emulation case study: Microgrid parameters.

Label	Value	Units	Description
S_N	500	kW	Microgrid nominal power.
U_N	400	V	Microgrid nominal rms line voltage.
$p_{L,0}$	0.2	pu	Initial active power demand from the load.
$p_{SG,0}$	0.2	pu	Initial active power generation from the SG.
$p_{BESS,0}$	0	pu	Initial active power generation from the BESS.
f_N	50	Hz	Microgrid nominal frequency.
t_p	10	ms	Sample time of the power circuit simulation.
l_G	0.1	pu	Equivalent inductance of the connection between the SG and the load.
l_F	0.2	pu	Equivalent inductance of the connection between the BESS and the load.

The SG has been implemented using the *Simplified Synchronous Machine pu Units* model of the *powerlib* library, which models both the electrical and mechanical characteristics of a simple synchronous machine. In this model , the electrical circuit consists solely of a voltage source behind a synchronous reactance and resistance.

A hydraulic turbine and governor model is used to control the mechanical power (p_m) injection to the SG. This model includes a PI governor system, and a servomotor as defined in [109]. The governor regulates the SG rotational speed to 1.0 pu. It is configured to perform a droop function between the valve opening and the speed reference. The SG voltage is fixed at 1.0 pu.

The parameters relative to the SG, turbine and governor are summarized in Table 4.5. The SG is rated to the MG nominal power in order to be able to support the load on its own. Based on this rating, the parameters have been selected based on the procedure presented in [110]. A small passive load rated at 0.05 pu is connected in parallel with the SG, to avoid its direct connection with the inductance l_G, as recommended by the *powerlib* documentation.

The MG load is modelled as a constant impedance. Variations in load demand are performed by connecting additional impedances in parallel though a three-phase circuit breaker.

The BESS is modelled as a controllable AC voltage source dependent on the control systems presented in Section 4.2.

Table 4.5: Inertia Emulation case study: Synchronous Generator (SG) parameters.

Label	Value	Units	Description
$S_{SG,N}$	500	kW	SG nominal power.
$U_{SG,N}$	400	V	SG nominal rms line voltage.
H_{SG}	3.7	s	SG inertia constant.
$K_{D,SG}$	0.1	pu	SG damping factor.
p	20	-	SG Pole pairs.
r_{SG}	0.02	pu	SG stator total resistance.
l_{SG}	0.3	pu	SG stator total inductance.
K_{SM}	3	pu	Servo-motor gain.
T_{SM}	0.07	s	Servo-motor time constant.
g_{min}	0.16	pu	Minimum gate opening.
g_{max}	0.96	pu	Maximum gate opening.
vg_{min}	-0.1	pu/s	Minimum gate opening speed.
vg_{max}	0.1	pu/s	Maximum gate opening speed.
$K_{Droop,G}$	0.05	pu	Governor permanent droop gain.
$K_{P,G}$	1.163	pu	Governor PID proportional gain.
$K_{I,G}$	0.105	pu	Governor PID integral gain.
ξ_{HT}	0.1	pu	Hydraulic turbine damping factor.
T_{HT}	1	s	Hydraulic turbine time constant.

4.3.2 VSM control systems comparison

Based on this case study, the frequency dynamics under the different control systems are compared. Specifically, the results show the behavior of the different systems regarding frequency dynamics when a sudden 0.1 pu active load variation occurs. All parameters are the same as in the base case given in Section 4.2, unless otherwise noted.

The variation of the SG speed, which serves as a measurement of the grid frequency, is presented in Fig. 4.9. It can be seen that, with the proposed solutions, the BESS can help the system to restore its frequency. In this time scale, the effect is similar for the Droop, VI and VSM implementations. On the other hand, the VOC effect is similar to the case where there is no support form the BESS.

The active power delivered by the BESS in each case is presented in Fig. 4.10. It can be seen that the behavior differs in the first instants following the load variation. The initial active power response is similar between the VOC, Droop and VI systems. With the VOC, there is an initial active power that

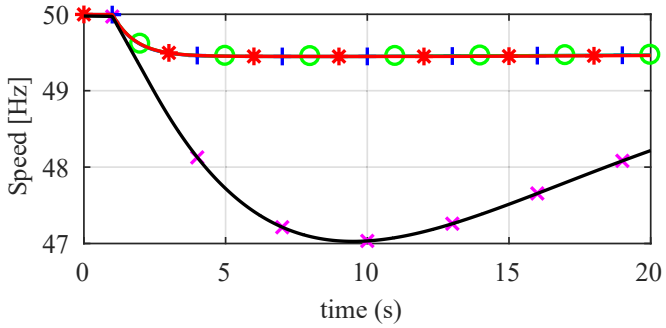

Figure 4.9: Synchronous generator speed variation on load change for VOC (black, solid line), VSM (red, * marked), VI (green, circle marked) and Droop (blue, + marked) control systems and no BESS connection (magenta, x marked).

drops very fast while for the Droop and VI systems, the active power is maintained due to the external active power regulation loops.

For the VSM, the active power is greater in the first moments but decays to the point where it is even lower than the initial active power generation of the BESS.

These initial differences have a direct effect on the rate of change of frequency (RoCoF) as seen in Fig. 4.11. This RoCoF is calculated as the rate of change of the SG rotational speed for the simulation time step t_p or

$$RoCoF_{tp}(t) = \frac{\omega_{t+1} - \omega_t}{t_p} \tag{4.10}$$

A numerical comparison between the frequency and power response of the different systems is presented in Table 4.6. Since RoCoF is usually measured on different time windows depending on the application, the RoCoF on a time window of 500ms ($RoCoF_{500ms}$) is also considered besides $RoCoF_{tp}$.

Table 4.6: Inertia Emulation case study: Comparison of control systems performance indicators.

Indicator	VOC	Droop	VI	VSM
f_{NADIR} [Hz]	47.028	49.448	49.448	49.448
$RoCoF_{tp}$ [mHz/s]	682.96	609.10	613.35	700.89
$RoCoF_{500ms}$ [mHz/s]	666.84	502.31	494.23	495.74
p_{MAX} [pu]	0.04	0.10	0.10	0.10
E [pu·s]	0.00	1.79	1.79	1.81

Under the VSM control system, the initial $RoCoF_{tp}$ is lower, as seen in Fig. 4.11. However the maximum $RoCoF_{tp}$ is higher due the transitorial oscillation of the power defined by the emulated swing

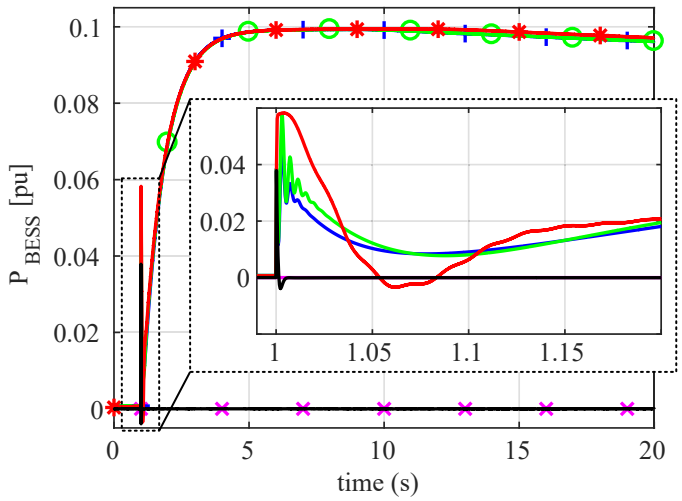

Figure 4.10: BESS active power variation on load change for VOC (black, solid line), VSM (red, * marked), VI (green, circle marked) and Droop (blue, + marked) control systems and no BESS connection (magenta, x marked).

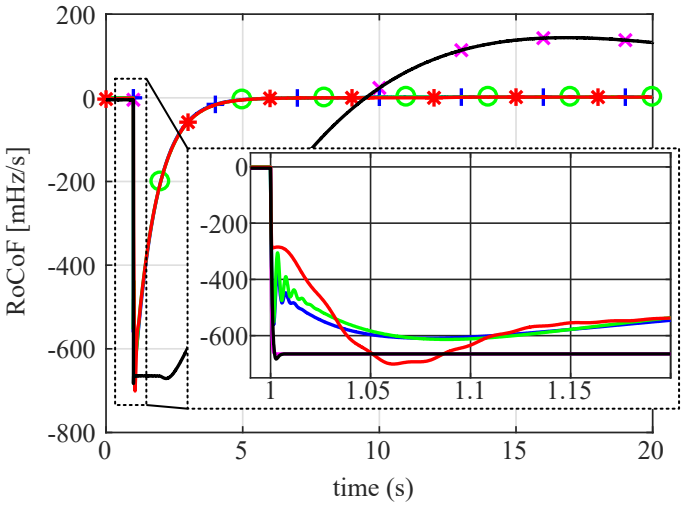

Figure 4.11: $RoCoF_{tp}$ variation on load change for VOC (black, solid line), VSM (red, * marked), VI (green, circle marked) and Droop (blue, + marked) control systems and no BESS connection (magenta, x marked).

equation. The response of the VSM system is also slower, so the initial power is maintained for a longer period of time leading to the exchange of an extra 2% of energy.

On the other hand, when $RoCoF_{500ms}$ is considered, the difference between systems is reduced. As expected from the speed variation represented in Fig. 4.9, the minimum frequency, or f_{NADIR} is the same for the different systems. Due to the steady state coupling between frequency and active power in both Grid-Tied and Grid-Supporting VSM systems, the maximum power is also the same.

To conclude, the influence of the steady-state relation between active power and frequency, K_P, that was analysed in Section 4.2, is also addressed. Its value will be reduced so that the BESS only compensates the 50% of the load variation. Note that this criteria can be used to define the proportional relation between active power and frequency in the Droop, VI and VSM control systems, as explained in Section 4.2.

The comparison of the effect on the SG speed in the full 20s time scale is depicted in Fig. 4.12.a. In order to compare this response with the response to previous value of K_P, the results of the Droop control system depicted in Fig. 4.9 are depicted here again as a reference.

It can be seen that the f_{NADIR} increases with respect to the original case with a higher K_P value. The frequency variation is similar for all the systems.

Again, in order to study the first instants following the load variation, the $RoCoF_{tp}$ for the case of low K_P is presented in Fig. 4.12.b. In this case, the difference on the system dynamics for the different inertia control implementations is more noticeable. The VSM damping is reduced significantly, due to the inherent relation between damping and steady-state gain explained in Section 4.2. On the other hand, the effect on the Droop and VI systems is significant for the steady-state value but not in the first moments, which are still dominated by the internal VOC, and thus the system dynamics are not compromised.

4.3.3 Final discussions

The presented results show the effect of the VSC synchronizing system on the emulated inertial response of BESSs based on the discrete implementation of representative solutions of both Grid-Tied and Grid-Supporting VSM control systems.

A case study where a BESS is connected to an isolated MG is used to compare the different control systems. The parameters of each system have been selected specifically for this case-study in order to provide equivalent inertia support characteristics.

The implemented Droop, VI and VSM systems were all able to improve the MG frequency stability. The most important parameters in frequency stability, including minimum frequency (f_{NADIR}) and RoCoF, have been obtained for each solution. Considering a wide time frame, results show a similar

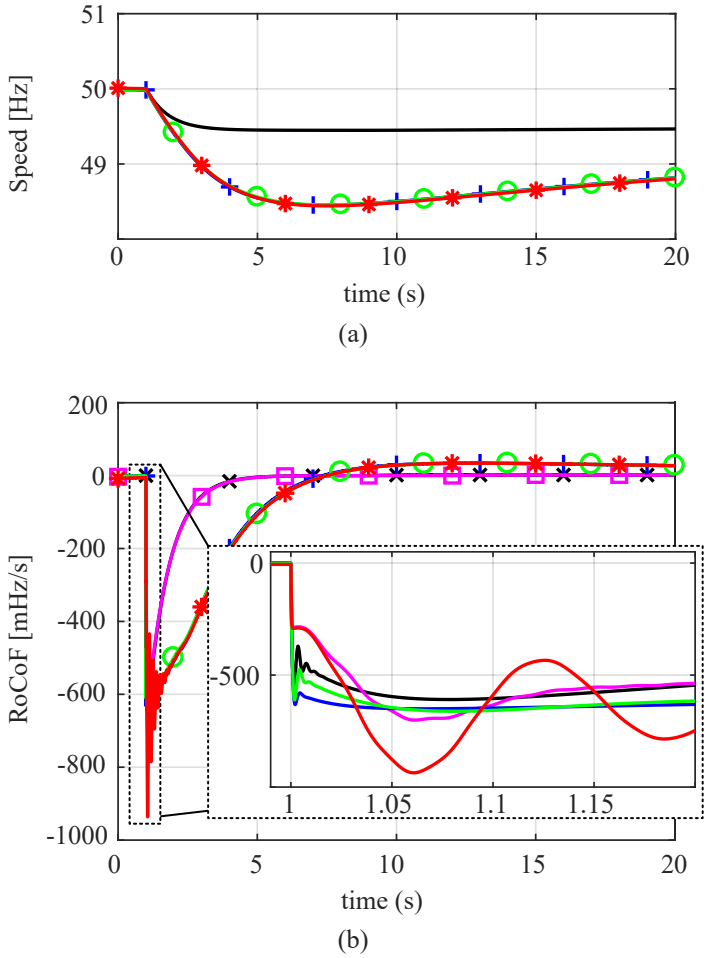

Figure 4.12: Synchronous generator (a) speed variation and (b) $RoCoF_{tp}$ on load change for VSM (red, * marked), VI (green, circle marked) and Droop (blue, + marked) control systems if the BESS assumes 100% of the load variation versus 50% with droop (black, x marked) and VSM (magenta, square marked) control systems.

behavior between the different systems, showing that all of them are suitable for the Inertia Emulation application.

Differences emerge when the analysis is performed for the first moments following a load disturbance. For the PLL-based solutions, the initial dynamics are dominated by the low-level current control. In fact, the system response is similar even if no specific emulated inertia control is considered, due to the internal control dynamics. The effect of the derivative component is small, as the results for the VI and Droop implementations are very close. On the other hand, for the VSM, the steady-state gain between active power frequency, which is imposed by the emulated inertia application, has an increased effect on the system dynamic performance compared to the VI and Droop control systems. Specifically, a reduction of the steady-state gain of the VSM reduces the damping of the system, which could lead to stability problems.

Chapter 5

Reactive Power Synchronization

Contents

5.1 Introduction 51

5.2 Proposed control 52

5.2.1 Reactive Power Synchronization concept 54

5.2.2 Description of the Reactive Power Synchronization control 57

5.2.3 Characteristic swing equation 58

5.3 Modeling and analysis 59

5.3.1 State-space model 60

5.3.2 Stability analysis 61

5.3.3 Damping of oscillations 62

5.4 Results and discussions 64

5.4.1 Simulations 64

5.4.2 Experimental results 65

5.1 Introduction

In previous chapters the problem of the synchronous operation of VSCs has been presented, and the solution of VSM has been studied in detail. In its core, VSM is based on a dependency between active power and frequency as synchronizing mechanism [68, 70].

In this chapter, a different approach is proposed where reactive power is used instead of active power for the synchronous operation of VSCs, thus decoupling the synchronization mechanism from the VSC

active power, while no PLL is required for frequency measurement. Active and reactive power are independently controlled using a dq-frame representation based on a current vector control scheme.

This proposal is based on a dynamic modeling of a grid-connected VSC from a new perspective that shows a dynamic coupling between the VSC reactive power and power angle, and therefore between reactive power and frequency. The relation between reactive power and frequency has been addressed in previous publications but with different purposes.

In [111], the steady-state cross-coupling between active and reactive power in an UPS (Uninterruptible Power Supply) systems is studied. Authors in [111] provide an analysis to show that this cross-coupling is related to the proposed UPS inverter control system. However, no insight is given on the dynamic coupling between reactive power and power angle.

In [112] the authors propose a frequency-reactive power control in order to share the reactive power among different converters in a MG. This control is based on the relation between the MG frequency and the reactive power demanded by the MG capacitance. In [113] the authors propose a modified droop control for load-sharing between UPS systems that uses a virtual resistive output impedance. Given a total resistive output impedance, the static relation between reactive power and frequency on resistive networks is used to propose a frequency-reactive power droop control that improves damping and reactive current sharing compared to previous solutions. Therefore, no insight is given on the coupling between reactive power and power angle on inductive networks. Moreover, in these publications, the application of the coupling between reactive power and frequency for grid synchronization is not addressed.

In section 5.2, the proposed RPS control system is presented and explained using a simplified model. A more detailed state-space model is presented in section 5.3. This analysis method has also been applied to droop [114, 115] and VSM [70] control systems. An eigenvalue analysis is performed to evaluate the system performance.

Experimental results, for a case study where a VSC is connected to a host grid, are presented in section 5.4 to validate the proposal. The set-up used for the real-time experiments is described in more detail in the appendix.

5.2 Proposed control

In this section, the proposed control system is presented. A small-signal model of a grid-connected VSC is used to demonstrate the relationship between reactive power and phase displacement. An analogy with the swing equation of traditional power systems, based on synchronous generators, is presented to illustrate the synchronizing system.

A general scheme of the proposed control system is depicted in Fig. 5.1. It is based on a dq-frame representation of the system voltages and currents. The reference for this dq-frame is obtained from

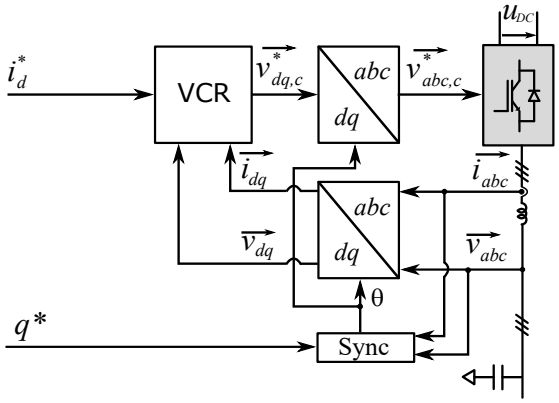

Figure 5.1: General scheme of the proposed control and system under study. VCR: Voltage and Current Regulation.

a novel synchronization mechanism based on the measurement of the exchanged reactive power. The inputs of this control system are the active current $i_d{}^*$ and the reactive power q^* references, both of which can be independently controlled.

Variables in lowercase are represented in pu with respect to the base values included in Table 5.1. These values were selected considering the set-up used for the real time experiments that will be presented in the appendix.

Table 5.1: Reactive Power Synchronization: Base values for per unit transformations

Label	Value	Units	Description
U_b	400	V	AC base voltage
$U_{dc,b}$	$2U_b$	V	DC base voltage
S_b	20	kVA	Base power
f_b	50	Hz	Base frequency
Ω_b	$2\pi f_b$	rad/s	Base frequency

The internal Voltage and Current Regulation (VCR) system of Fig. 5.1 is based on the current vector control. A more detailed scheme is depicted in Fig. 5.2. As in current vector control, it is possible to decouple active and reactive current control as well as limit the current injected by the VSC.

A high-pass filter (HPF) is included in the voltage controller of Fig. 5.2 as an oscillation damping mechanism. This will be further discussed in section 5.3.3.

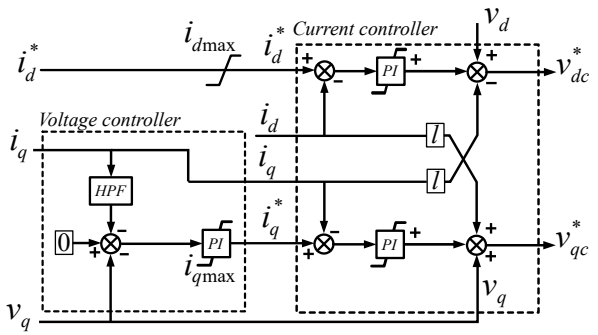

Figure 5.2: Internal Voltage and Current Regulation (VCR) system for the Reactive Power Synchronization (RPS) control. HPF: High-pass filter.

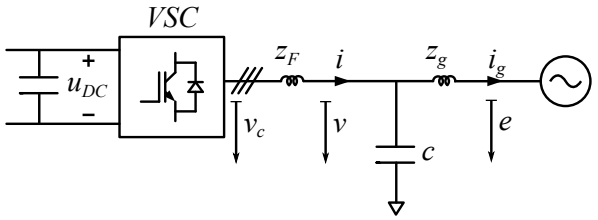

Figure 5.3: Case study scheme. VSC: Voltage Sourced Converter.

5.2.1 Reactive Power Synchronization concept

Traditionally, as an approximation to synchronous generators, a relation has been established between a VSC active power generation and its frequency [75], emulating the behavior of synchronous generators synchronizing torque. However, in VSCs there is no relation between the phase of electrical variables and a mechanical system requiring a force to restore position.

Another argument for using active power for the synchronous operation of VSCs is the relationship between transmitted active power and power angle in power systems. Most studies use this relationship for synchronizing based on a steady-sate model of the grid short circuit impedance. On the other hand, in this section a detailed dynamic model of a VSC connected to a host grid is used to demonstrate the relationship between phase displacement and reactive power that it is the basis of the proposed synchronizing method.

The system under study is depicted in Fig. 5.3. It represents a VSC connected to grid through an LC filter and an interfacing impedance z_g.

The power angle δ can be defined from the dq-frame angular frequency ω and the grid frequency ω_g as

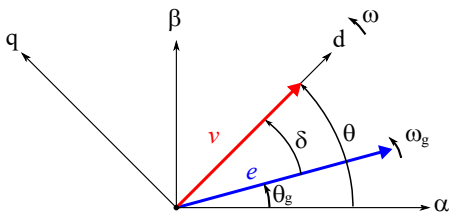

Figure 5.4: Vector diagram of the system under study. δ: power angle. e: grid voltage vector. v: converter voltage vector. ω: dq frame angular frequency. ω_g: grid frequency.

$$\frac{1}{\Omega_b}\frac{d\delta}{dt} = \omega - \omega_g \tag{5.1}$$

A graphical representation of these variables together with the grid voltage vector e and converter voltage vector v is depicted in Fig. 5.4.

The internal VCR system of Fig. 5.2 is responsible of tracking the active current reference ${i_d}^*$ and also of keeping the internal voltage vector aligned with the reference dq axis, which is achieved by a regulation of the quadrature component of the capacitor voltage v_q [60]. The dynamics of this internal VCR loops are considered faster than the synchronizing system loop so it can be assumed that

$$i_d = {i_d}^* \tag{5.2}$$

$$v_q = 0 \tag{5.3}$$

This assumption will be validated in section 5.3. The relationship between the VSC and grid voltages is given by

$$\frac{l_g}{\Omega_b}\frac{d\vec{i_g}}{dt} = \vec{v} - \vec{e} - r_g\vec{i_g} - j\omega l_g\vec{i_g}, \tag{5.4}$$

where i_g is the current flowing through the grid impedance $z_g = r_g + j\omega l_g$ as seen in Fig. 5.1. Given (5.3), active and reactive power delivered by the VSC to the grid can be defined as

$$p = i_{dg}v_d \tag{5.5}$$

$$q = -i_{qg}v_d \tag{5.6}$$

From (5.6), it can be seen that reactive power q is related to i_{qg}. From (5.4), it is obtained that

$$\frac{l_g}{\Omega_b}\frac{di_{qg}}{dt} = -e_q - r_g i_{qg} - \omega l_g i_{dg} \tag{5.7}$$

From Fig. 5.4, it can be seen that e_q is related to the phase displacement δ as

$$e_q = -|e|\sin\delta \tag{5.8}$$

This introduces a non-linear relationship in (5.7) so a small-signal model will be considered. A base case operating point for linearization is defined in Table 5.2.

Table 5.2: Reactive Power Synchronization: Base case operating point in pu

Label	Value	Description
e_0	1	Grid voltage vector amplitude
w_{g0}	1	Grid voltage frequency
i_{d0}	1	VSC active current generation
q_0	0	VSC reactive power generation

Linearizing (5.7) around this operating point leads to

$$\frac{l_g}{\Omega_b}\frac{d\Delta i_{qg}}{dt} = e_0 \cos\delta_0 \Delta\delta - r_g \Delta i_{qg} - \omega_0 l_g \Delta i_{dg}, \tag{5.9}$$

where the product $i_{qg0}\Delta\omega$, which depends on the synchronizing mechanism, has been neglected. Equation (5.9) shows that there is a relationship between i_{qg}, or reactive power, and the power angle δ.

Note that if only the steady-state is considered, neglecting $\frac{d\Delta i_{qg}}{dt}$ in (5.9), and assuming a small filter resistance r_g and initial angle δ_0, it will follow that only Δi_{dg}, or active power, is related to δ, as is commonly stated. Therefore, from (5.9) it is concluded that, although there is only a small steady-state relationship between reactive power and phase displacement, there is a stronger dynamic relationship.

To clarify the explanation, the filter capacitor is not considered here. Therefore, based on (5.2) it is deduced that $\Delta i_{dg} = \Delta {i_d}^*$. From (5.9) it can be written that

$$\Delta i_{qg} = \frac{\omega_0 l_g}{\frac{l_g}{\Omega_b}s + r_g}\left(\frac{e_0 \cos\delta_0}{\omega_0 l_g}\Delta\delta - \Delta {i_d}^*\right) \tag{5.10}$$

For reactive power, based on (5.6) and for the operating point defined in Table 5.2, it is obtained that

$$\Delta q = \underbrace{\frac{\omega_0 l_g}{\frac{l_g}{\Omega_b}s + r_g}}_{G_{qp}}\left(\Delta p^* - \underbrace{\frac{v_{d0} e_0 \cos\delta_0}{\omega_0 l_g}}_{G_{p\delta}}\Delta\delta\right), \tag{5.11}$$

where $\Delta p^* = v_{d0}\Delta {i_d}^*$. Note that $G_{p\delta}$ is in fact the commonly considered coupling between active power and power angle, while G_{qp} represents the coupling between active and reactive power through the dynamics of the grid inductance.

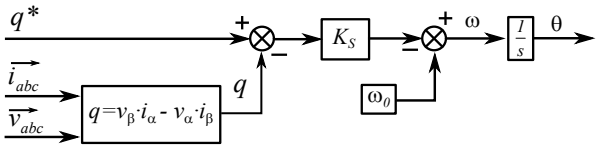

Figure 5.5: Reactive power synchronization loop.

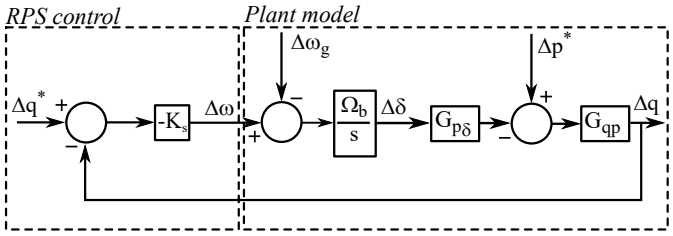

Figure 5.6: Block diagram of the complete system. RPS: Reactive Power Synchronization.

5.2.2 Description of the Reactive Power Synchronization control

Equation (5.11) demonstrates that phase displacement variations are related to reactive power and consequently that reactive power can be used as a synchronizing mechanism.

Considering this coupling, the proposed control system is depicted in Fig. 5.5. The internal frequency of the control system ω is defined by the control law

$$\omega = \omega_0 - (q^* - q) * K_s, \tag{5.12}$$

where ω_0 and K_s are the control parameters and q^* is the VSC reactive power set-point.

With this system, the VSC will deliver a reactive power q^* if the frequency is ω_0, but otherwise reactive power will vary proportionally to the frequency deviation. Thus, synchronization can be independent of active power generation.

The small-signal block diagram, including the proposed control system and the plant model, is depicted in Fig. 5.6. The resulting open loop transfer function can be obtained combining equations (5.1), (5.11) and (5.12) as

$$G_{OL} = \frac{K_s \Omega_b v_{d0} e_0 \cos\delta_0}{s(\frac{l_g}{\Omega_b} s + r_g)} \tag{5.13}$$

A bode diagram of this transfer function is presented in Fig. 5.7, for the base case parameters given in Table 5.3.

The open-loop transfer function already comprises a good reference-tracking behavior, due to the intrinsic integrator, and thus a proportional controller is enough to ensure synchronous operation. If the

Table 5.3: Reactive Power Synchronization: Base case system parameters in pu

Label	Value	Description
l_f	0.2	Filter inductance
r_f	0.003	Filter resistance
c	0.05	AC capacitance
l_g	0.1	Grid inductance
r_g	0.001	Grid resistance
c_{DC}	0.35	DC capacitance
k_{pc}	2	AC current proportional gain
k_{ic}	0.637	AC current integral gain
k_{pv}	2.5	AC voltage proportional gain
k_{iv}	0.127	AC voltage integral gain
k_s	0.1	Synchronization loop gain

system is stable, $\Delta\omega = \Delta\omega_g$ and the VSC will be operating in synchronism with the grid. The cross-over frequency is located at

$$\Omega_{co} = \Omega_b \sqrt{\frac{K_s}{l_g} v_{d0} e_0 \cos\delta_0} \tag{5.14}$$

discarding the effect of r_g. For the given parameters $\Omega_{co} \approx \quad \Omega_b$.

Both active power and grid frequency variations act as perturbations of the proposed control system. Thus, the angle varies to reject active power variations, allowing the system to remain in synchronism regardless of the required power angle. In contrast, when using active power for synchronization, as in PSC, the active power reference must be varied in order to change the power angle, which is usually performed by an outer DC-voltage control loop [15].

Also, it is worth noting that there is no need to measure the grid frequency, which improves the robustness of the method over classical PLLs.

5.2.3 Characteristic swing equation

In this section the model of the RPS control system is analyzed from the point of view of the characteristic swing equation, in an analogy to the operation of synchronous generators presented in Section 5.2.

From the block diagram of Fig. 5.6, considering only the effect of active power variations, i.e. con-

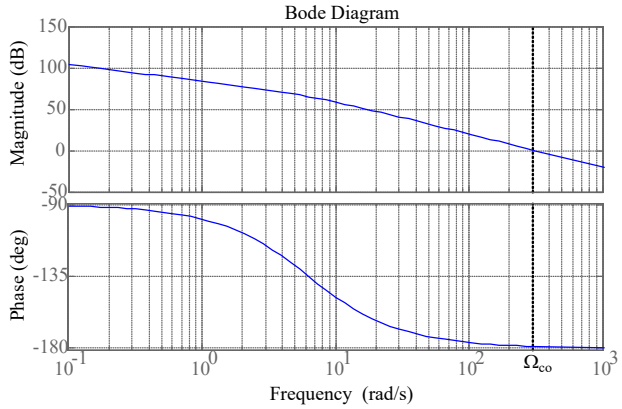

Figure 5.7: Bode diagram of the open-loop transfer function for the reactive power synchronization model. Ω_{co}: Cross-over frequency.

sidering $\Delta\omega_g = 0$ and $\Delta q^* = 0$, it can be written that

$$\Delta p^* = \frac{1}{G_{qp} K_s \frac{\Omega_b}{s}} \Delta\delta + G_{p\delta}\Delta\delta \tag{5.15}$$

If G_{qp} and $G_{p\delta}$ are defined as in (5.11) it follows that

$$\frac{1}{K_s {\Omega_b}^2} s^2\Delta\delta + \frac{r_g}{\omega_0 l_g K_s \Omega_b} s\Delta\delta + G_{p\delta}\Delta\delta = \Delta p^* \tag{5.16}$$

which is analogous to the synchronous machine swing equation

$$\frac{2H}{\Omega_b} s^2\Delta\delta + \frac{D}{\Omega_b} s\Delta\delta + K\Delta\delta = \Delta p_m \tag{5.17}$$

where H is the inertia constant, D the damping constant, K the synchronizing component and p_m the input mechanical power. For the proposed system

$$H = \frac{1}{K_s \Omega_b} \tag{5.18}$$

$$D = \frac{r_g}{\omega_0 l_g K_s} \tag{5.19}$$

$$K = \frac{v_{d0} e_0 \cos\delta_0}{\omega_0 l_g} \tag{5.20}$$

Note that the syncronizing torque is the same as in the SG model of section 3.3.

5.3 Modeling and analysis

In this section the system presented in Fig. 5.3, including the control system of Fig. 5.1, is modeled in the state space discarding the assumptions made in section 5.2.

In order to assess the dynamics and stability of the overall system, the eigenvalue and sensibility analysis of this model are also performed. Since the system is non-linear the operation point also affects the stability of the system. The base-case operating point values are given in Table 5.2.

5.3.1 State-space model

Using a transformation to a dq-frame rotating at ω, as depicted in Fig. 5.4, the VSC terminal voltage v_c and the capacitor bank voltage v are related by the equation

$$\vec{v} = \vec{v_c} - R\vec{i} - L\frac{d\vec{i}}{dt} - j\omega L\vec{i} \tag{5.21}$$

On the other hand, at the capacitor bank, the converter and grid currents are related by

$$\vec{i} - \vec{i_g} = C\frac{d\vec{v}}{dt} + j\omega C\vec{v} \tag{5.22}$$

These equations are used by the VCR of Fig. 5.2 to control the converter current. As seen in Fig. 5.2, the VCR calculates the reference for the PWM system ${v_c}^*$ as

$${v_{dc}}^* = k_{pc}(i_d^* - i_d) + k_{ic}x_{dc} - li_q \tag{5.23}$$

$${v_{qc}}^* = k_{pc}(i_q^* - i_q) + k_{ic}x_{qc} + li_d, \tag{5.24}$$

where k_{pc} and k_{ic} are the current controller proportional and integral gains, respectively, and the compensating cross terms have been added. x_{dc} and x_{qc} are the d-q current error states, given by

$$\frac{1}{\omega_0}\frac{dx_{dc}}{dt} = i_d^* - i_d \tag{5.25}$$

$$\frac{1}{\omega_0}\frac{dx_{qc}}{dt} = i_q^* - i_q \tag{5.26}$$

Similarly, the voltage controller input is the voltage error, while the output is the current reference, given by

$$i_q^* = k_{pv}(u_{qg}^* - u_{qg}) + k_{iv}x_{qv} - cu_{dg}, \tag{5.27}$$

where k_{pv} and k_{pv} are the voltage controller proportional and integral gains, respectively, and the compensating cross terms have been added. As in the current controller, x_{qv} is the q voltage error state, given by

$$\frac{1}{\omega_0}\frac{dx_{qv}}{dt} = u_{qg}^* - u_{qg} \tag{5.28}$$

The equations of the filter inductance, (5.21), and capacitance, (5.22), the VCR states, (5.25),(5.26) and (5.28), together with the power angle definition, (5.1), and the equation from the grid impedance, (5.4), form a dynamic non-linear system that can be represented in the state-space as

$$\frac{d\Delta x}{dt} = A\Delta x + B\Delta u, \tag{5.29}$$

where

$$x = [u_{gd}, u_{gq}, x_{vq}, i_d, i_q, x_{cd}, x_{cq}, i_{gd}, i_{gq}, \delta] \tag{5.30}$$

$$u = [{i_d}^*, q^*, w_g]. \tag{5.31}$$

5.3.2 Stability analysis

In this section, the influence of the system parameters on the loci of dominant eigenvalues is studied considering the base-case scenario given in Table 5.3.

For this base case, the eigenvalues are computed and presented in Table 5.4. Frequency and damping ratio are also given, as well as the dominant states according to their participation factors. A graphical representation is presented in Fig. 5.8.

It can be seen that the dominant eigenvalues are related to phase and voltage amplitude variations. This validates the assumption made in section 5.2.1 of considering that the VCR dynamics are significantly faster than the synchronizing system ones. All the eigenvalues have a negative real part and thus the system is stable.

Table 5.4: Reactive Power Synchronization: Base-case eigenvalue analysis.

λ_i	Eigenvalues [rad/s]	Frequency [Hz]	Damping ratio [p.u.]	Dominant states
$1-2$	$-490.6 \pm 10\,870.8$i	1730.1	0.045	u_{gq}, i_q
$3-4$	-6.1 ± 4433.0i	705.5	0.001	u_{gd}, i_{gd}
5	-1348.8	0	1	i_d
6	-459.1	0	1	x_{vq}, i_q, i_{gq}
$7-8$	-70.3 ± 208.4i	33.16	0.32	δ, i_{gq}
9	-10.5	0	1	x_{vq}, x_{cq}
10	-233.7	0	1	x_{cd}

A common concern in synchronization systems is their sensitivity to the grid "strenght" or Short Circuit Ratio (SCR). Fig. 5.9.(a) shows the effect on the system eigenvalues of a grid impedance variation from 0.1 pu (low SCR) to 0.02 pu (high SCR). It can be seen how the eigenvalues related to the phase displacement δ become more damped while the frequency of the eigenvalues related to the voltage

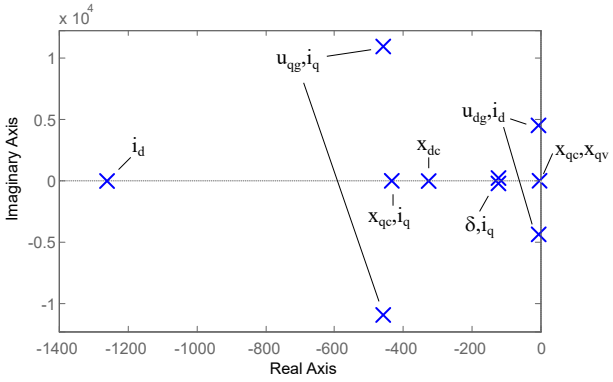

Figure 5.8: Base case eigenvalues and related states according to their participation factors.

amplitude increases. However, the system remains stable regardless of such a high variation of the grid impedance.

Another concern, specially in droop control systems, is the dependency with the grid impedance inductive or resistive behavior. This can be defined by the inductive to resistive ratio (X/R). In most electrical systems this ratio is very high and thus grid impedance can be considered purely inductive. However, this might not be the case in MGs, where more resistive networks are likely to appear [82].

A variation of X/R from 20 to 1 has been tested. Results are depicted in Fig. 5.9.(b). It can be seen how the system improves its stability for a more resistive impedance. This is due to the stronger coupling between frequency and reactive power that appears on resistive networks [65]. The resistive nature also helps to damp oscillations related to δ. However, as seen from the base case, the systems is also stable for highly inductive networks.

Besides, in order to illustrate the effect of the regulation parameter K_s, a variation from 0.1 to 1 is performed. As with other proportional control systems, this parameter must be chosen regarding both the steady-state relation between reactive power and frequency and the desired dynamic performance. From the results in Fig. 5.9.(c), it can be seen how the poles related to δ become faster and less damped, as expected from the characteristic swing equation (5.16). Thus, a compromise must be achieved between the control bandwidth and stability margin.

5.3.3 Damping of oscillations

The state-space model shows two prominent oscillations, one appearing close to Ω_b, as expected from (5.14), and another at around the filter resonance frequency. Since the grid resistance has been considered to be very low, these resonances are poorly damped.

The resonance related to the filter is common in VSC based systems. Its frequency is usually de-

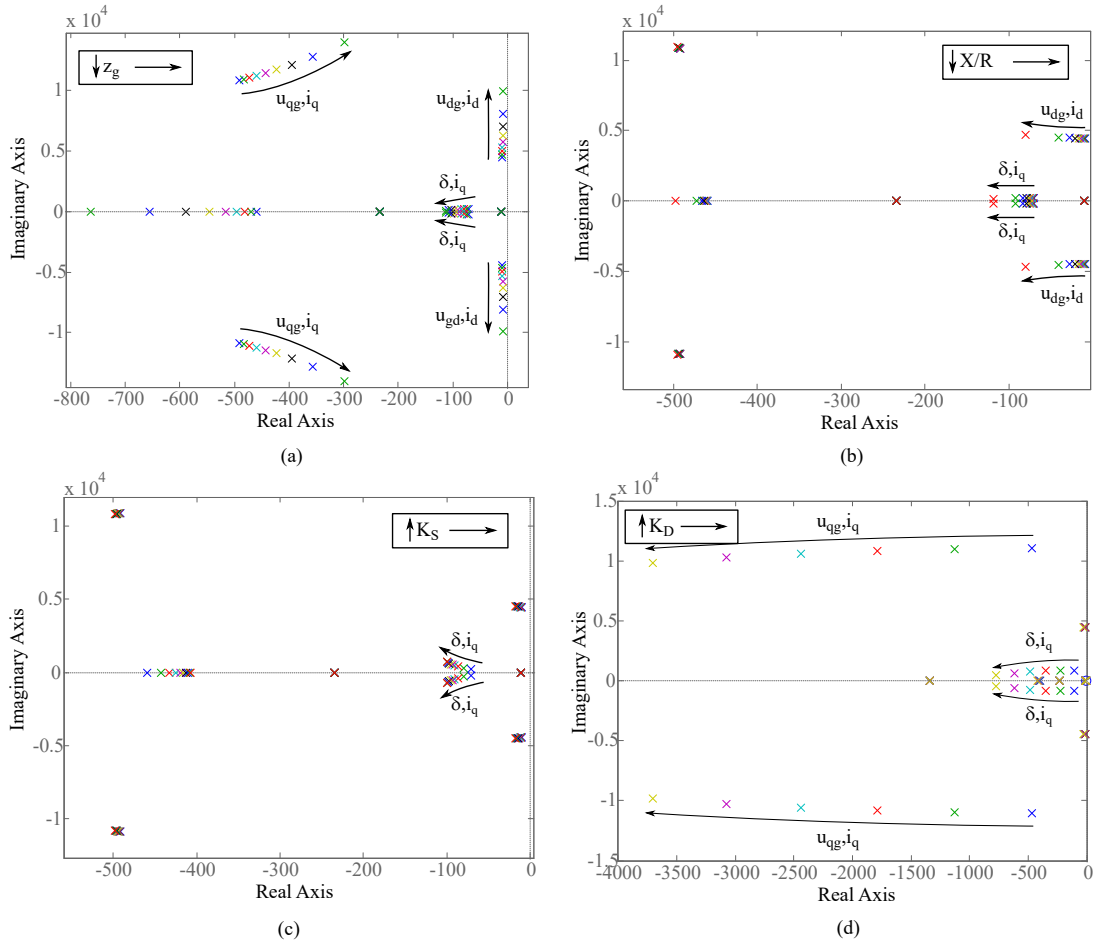

Figure 5.9: System response against variations on (a) the grid impedance z_e, (b) the grid inductive to resistive ratio X/R_e, (c) the synchronization loop gain K_s and (d) the damping gain K_D.

signed as a compromise between economic and technical parameters. Damping of these high-frequency oscillations through the control system, or active damping, is a developing topic in the literature. A comparison between some of the most common methods was recently presented in [116]. For this work, these oscillations have been passively damped with a resistor connected in series with the filter capacitor.

The low-frequency resonance appears as a direct consequence of the link established between reactive power and phase displacement, as can be deduced from (5.14). A similar resonance appears in [15], where the PSC was proposed, for the relation between active power and phase displacement.

In order to damp these oscillations, the authors of [15] introduce variations in the generated voltage amplitude related to the current oscillations by means of a high-pass filter. This structure for damping oscillations is similar to the traditional "washout" filter used in the excitation system of synchronous generators [1].

Here, these oscillations are compensated by introducing an opposite-sign variation in the internal phase, which is related to v_q. Since these variations will appear in i_q, measurements of i_q are used to implement the damping through v_q reference variations. A high-pass filter (HPF) is used to avoid steady-state variations. This structure is depicted in Fig. 5.2. The gain introduced by this HPF is

$$G_{HPF} = K_D \frac{T_w s}{1 + T_w s} \tag{5.32}$$

An illustrating approach to show the effect of this system, following the simplified model of section 5.2, is studying the modification of the swing equation (5.16), which becomes

$$\frac{1}{K_s {\Omega_b}^2} s^2 \Delta\delta + \frac{r_g + G_{HPF}}{\omega_0 l_g K_s \Omega_b} s\Delta\delta + G_{p\delta}\Delta\delta = \Delta p^* \tag{5.33}$$

It can be seen how the equivalent D parameter is modified by the damping mechanism.

The effect of this system on the complete model, varying K_D from 0 to 0.5 pu, is shown in Fig. 5.9.(d). It can be seen how the damping of the eigenvalues related to the synchronizing system increases.

5.4 Results and discussions

In this section, the simulation and experimental results are presented to demonstrate the performance of the proposed control system as well as to validate the developed dynamic models.

5.4.1 Simulations

Simulations were developed using a detailed switching model implemented in MATLAB/Simulink in co-simulation with PSIM. Simulink was used to implement the control system whereas PSIM was used for simulating the power system components.

The simulated system response is tested against frequency and active and reactive power reference step variations. First, the synchronizing system is tested by performing a frequency step. Then, it is demonstrated how active and reactive power can be independently controlled. To conclude, the system inherent capability to limit the VSC current under fault conditions is tested.

Results are depicted in Fig. 5.10. At t=0.1s the grid frequency f_g suffers a step from 50Hz to 60Hz. It can be seen how the internal frequency of the control f, which is the representation in Hz of the angular frequency ω calculated through the RPS loop of Fig. 5.5, follows this change. This demonstrates that the proposed control system can track this new frequency even for such a high and sharp variation. To track this new frequency, the control system varies the reactive power reference proportionally by a K_s factor. The active power reference remains unchanged, showing that it was not needed for the synchronization

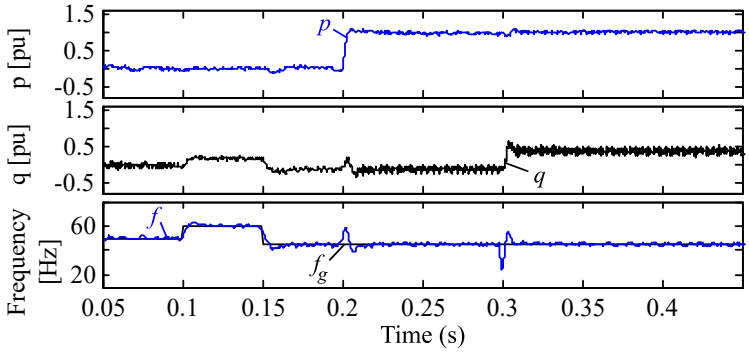

Figure 5.10: Simulation results against frequency, active power reference and reactive power reference variations.

process. At t=0.15s the grid frequency suffers a falling step from 60Hz to 45Hz to show that the previous variation is not a particular simulation case.

An active power reference step, from 0 to 1 pu, is performed at t=0.2s. Active power rises accordingly, showing that the control system is able to track this reference. The frequency changes during the transient, as expected from the block diagram of Fig. 5.6 where active power is a disturbance in the control loop. The control system is able to compensate this perturbation so the frequency f is restored to f_g and the system remains in synchronism with the grid. Note that this transient frequency variation is needed for achieving the new power angle required by the power variation

Finally, a reactive power reference step, from 0 to 0.5 pu, is performed at t=0.3s. As with active power, the control system is able to track this reference while maintaining synchronism with the grid. The final reactive power is not exactly 0.5 pu because of the open-loop configuration of the reactive power channel.

The proposed synchronization system presents the advantage of being built upon the well-known current vector control. This provides the capability of limiting the VSC current under faults without any additional systems. This capability has been tested in the proposed system as shown in Fig. 5.11. A fault is produced at $t = 0.5s$. The converter active current is limited, so the active power is reduced. When the fault is cleared at $t = 0.7s$, the control is able to return to pre-fault levels.

5.4.2 Experimental results

In this section, the simulation results are contrasted with a real-time implementation. The experimental set-up used to obtain the real-time results emulates the simulated system as described in Fig. 5.3. It will be described in more detail in the Appendix A.1.

Results are shown Fig. 5.12. It was not possible to test the frequency variation presented in the

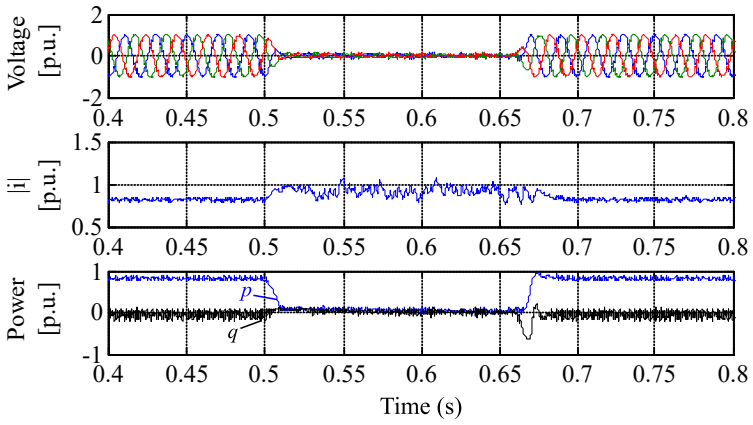

Figure 5.11: Simulated system response against a grid fault.

simulation since the system was connected to a stiff grid. Therefore, only the response to active and reactive power variations is included. The grid frequency f_g could not be directly measured so a constant value of 50 Hz is presented as a reference.

An active power reference step is applied at t=0.2s as shown in Fig. 5.12.(a). As in the simulation case, the control system is able to track this reference while maintaining a constant frequency. The transient frequency variation is significantly smaller than in the simulated case, probably due to the damping provided by the electrical power losses.

The response to the reactive power reference change is shown in Fig. 5.12.(b). It can be seen that the behavior is similar to the one expected from the simulation. The transient frequency variation is again smaller than in the simulated case. However, note that it is significantly higher than in the active power variation scenario of Fig. 5.12.(a), which is in accordance with the dynamic coupling studied in section 5.2. Regarding the synchronizing capabilities, it can be seen that the system behavior is similar to the one observed in simulation, validating the presented models.

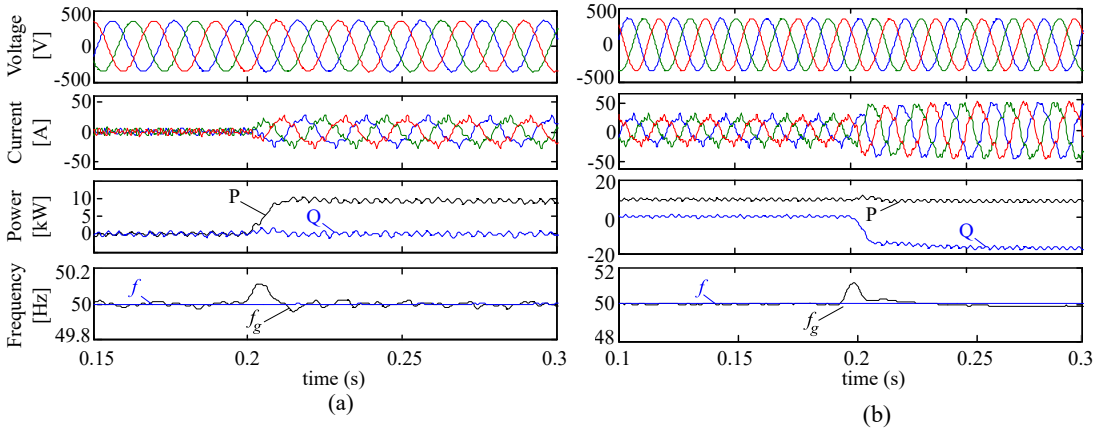

Figure 5.12: Experimental results for (a) an active power reference step variation and (b) a reactive power reference step variation.

Chapter 6

Black start of Full Converter Wind Energy Conversion Systems

Contents

6.1 Introduction 69

6.2 Isolated operation of FC WECSs 71

6.2.1 System model 72

6.2.2 Proposed control 76

6.2.3 Stability analysis 81

6.2.4 Results and discussions 83

6.3 Control system for parallel operation 87

6.3.1 LSC control for parallel operation 88

6.3.2 Results and discussions 89

6.1 Introduction

In this chapter, the RPS method presented in Chapter 5 is applied for the support of restoration following a black-out or Power System Restoration (PSR) through WECSs.

For any power system, PSR is a complex process. Even for conventional power systems, the number of generation units for the restoration phase can be limited due to the high capacity requirements and the time constraints for the start-up and connection to the grid [117].

Due to these requirements, PSR has been traditionally carried out by large SGs at the transmission level. However, transmission system operators are recognizing the need for DERs to support PSR as

penetration of renewable energy increases [14].

A possible solution for DERs to contribute to PSR are islanded MGs that are able to perform a black-start. One of the problems associated to PSR is that a few generators have to energize a large portion of the grid before others can follow. If MGs are able to perform a black-start, they could energize their share of the network, thus reducing the requirements for traditional PSR generators [14].

If MGs have to account for a high penetration of renewable energies, the capacity of WECSs to support the PSR is of high importance.

However, there has not been much research on supporting PSR through WECSs. Most studies focus on the planned coordination between WECSs and additional elements such as gas turbines [118]. However, for WECSs to effectively support PSR, they cannot rely on a wider power system and thus must be able to operate as islanded systems.

As noted in section 2.3, a key concern for islanded WECSs is how to balance generation and load. To face this problem several authors have suggested the integration of more than a source in the so-called hybrid systems [61–63, 119, 120], where energy storage systems (ESSs) and diesel generators play a significant role in power balancing. In [61] a WECS is connected in parallel to a battery ESS with little insight in the voltage and frequency control. The WECS is commanded to follow a Maximum Power Point Tracking (MPPT) strategy and the ESS closes the power balance. In [63] the diesel generator is replaced by a photovoltaic (PV) system. A small battery ESS and a dump load are used to balance power. In [119] the isolated system is fed through a fixed speed Wind Turbine (WT) and a battery ESS.

In order for WECSs to operate isolated from the grid and without additional elements, they must be able to control the system voltage and frequency. Moreover, this control should not be limited to a single unit but shared among different WECSs.

One of the first studies concerning the supply of an isolated load from a WECS was carried out by [59] employing a doubly-fed induction generator (DFIG). Further studies on this topic, when the generator is connected to an unbalanced system, have been published by the same research group [121, 122]. A different approach using a direct flux control is proposed in [123].

However, there has been little research about full converter (FC)-based WECSs, where the role of the power converters changes significantly compared to DFIGs [124]. Moreover, since MG applications usually require low to medium power WECSs, FC solutions using Permanent Magnet Synchronous Generators (PMSGs) and Squirrel-Cage Induction Generators (SCIGs) might be more suitable than DFIGs [125, 126].

As noted earlier, a critical problem during black-start is that the WECSs active power generation must be balanced with the local demand. Moreover, if there are multiple WECSs, this demand should be shared between them. As opposed to VSM solutions, in RPS active power sharing is not imposed by the

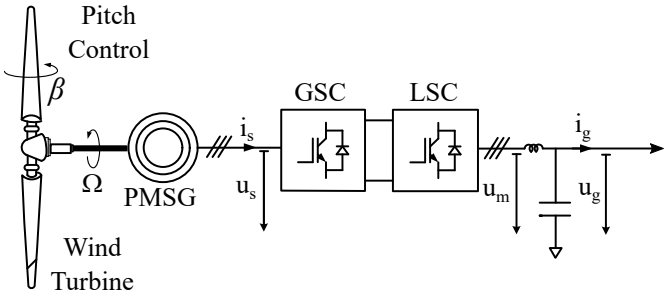

Figure 6.1: Scheme of an isolated Full-Converter Wind Energy Conversion System. PMSG: permanent magnet synchronous generator; LSC: line side converter; GSC: generator side converter.

synchronization system. It will be seen how this allows WECSs to provide a black-start solution where the available load is shared according to each WECS wind availability.

In this chapter, a solution for the black-start of a wind farm is proposed. It is based on the RPS method presented in chapter 5. A case study system with 2 WECSs connected in parallel is used to demonstrate that WECSs can be controlled to perform a black start without relying on any additional systems. In section 6.2, the basis for controlling active power on isolated WECSs are presented based on the operation of a single WECS. This is used in section 6.3 to introduce the proposed control system operation. Simulation and experimental results are presented to validate the proposals.

6.2 Isolated operation of FC WECSs

As noted in the introduction, control systems for islanded FC WECSs , as the one shown in Fig. 6.1, have not been widely studied in the literature. Control solutions are proposed in [127–131]. In [127], the generator side converter (GSC) is controlled using a MPPT strategy, while the line side converter (LSC) controls the DC voltage as in traditional grid-connected applications. Power balance is achieved by a dump resistor connected at the DC bus. In [128] and [129] the voltage control is performed in an open loop and there is no control of the inverter current. Moreover, in these studies the effect of wind variation on the load balancing is not analysed. A similar study is presented in [130] but employing a current-sourced converter. The scheme in [130] is analyzed in [131] for sudden unbalanced operating conditions when feeding three isolated single phase loads.

In this section, a different approach is presented where the voltage and frequency are controlled by the WECS without relying on additional systems. The roles of the converters in the WECS are inverted from usual FC applications so the LSC controls AC voltage and frequency while the GSC is responsible for maintaining constant voltage in the DC link. Also, instead of using a dummy load or an additional power source, as in hybrid systems, power balance is achieved by the speed regulation of the WT through

pitch angle control.

A Voltage and Frequency Controller (VFC) is presented, based on the orientation of the output voltage vector along a synchronous axis rotating at the reference frequency. The ability of the VFC to maintain the stator voltage oriented toward the synchronous reference axis means that constant voltage and frequency are obtained, which in turn means that the demanded active and reactive powers are supplied by the LSC. In order to implement such principles, a new approach is proposed where the variations in the AC filter capacitor voltage will provide the information needed for balancing active and reactive power in the isolated system. The LSC currents are also controlled to avoid large excursions and protect the converter against overcurrents [3].

Simulation results, using both a state-space model and a detailed switching model, are presented to demonstrate the capabilities and contributions of the proposed control scheme. The proposal is validated by experimental results on a real-time test bench.

6.2.1 System model

To analyze the system behavior, mathematical models of the different components of the system are presented. A scheme of the system under study, which includes the WT, the PMSG, the GSC and LSC stations and the isolated load, is depicted in Fig. 6.1 .

The system model is divided in three subsections. First, the WT model presents the relationship between the blade pitch angle β and the WT power and rotational speed. Then, an electrical model of the PMSG is defined as the basis for the GSC control, responsible for maintaining constant DC link voltage despite variations in the generator voltage and frequency. Finally, the LSC operation in the isolated system is modeled in the state space. This model will be used later to derive the VFC.

Wind Turbine Model

The mechanical power of the WT is given by the aerodynamic equation

$$P_m = \frac{1}{2}\rho A v^3 C_p(\lambda,\beta), \tag{6.1}$$

where ρ is the air density, A is the WT rotor area, v is the wind velocity and C_p is the power coefficient of the WT.

C_p is a function of the tip speed ratio, λ, and the blade pitch angle, β. A generic equation was used to model the function $C_p(\lambda,\beta)$. This equation is based on the turbine characteristics of [132]. The relation between the power coefficient C_p and the tip speed ratio λ for various pitch angles can be seen in Figure 6.2.a. This figure shows how β affects C_p and therefore the WT power, meaning that β can be used for controlling the WT power. In most of the literature related to WECSs, this relation is employed

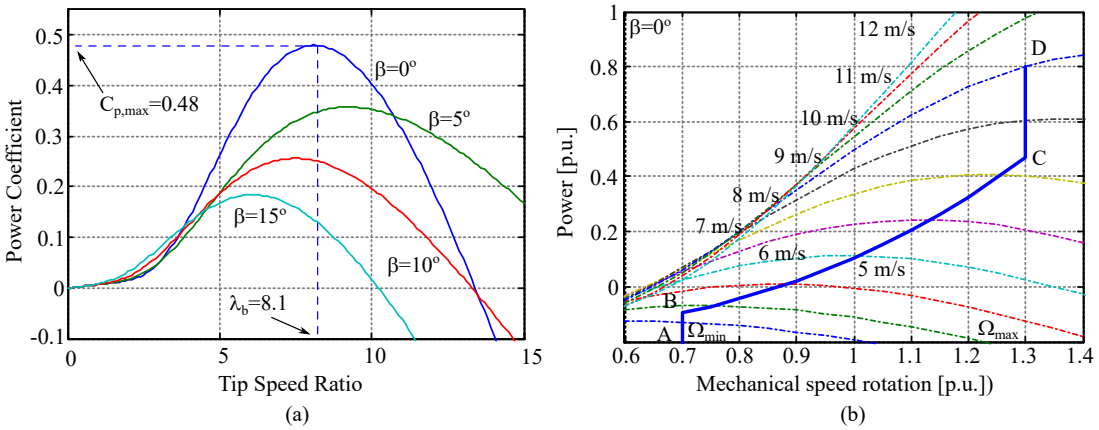

Figure 6.2: Graphical representation of wind turbine (WT) equations: (**a**) C_p versus λ for different β values; (**b**) WT power (p_m) for different wind speeds and maximum power loci (curve BC).

to limit the power extracted at high wind speeds. However, in this work this relation will be used to achieve the power balance by a load following strategy.

From the $C_p(\lambda,\beta)$ relationship at constant β, Figure 6.2.b shows the WT power characteristics (WT power vs. WT rotational speed Ω), for different wind speeds. More importantly, this figure also shows the maximum power loci, which are obtained when the WT is operated with the maximum power coefficient, $C_p = 0.48$, at $\lambda = 8.1$ and $\beta = 0$. As it will be shown later, the maximum power curve is particularly relevant because it defines the steady-state stability limit of the WT. If the demanded power is increased beyond this curve, the subsequent reduction in the rotational speed will lead to a further reduction of the WT power, making the system unstable. This curve will be used in the control strategy of the LSC to limit the maximum active power that the WECS can supply to guarantee a stable operation.

PMSG Model

The electrical behavior of a PMSG can be expressed in a stationary reference frame as

$$\vec{u_s} = \psi \frac{d}{dt} e^{j\varepsilon} - R_s \vec{i_s} - L_s \frac{d}{dt} \vec{i_s}, \tag{6.2}$$

where subscript s stands for stator, $\vec{u_s}$ and $\vec{i_s}$ are the stator voltage and current, respectively, ψ is the stator total magnetic flux linkage, ε is the angular position of the rotor, and R_s and L_s the stator resistance and inductance, respectively.

In order to implement a dynamic control of the PMSG active power, a transformation to a dq rotating frame oriented to the rotor is used. The orientation to the rotor results in steady-state constant values for

the control variables. Applying this transformation to equation (6.2) leads to

$$u_{sd} = -R_s i_{sd} - L_s \frac{d}{dt} i_{sd} + \omega_r L_s i_{sq}, \tag{6.3}$$

$$u_{sq} = \omega_r \psi - R_s i_{sq} - L_s \frac{d}{dt} i_{sq} - \omega_r L_s i_{sd}. \tag{6.4}$$

For a balanced three-phase system, the output power can be calculated as

$$P_s = \frac{2}{3} \Re(\vec{u_{s,dq}} \cdot \vec{i^*_{s,dq}}) \tag{6.5}$$

where the asterisk indicates the complex conjugate. Using equations (6.3)–(6.5) the output power can also be expressed as

$$P_s = \frac{2}{3} (\omega_r \psi i_{sq} - R_s |\vec{i_{s,dq}}|^2) \tag{6.6}$$

The term related to the stator resistance can be interpreted as power losses and thus the electromagnetic torque is derived as

$$T_{em} = \frac{P_{em}}{\Omega} = P_{em} \frac{p_n}{\omega_r} = \frac{2}{3} (\psi p i_{sq}) \tag{6.7}$$

where p is the pole pair number.

Equation (6.7) shows that torque can be controlled by means of the q-component of the stator current i_{sq}. In a grid-connected FC, i_{sq} is regulated to control the rotational speed of the WT and in this way control the WT power. However, in the off-grid application power is imposed by the load and i_{sq} will be used to balance the power at the DC bus. This means that this current component will be obtained by the DC voltage controller to maintain constant DC voltage, which in turns means that the generator supplies the power that is demanded by LSC to supply the load. This is further developed in Section 6.2.2.

Isolated VSC Model

In this section, the model of an isolated VSC is used as a reference for the implementation of the VFC. In contrast with the model developed in section 5.3, in this case it is an isolated system so the dynamics are affected by the load instead of the grid. Although some of the equations, particularly the equations of the current controllers of the VOC and the dynamic equations of the AC filter, are shared with the model of section 5.3, they are reproduced here again for the sake of clarity.

The AC-side of a VSC can be represented by a three-phase AC voltage source connected to the system through a interfacing reactor, modelled by its inductance L and resistance R [133–135] as seen in Figure 6.3.

The dynamics of the DC link have been modelled by a controlled current source i_{DC} in parallel with the DC bus capacitor C_{DC}. This is useful to study the effects of the VFC on the DC-link, considering the voltage control performed by the GSC.

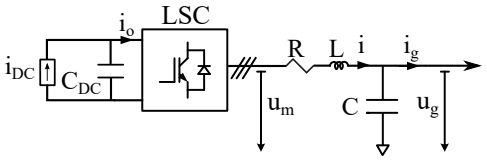

Figure 6.3: Scheme of the Line-Side Converter (LSC) operating in isolated mode.

Using pulse-width modulation (PWM), the relation between DC and AC voltages can be expressed as

$$u_{mk} = m_k \frac{U_{DC}}{2}, \tag{6.8}$$

where m_k is the modulating signal corresponding to phase k [134].

At the AC side, the total capacitance connected is represented by C. This includes the high frequency filter, which is considered purely capacitive at the fundamental frequency [136], and other capacitor banks connected at the point of common coupling (PCC). The VSC terminal voltage u_m and the capacitor bank voltage u_g are related by the equation

$$u_{gk} = u_{mk} - Ri_k - L\frac{d}{dt}i_k, \tag{6.9}$$

where i_k is the converter current and subscript k stands for the system phase ($k = a,b,c$).

The phase currents and voltages and the modulating signals can be expressed in a rotating dq reference frame as $\vec{i} = i_d + ji_q$, $\vec{i_g} = i_{gd} + ji_{gq}$, $\vec{u_g} = u_{gd} + ju_{gq}$, $\vec{u_m} = u_{md} + ju_{mq}$ and $\vec{m} = m_d + jm_q$, respectively. Therefore, by applying the Park transformation, equation (6.9) can be expressed in a synchronous dq reference frame, rotating at constant frequency ω_0, as

$$\vec{u_g} = \vec{u_m} - R\vec{i} - L\frac{d}{dt}\vec{i} - j\omega_0 L\vec{i}, \tag{6.10}$$

On the other hand, at the capacitor bank, the voltage equations per phase are

$$i_k - i_{gk} = C\frac{d}{dt}u_{gk}, \tag{6.11}$$

where i_{gk} is the phase k current demanded by the load. Equation (6.11) can be expressed in a synchronous dq reference frame as

$$\vec{i} - \vec{i_g} = C\frac{d}{dt}\vec{u_g} + j\omega_0 C\vec{u_g} \tag{6.12}$$

The load is modelled as a constant power source that demands a given value of active power P_L and reactive power Q_L. This introduces a non-linear relation between the controlled voltage $\vec{u_g}$ and the demanded current $\vec{i_g}$. This relation can be expressed in dq as

$$i_{gd} = \frac{P_L u_{gd} + Q_L u_{gq}}{u_{gd}^2 + u_{gd}^2}, \tag{6.13}$$

$$i_{gq} = \frac{P_L u_{gq} - Q_L u_{gd}}{u_{gd}^2 + u_{gd}^2}. \tag{6.14}$$

Finally, the dynamics on the DC-link capacitor, considering the relationship between the VSC DC and AC variables, is expressed as

$$C_{DC}\frac{d}{dt}U_{DC} = I_{DC} - \frac{1}{U_{DC}}\frac{3}{2}\Re(\vec{u_m}\cdot\vec{i}^*), \tag{6.15}$$

where the last term is the derived from the active AC power, neglecting the VSC losses.

The complete system dynamic equations can be obtained by separating the real and imaginary parts of Equations (6.10) and (6.12). Moreover, these equations plus Equation (6.15) can be expressed per unit as

$$\frac{c}{\omega_0}\frac{d}{dt}u_{gd,pu} = i_{d,pu} + cu_{gq,pu} - i_{gd,pu}, \tag{6.16}$$

$$\frac{c}{\omega_0}\frac{d}{dt}u_{gq,pu} = i_{q,pu} - cu_{gd,pu} - i_{gq,pu}, \tag{6.17}$$

$$\frac{l}{\omega_0}\frac{d}{dt}i_{d,pu} = m_d u_{DC,pu} - u_{gd,pu} - ri_{d,pu} + li_{q,pu}, \tag{6.18}$$

$$\frac{l}{\omega_0}\frac{d}{dt}i_{q,pu} = m_q u_{DC,pu} - u_{gq,pu} - ri_{q,pu} + li_{q,pu}, \tag{6.19}$$

$$\frac{c_{DC}}{\omega_0}\frac{d}{dt}u_{DC,pu} = i_{DC,pu} - m_d i_{d,pu} - m_q i_{q,pu}. \tag{6.20}$$

Base values for per unit transformation have been selected considering the ratings of the PMSG used for the real-time implementation. They are presented in Table 6.1.

Table 6.1: Isolated FC WECS: Base values for per unit transformations

Label	Value	Units	Description
U_b	132.8	V	AC base voltage
$U_{dc,b}$	$2U_b$	-	DC base voltage
S_b	3000	VA	Base power
f_b	50	Hz	Base frequency
Ω_{WT}	375	rpm	Base rotational speed

In conclusion, the system has five state variables, u_{gd}, u_{gq}, i_d, i_q and u_{DC}, two external inputs, p_L and q_L, and three controlled inputs, m_d, m_q and i_{DC}.

6.2.2 Proposed control

As explained in the introduction, the control system must be able to maintain constant voltage and frequency at the generator terminals despite a variable wind energy source while delivering the demanded amount of active and reactive power. The proposed control system is divided into WT, GSC, and LSC control.

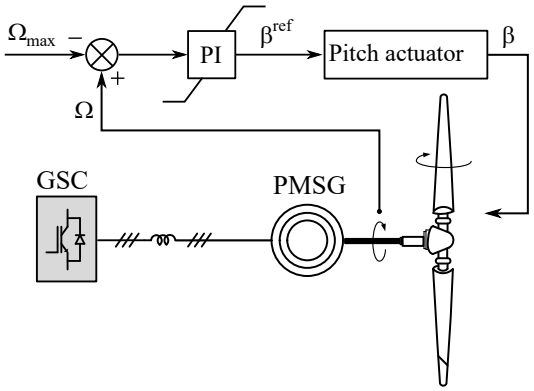

Figure 6.4: Control scheme for the WT Rotational speed

Wind Turbine Power Control

In order to ensure a stable operation, the power demanded by the load must be equal to the power delivered by the WT. Due to the proposed control, the PMSG power is fixed by the load while the power extracted from the WT is given by Equation (6.1). The power exchange between both systems is given by the mechanical equation of the WT as

$$\frac{d\Omega}{dt} = \frac{1}{J}(T_{WT} - T_{em}), \tag{6.21}$$

where T_{WT} is the torque produced by the WT and T_{em} is the torque produced by the PMSG.

Equation (6.21) shows that if the turbine power is higher than the load power, the rotational speed will increase, or decrease in the opposite case. Therefore, power balance can be achieved by means of a speed control loop: only when the turbine power equals the load power is the rotational speed maintained constant. This speed control loop is shown in Figure 6.4.

The speed control loop will ensure that the maximum rotational speed of the WT is not exceeded by acting on the pitch control system. The blade pitch angle is adjusted, thus reducing or increasing the turbine power until it matches the load power. Note that this control system is similar to the one used in grid-connected WECS for limiting power when the wind velocity is higher than rated. The only difference is that here maximum rotational speed can be achieved at any wind velocity. By regulating the rotational speed, pitch control allows the WT to supply a specific load in a wider range of wind velocities or alternatively to deliver a wider range of power values for a specific wind velocity.

When operating at the minimum pitch angle ($\beta = 0$), WT operation will still be stable but only below a defined stability limit, as shown in Figure 6.2b. This is why the power extracted from the WT must be limited at this value in the LSC.

Note that instantaneous power variations will be supplied by the WT stored kinetic energy since the pitch actuation is normally limited between $5\,^{\circ}/\mathrm{s}$ and $10\,^{\circ}/\mathrm{s}$ [137].

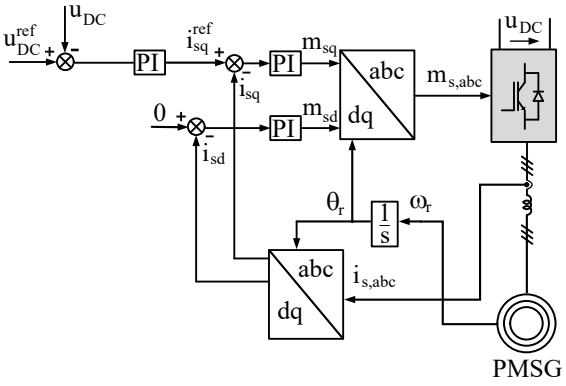

Figure 6.5: Control scheme for the Generator Side Converter (GSC)

Generator Side Converter Control

The GSC will be responsible for maintaining the DC-link voltage constant despite the WT speed and torque variations. This is achieved by the regulation of the active power drawn from the PMSG using the stator current q-component, which is related to active power as seen in Equation (6.7). The control scheme is depicted in Figure 6.5.

There are several criteria for selecting the stator d-component current, related to the efficient use of the PMSG [138]. Here, maximum torque per ampere ($i_d = 0$) is employed.

The DC voltage control loop is included in the VSC model of section 6.2.1 through the controlled current source i_{DC} as

$$i_{DC} = k_{pDC}(u^*_{DC} - u_{DC}) + k_{iDC}x_{DC}, \tag{6.22}$$

where k_{pDC} and k_{iDC} are the DC voltage controller proportional and integral gains, respectively. The dynamics of the internal current control loops are not considered since their bandwidths are tuned at more than one order of magnitude higher than that of the DC voltage control loop. Therefore, their effect on the DC voltage variation can be neglected. x_{DC} is the DC voltage error state, given by

$$\frac{1}{\omega_0}\frac{d}{dt}x_{DC} = u^*_{DC} - u_{DC}, \tag{6.23}$$

LSC Voltage and Frequency Control

The VFC objective is to maintain constant voltage and frequency on the AC system. It is based on the orientation of the output voltage vector along a synchronous reference axis (d axis). The rotational speed of the synchronous reference axis is the reference frequency of the system ω_0. If the control can maintain the voltage vector orientated along the synchronous reference axis, the frequency is kept constant.

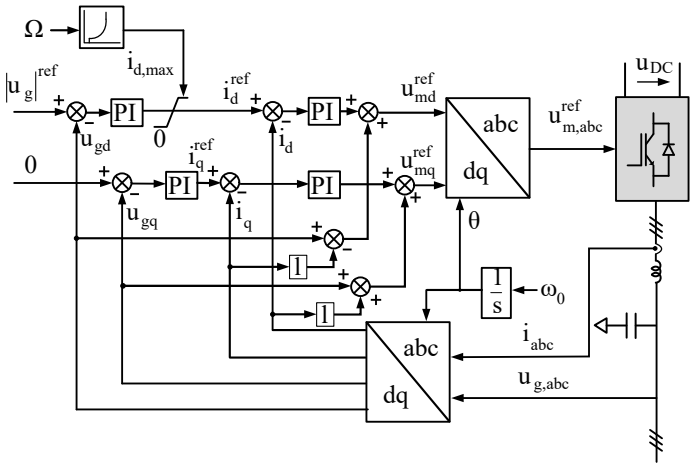

(c)

Figure 6.6: VFC scheme for the LSC

A linear approximation can be made between the magnitude and angle of the voltage and its d and q components, respectively. Considering that

$$u_{gd} = |\vec{u_g}|cos(\delta), \tag{6.24}$$

$$u_{gq} = |\vec{u_g}|sin(\delta), \tag{6.25}$$

where δ is the angle between $\vec{u_g}$ and the d axis, the following can be deduced for small variations of δ around 0:

$$\Delta u_{gd} = \Delta|\vec{u_g}|, \tag{6.26}$$

$$\Delta u_{gq} = \Delta(\delta). \tag{6.27}$$

In steady state, if the LSC keeps the voltage and frequency constant, then it will act as the system slack node, supplying the active and reactive power demanded by the load. Moreover, considering Equations (6.16) and (6.17), the control of the voltage magnitude (u_{gd}) and angle (u_{gq}) is related to the control of the LSC active (i_d) and reactive (i_q) currents, respectively, with a certain coupling between axes.

These principles are the basis of the proposed VFC. There are two control channels, the first one to obtain constant voltage, and the second one to obtain $u_{gq} = 0$, as seen in Fig. 6.6, which in turns means that the voltage vector is kept orientated to the reference axis.

The reference for the orientation of the d-axis is obtained by the integration of the desired frequency ω_0. Note that a PLL is not needed because the whole control is oriented to a synchronous axis obtained directly from integration of the desired angular frequency. Therefore, the angular position is not subject to any measurement noise or grid disturbance.

A dynamic saturation for i_d^{ref} also included to ensure that the WT never exceeds its stability limit as explained in section 6.2.1. When the available wind power is not enough to supply the load, the voltage magnitude will drop. This will be used as the principle to share the load between multiple WECSs in Section 6.3.

To complete the state-space model, the dynamics of the VFC are included. In the current controllers, the modulating signals m_d and m_q can be expressed as

$$m_d = k_{pc}(i_d^{ref} - i_d) + k_{ic}x_{cd} - li_q, \tag{6.28}$$

$$m_q = k_{pc}(i_q^{ref} - i_q) + k_{ic}x_{cq} + li_d, \tag{6.29}$$

where k_{pc} and k_{ic} are the current controller proportional and integral gains, respectively, and the compensating cross terms have been added. x_{cd} and x_{cq} are the d-q current error states, given by

$$\frac{1}{\omega_0}\frac{d}{dt}x_{cd} = i_d^{ref} - i_d, \tag{6.30}$$

$$\frac{1}{\omega_0}\frac{d}{dt}x_{cq} = i_q^{ref} - i_q. \tag{6.31}$$

Similarly, the voltage controller input is the voltage error, while the output is the current reference, given by

$$i_d^{ref} = k_{pv}(u_{gd}^{ref} - u_{gd}) + k_{iv}x_{vd} + cu_{gq}, \tag{6.32}$$

$$i_q^{ref} = k_{pv}(u_{gq}^{ref} - u_{gq}) + k_{iv}x_{vq} - cu_{gd}, \tag{6.33}$$

where k_{pv} and k_{pv} are the voltage controller proportional and integral gains, respectively, and the compensating cross terms have been added. As in the current controller, x_{vd} and x_{vd} are the d-q voltage error states, given by

$$\frac{1}{\omega_0}\frac{d}{dt}x_{vd} = u_{gd}^{ref} - u_{gd}, \tag{6.34}$$

$$\frac{1}{\omega_0}\frac{d}{dt}x_{vq} = u_{gq}^{ref} - u_{gq}. \tag{6.35}$$

These equations the proposed state-space model, which is composed of the set of non-linear dynamic equations given by the LSC station model (6.16)–(6.20), the GSC DC-link voltage control (6.23), the VFC current controllers (6.30)-(6.31) and the VFC voltage controllers (6.34)-(6.35).

A Linear Time-Invariant (LTI) state-space representation of the system can be obtained through the Jacobian matrix of these equations around the operating point given by $|\vec{u_g}|_0$, δ_0, p_{L0}, q_{L0} and u_{DC0} as

$$\frac{d}{dt}\Delta x = A\Delta x + B\Delta u, \tag{6.36}$$

$$\Delta y = C\Delta x + D\Delta u, \tag{6.37}$$

where

$$x = [u_{gd}, u_{gq}, x_{vd}, x_{vq}, i_d, i_q, x_{cd}, x_{cq}, u_{DC}, x_{DC}], \tag{6.38}$$

$$u = [p_L, q_L, u_{gd}^{ref}, u_{gq}^{ref}, u_{DC}^{ref}], \tag{6.39}$$

$$y = [u_{gd}, u_{gq}]. \tag{6.40}$$

and A, B, C and D contain only linear time-invariant coefficients.

Note that the dynamics of the WT model and control are not considered in this model since the DC voltage is only dependent on the GSC control. This implies that the GSC control is considered significantly faster than the WT dynamics so both models can be considered dynamically independent.

6.2.3 Stability analysis

In order to assess the dynamics and stability of the overall system, the eigenvalue and sensibility analysis are performed in the following paragraphs. For such purpose, the influence of the system parameters on the loci of dominant eigenvalues is studied considering the base-case scenario given in Table 6.2.

Table 6.2: Isolated FC WECS: Base case system parameters in pu.

Label	Value	Description
l	0.1	AC filter inductance
r	0.003	AC filter resistance
c	0.1	AC capacitance
c_{DC}	0.35	DC capacitance
k_{pc}	2	AC current proportional gain
k_{ic}	0.637	AC current integral gain
k_{pv}	2.5	AC voltage proportional gain
k_{iv}	0.127	AC voltage integral gain
k_{pDC}	3	DC voltage proportional gain
k_{iDC}	0.064	DC voltage integral gain

Since the system is non-linear, the operation point, or quiescent point, also affects the stability of the system. The base-case operating point values are given in Table 6.3.

For this base case, the eigenvalues are computed and presented in Table 6.4. The frequency and damping ratio are also given, as well as the dominant states according to their participation factors [1].

All the eigenvalues have a negative real part and thus the system is stable.

Table 6.3: Isolated FC WECS: Base case operating point in p.u.

Label	Value	Description
$\|\vec{u_g}\|_0$	1	AC voltage vector amplitude
δ_0	0	AC voltage vector deviation
p_{L0}	0.5	Active power demand
q_{L0}	0	Reactive power demand
u_{DC0}	1	DC voltage amplitude

Table 6.4: Isolated FC WECS: Base-case eigenvalue analysis.

λ_i	Eigenvalues [rad/s]	Frequency [Hz]	Damping Ratio [p.u.]	Dominant States
1–2	-2820.1 ± 4989.1i	911.96	0.492	u_{gq}, i_q
3–4	-1254.7 ± 4261.3i	706.65	0.282	u_{gd}, i_d
5	-2.2311	0	1	u_{DC}
6–7	-0.1	0	1	x_{cd}, x_{cq}
8	-0.0268	0	1	x_{DC}
9–10	-0.01	0	1	x_{vd}, x_{vq}

The proposed VFC is based on the regulation of the filter capacitance voltage. Therefore, one of the system more relevant parameter is the total capacitance connected at the PCC. Figure 6.7a shows the system eigenvalue map, together with the associated states, for a variation in c from the base case of 0.1 to 0.3. It can be concluded that a higher capacitance damps voltage variations and reduces the frequency of the associated eigenvalues. Consequently, a very small capacitance could compromise the system stability.

Due to the non-linearities of the load and the VSC models, the system is also dependent on the active and reactive power demand. Figure 6.7b shows the eigenvalues evolution for a variation of p_L from 0.1 to 1 p.u. It can be noted how the eigenvalues associated with u_{gd}, and thus with voltage amplitude, move towards the imaginary axis. This means they tend to become more dominant and less damped. The opposite happens with the eigenvalues associated with u_{gq}, and thus with voltage frequency.

Variations of q_L produce a similar effect but without influence on the eigenvalues related to DC voltage. Note that power variations could make the system unstable if the control gains are not selected correctly.

This stability analysis shows the proposed system robustness against variations in both the operating point and internal parameters.

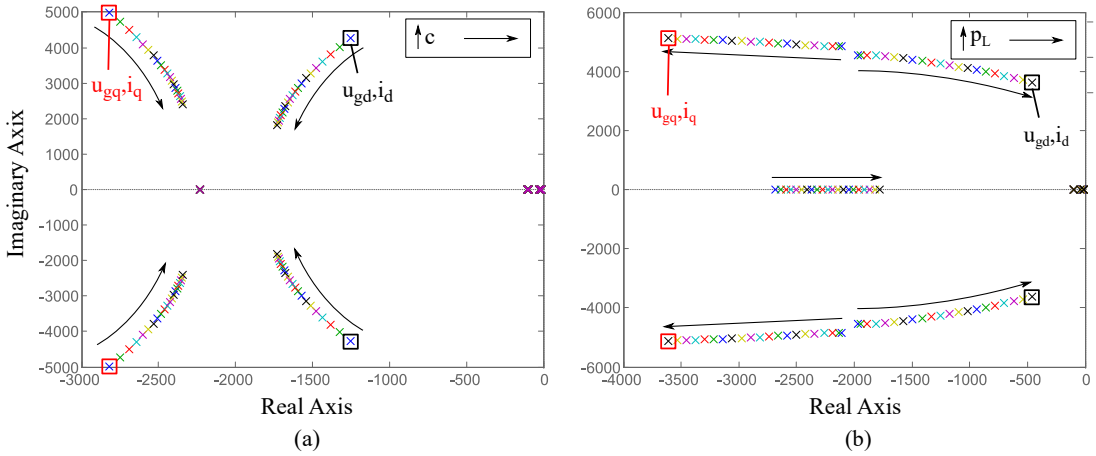

Figure 6.7: Model sensitivity to:

(**a**) Point of common coupling (PCC) capacitance variation and (**b**) active load variation.

6.2.4 Results and discussions

In this section, the detailed switching model simulations and real-time results are presented to demonstrate the capability of the proposed control operation as well as to validate the developed dynamic models.

These detailed simulations were developed using MATLAB/Simulink in co-simulation with PSIM Simulink was used to implement the control algorithms, whereas PSIM was used for simulating the power system elements.

Using this structure, the implementation of the models represented in Fig. 6.1–6.6 is fairly straightforward. The model has been discretized according to the simulation parameters given in Table 6.5. Other parameters, such as control proportional and integral gains, are the same as in the base case presented in Tables 6.2 and 6.3.

Table 6.5: Isolated FC WECS: Simulation parameters. WT: wind turbine.

Label	**Value**	**Units**	**Description**
$Ts, cont$	200×10^{-6}	s	Control sampling time
$Ts, power$	10×10^{-6}	s	Power circuit sampling time
D_{WT}	4	m	WT diameter
H_{WT}	3	s	WT time constant
ρ	1.225	$\mathrm{kg\,m^{-3}}$	Air density

In order to obtain a further demonstration of the capabilities of the proposed control, the system

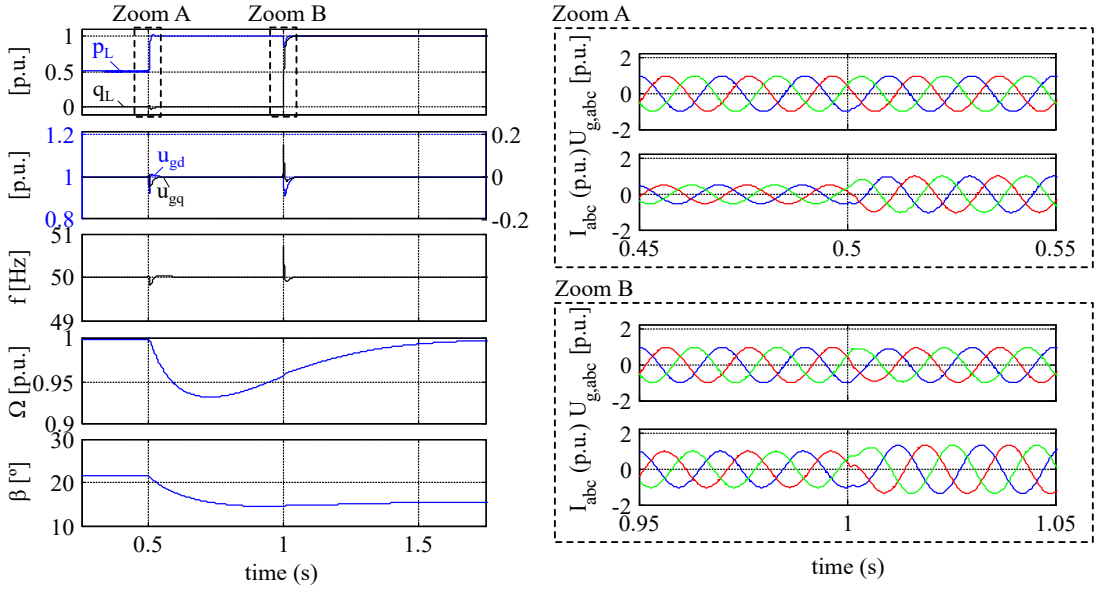

Figure 6.8: Load step response in simulation

was tested on a real-time test bench. The WT was emulated based on the hardware-in-the-loop scheme developed in [139]. A more detailed explanation is given in the Appendix A.2. The load could not be emulated as a constant power source so a resistor and a reactance were used instead.

Responses to both wind and load variations were studied showing the effect on both the WT and the VSC. First, a load step at a constant wind speed is performed and then a variable wind speed is applied under constant load.

Load Step Response

Despite load variations, the VFC must be able to maintain constant voltage and frequency. Also, the pitch control must ensure steady-state power balance between the WECS and the load to ensure a stable operation.

Simulation results are shown in Fig. 6.8. Both active and reactive power variations are included. A 0.5 pu to 1 pu an active load step is applied at $t = 0.5$ s, while a 0 pu to 1 pu reactive power step is applied at $t = 1$ s. The dq components of the voltage only suffer small deviations at the changes, despite the load variation and therefore voltage and frequency are maintained constant after the transience. Frequency is influenced by both active and reactive power variations due to the coupling between axes. However, in contrast with most power systems, reactive power variations have a more significant influence. Zooms of the AC voltages and currents during load transitions are also included.

To obtain a stable operation, the power demanded by the load must equal the power extracted from

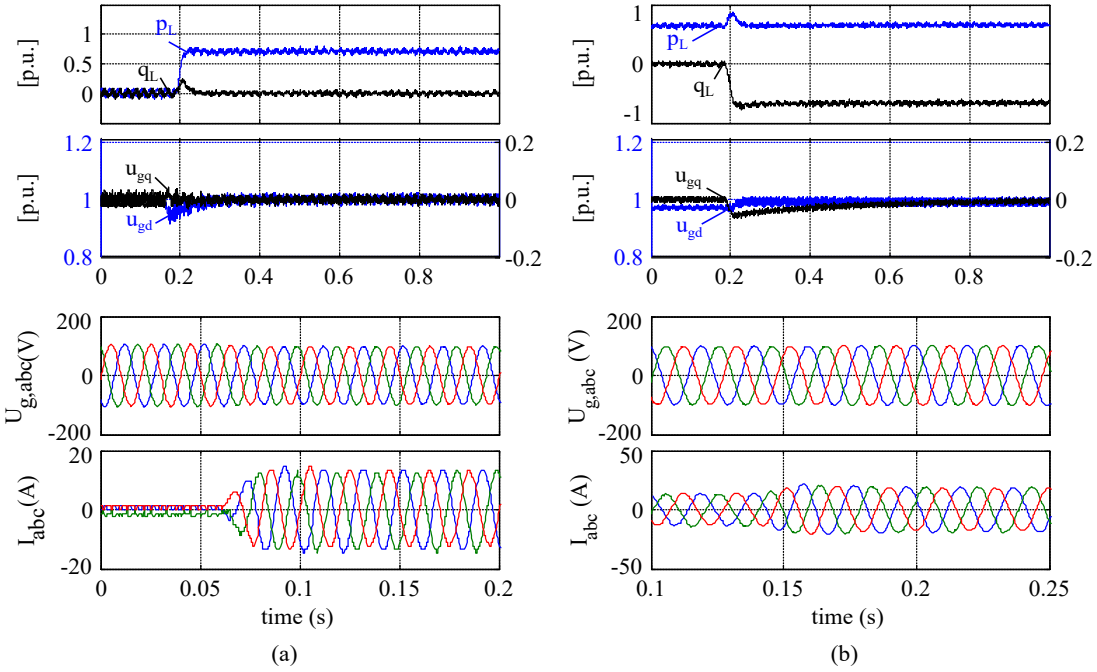

Figure 6.9: Load step response in real-time system including (**a**) an active power step variation and (**b**) a reactive power step variation.

the WT. For this purpose, the pitch angle must be decreased in order to increment power extraction. Note that pitch angle variations are considerably slower than the converter actuation. The difference between the load and WT power during this transience is drawn from the WT kinetic energy, producing a transience in the rotational speed, closing in this way the instantaneous power balance.

Reactive power demand is supplied by the VSC and thus has no influence on the WT power control.

Real-time results are shown in Fig. 6.9. Active and reactive power variations were also applied to the real-time system. It can be seen how these results validate the ones obtained in simulation and thus the same conclusions can be deduced.

Wind Variation Response

To study the system response to wind variations, the wind profile of Fig. 6.10 has been used. The profile consists of a turbulent variation around 12 m/s. Load is kept constant, so the WECS power must be constant despite the wind velocity variations. Only real-time results are shown to avoid a redundancy of information.

To balance the system, the objective of the pitch angle control is to maintain a constant WT speed. Fig. 6.10 shows that pitch angle follows wind velocity variations, increasing pitch angle if wind velocity increases or decreasing pitch angle if wind velocity decreases, in order to maintain constant rotational

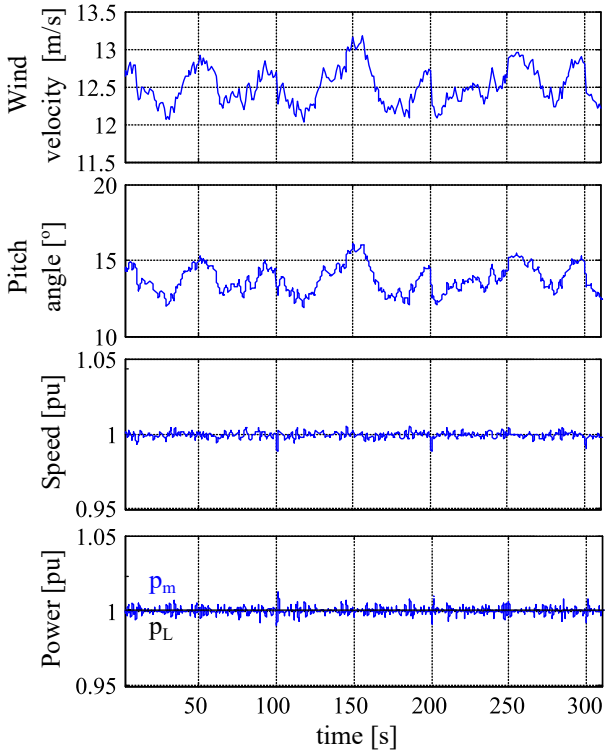

Figure 6.10: Real-time system response to wind variations.

speed. Nevertheless, as the pitch actuator has a low bandwidth, there are some variations on the rotational speed and the WT power (p_m). This rotational speed variation precisely balances the WT power and output power of the WECS, as commented before.

Note that the power measured in the load terminals (p_L) is kept constant despite the variations in the wind.

Final discussions

This section has presented the design and implementation of a VFC strategy for WECSs and its application for supplying an isolated load.

The decoupled control of the capacitor d-q voltage allows us to achieve a balance between demanded and generated active and reactive power, respectively, while maintaining constant voltage and frequency. Frequency control is achieved through the orientation of the voltage vector along an axis rotating at the reference frequency, avoiding the use of a PLL for frequency measurement.

The roles of the converters of the FC system are inverted. The LSC controls AC voltage and frequency, while the GSC is responsible for maintaining constant voltage in the DC link. Therefore, power is fixed by the load demand instead of the WECS.

The use of the proposed VFC allows the LSC active power to precisely match the load demand. In contrast with previous works, which focused on the integration of the WT with additional systems, here balance is achieved by the speed regulation of the WT through pitch angle control and thus no additional power sources, dump resistors, or ESSs are required to ensure the system stability.

Active power unbalance situations provoke voltage amplitude variations, instead of frequency variations as is the case in power systems with synchronous generators. This will be used in the next section to share the power demand between multiple WECSs. Nevertheless, once the power balance is restored, due to load regulation or wind speed rise, the algorithm operation is resumed automatically thanks to the included i_d limitation, which avoids wind-up situations and dynamic instabilities.

The proposed control scheme has been completely modelled and validated by simulation and real-time implementation, demonstrating its capability to maintain constant voltage and frequency despite load and wind speed variations.

6.3 Control system for parallel operation

As presented earlier, during black-start active power generation must be balanced with the local demand. For a single WECS, this can be guaranteed by the load balancing control presented in the previous section. However, if there are multiple WECSs, the system load must be shared between them. Moreover, depending on the wind, power availability might vary between different WECSs so the load share must vary accordingly.

The different WECSs must operate in synchronism in both isolated and grid-connected modes. In this section, the synchronization system presented in Chapter 5 is merged with a new proposal for active power sharing that does not affect synchronization. It is demonstrated that this allows WECSs to provide a black-start solution while sharing the available load according to each unit wind availability.

A case study system with 2 WECSs connected in parallel is used to demonstrate the proposed control operation. The case study considers both grid-connected and islanded operation modes. A scheme of this system is depicted in Fig. 6.11.

As with the case of a single WECS, the control objective is to ensure the stable operation of the system through the restoration process. This implies maintaining the AC voltage and frequency and ensuring that the power extracted from the WTs equals the load demand.

The WT and GSC control systems developed in section 6.2.2 are still applicable. In this case, the WT pitch angle control ensures that the power extracted from the wind equals the power demanded by the LSC. The GSC is again responsible for regulating the DC-link voltage. However, in this case each LSC control cannot regulate the system frequency and voltage on its own since the control systems of the different WECSs will conflict. Therefore, the control system of the LSC must me modified.

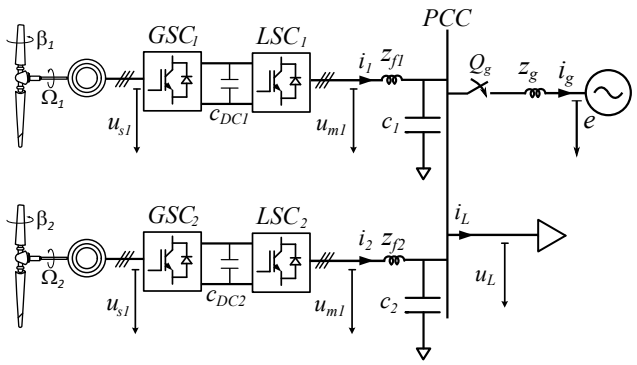

Figure 6.11: General scheme of the system under study with 2 wind energy conversion systems connected in parallel.

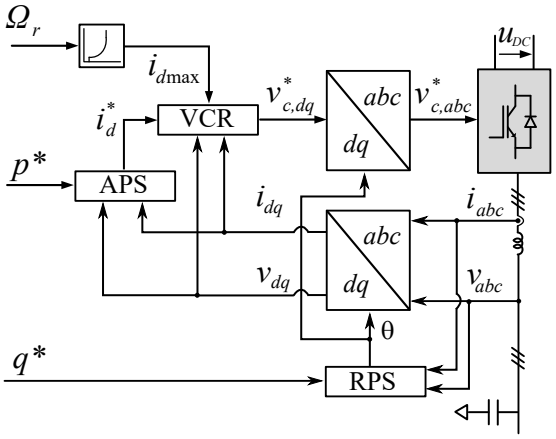

Figure 6.12: Line Side Converter (LSC) control for the parallel operation solution. RPS: Reactive Power Synchronization, APS: Active Power Sharing, VCR: Voltage and Current Regulator.

6.3.1 LSC control for parallel operation

A scheme of the proposed control system for the LSC is depicted in Fig. 6.12. It includes the RPS control presented in Chapter 5, including the internal Voltage and Current Regulators (VCR) depicted in Fig. 5.2.

In the solution for a single WECS, the LCS was responsible of ensuring the active power balance by the regulation of the system voltage. In this case, since two WECSs are operating in parallel, the voltage control must be shared between them.

For this purpose, an active power/voltage droop is implemented as seen in Fig 6.13. Thus, the active current current reference $i_d{}^*$ is obtained from the control law

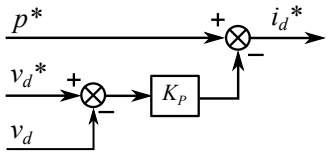

Figure 6.13: Active Power Sharing control.

$$i_d{}^* = p^* - (v_d{}^* - v_d) * K_P, \tag{6.41}$$

where p^* and K_P are the control parameters and $v_d{}^*$ is the voltage set-point.

Moreover, if for one WECS $i_d{}^*$ cannot be ensured, because there is not enough wind available, voltage will decrease. Due to the droop relation, the other WECS $i_d{}^*$ will increase automatically and a new stable operating point at a different voltage will be reached. Therefore, two WECSs can operate in parallel even if the $i_d{}^*$ provided by (6.41) cannot be fulfilled in one of them. This will be validated in section 6.3.2.

Note that if a traditional active power/frequency droop was used for active power sharing and synchronization, in case one of the WECSs could not ensure a given $i_d{}^*$, i.e. active power generation, that unit will lose the frequency reference and thus synchronism with the system.

If needed, voltage could also be controlled to the desired value by varying the WECSs voltage reference $v_d{}^*$. This could be performed by a secondary controller as it is usually done in traditional power systems [1] or hierarchical Microgrids [31].

6.3.2 Results and discussions

In this section, simulation results for the case study given in Fig. 6.11 are presented to validate the proposed control. Simulations were developed with the same method as in Section 6.2, using a detailed switching model implemented in MATLAB/Simulink in co-simulation with PSIM. Simulink was used to implement the control system whereas PSIM was used for simulating the power system components.

First, it will be seen how the WECSs can be started on their own in a complete black-out situation. Then, a change in the wind will be simulated so both WECSs are not able to share the load equally. To conclude, a hot-swapping from isolated operation to grid-connected operation is performed without changing the control system.

Results are depicted in Fig. 6.14. When the simulation starts, the system is disconnected from the grid (Q_g opened) and both WECS are disabled so no power is extracted from the wind ($p_1 = p_2 = 0$).

At t=0.01s, the first WECS is enabled. Since the system is operated disconnected from the grid, generated and consumed active and reactive power must be balanced to ensure a stable operation. It can

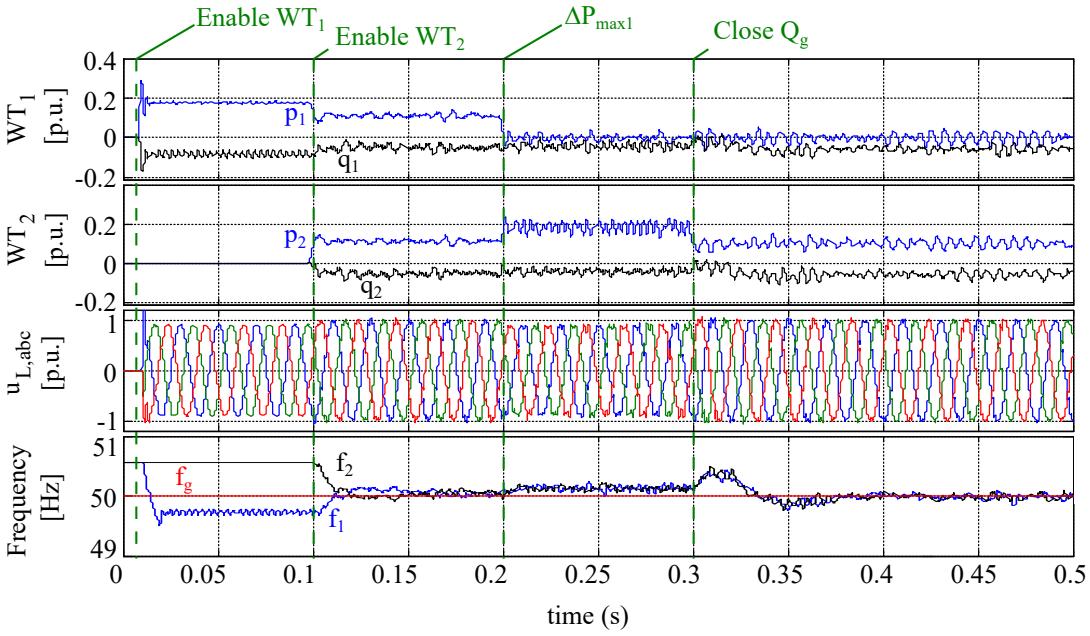

Figure 6.14: Results for: the black-start connection of WT_1 (t=0.01 s), the subsequent connection of WT_2 (t=0.1 s), a variation in the wind power available in WT_1 (t=0.2 s) and the connection to the main grid (t=0.3 s).

be seen how p_1 and q_1 are automatically regulated to the required values so the WT_1 is supplying the active and reactive power required by the loads, which gives broadly $p_1 = 0.2pu$ and $q_1 = 0.1pu$. Given these active and reactive power values, frequency and voltage are established at an operating point given by equation (5.12) of the RPS control and equation (6.41) of the APS control, respectively.

At t=0.1s, the second WECS is enabled. Its active and reactive power generation, p_2 and q_2, varies so the system active and reactive power demand is shared between both WECSs and a new frequency and voltage operating point is reached. It can be seen that the system is operating in synchronism since both frequencies, f_1 and f_2, converge to the same value. Note that reactive power varies accordingly to frequency due to the RPS control, while active power varies following the voltage variation due to the APS control. The resulting frequency is close to f_g because of the selected control parameters ω_0 and K_s.

In order to show that synchronism is possible even if wind is unequally available, a variation on the available wind power is simulated at t=0.2s. It can be seen that p_1 is limited so the WT_2 must supply the load on its own. Due to the voltage variation produced by the proportional relation in (6.41), reactive power is affected so a new frequency operating point is reached. However, it can be seen that both WECSs remain in synchronism despite the variation in wind availability.

Finally, in order to test the ability of the system to perform a hot-swapping between isolated and grid-connected modes, the system is connected to the grid by closing Q_g at t=0.3s. It can be seen how the system can perform this transition smoothly and both WECSs synchronize to the grid frequency. In this situation, if desired, active and reactive power generation of the WECSs could be freely controlled by p^* and q^*, respectively, for instance to follow a MPPT strategy.

Chapter 7

Conclusions

Contents

7.1 General conclusions **93**

7.2 Original contributions **95**

7.3 Publications **96**

7.4 Funding **97**

This chapter includes a summary of the main conclusions extracted during this thesis. Section 7.1 includes a general discussion on the thesis work. Section 7.2 enumerates the most relevant contributions. Publications resulting from this thesis are included in Section 7.3. Fundings used for the development of this thesis are acknowledge in Section 7.4.

7.1 General conclusions

This thesis has analyzed the Microgrid concept and its implications, focusing on the control systems that can be implemented to overcome technical requirements of Microgrid applications. This analysis highlights the importance of Microgrids for future power systems, specially due to the increased opportunities for the integration of distributed renewable energy generation. A literature review is used to study control problems related to renewable energy integration in Microgrids. Solutions based on a hierarchical control structure are presented. The study of the different control levels in the hierarchical structure is used to frame the rest of the Thesis work, which is devoted to the low level control solutions for renewable energy systems interfaced by Voltage Sourced Converters (VSCs). Studying the Microgrid control system as a whole has helped to understand the requirements of VSCs in Microgrids and the problems that have to be solved by the VSC control system.

The most relevant solutions for the control of VSCs have been categorized, according to their interaction with the Microgrid, in Grid-Tied, Grid-Forming and Grid-Supporting solutions. Grid-Supporting solutions allow the synchronous operation of VSCs in both grid-connected and islanded modes. Operation in both modes is possible because Grid-Supporting systems are able to operate in synchronism with other sources without relying on external frequency measurement units, such as PLLs, that cause stability problems in converter-dominated grids.

The review of VSC control systems shows that there are both Grid-Tied and Grid-Supporting systems that can contribute to maintain the Microgrid stability through the emulation of traditional Synchronous Generators. The Virtual Synchronous Machine concept is used to integrate control systems that are based on emulating Synchronous Generators. A review of VSC control systems based on the operation of SGs for Microgrid applications is presented, whether or not they use of the VSM notation. This review shows that the interest in VSM solutions comes from two inherent features of SGs: inertial response and synchronizing torque.

Emulation of inertial response, or inertia emulation, of both Grid-Tied and Grid-Supporting VSM systems has been compared in an isolated Microgrid case study. For this comparison, representative solutions of both categories have been implemented with equivalent inertial response requirements in a dynamic simulation. The results obtained from this simulation show that, in spite of the equivalent settings, the effect Grid-Tied and Grid-Supporting VSMs is different in the first moments following a power unbalance. Grid-Tied systems response is dominated by the internal current control and therefore is faster and less sensitive to the inertia support requirements while Grid-Supporting systems response is coupled to inertia requirements due to the emulation of a SG swing equation. Grid-Supporting systems present a slower response, thus providing more energy to the system. It is shown that the coupling of Grid-Supporting systems dynamic response to inertia requirements can lead to stability problems in the Microgrid.

A model of different Grid-Supporting VSM implementations is presented in order to understand the underlying synchronizing mechanism. It is shown that the synchronism is possible because of the existing coupling between active power and power angle on power systems that introduces a negative feedback of the phase displacement when power and frequency are coupled by the VSM control system, leading to a stable operation. This effect is analogous to the synchronizing torque of traditional Synchronous Generators. Several grid-supporting VSM models are compared in order to show that this effect is common to all of them.

A model of a grid-connected VSC is used to demonstrate that there is a dynamic coupling between reactive power and power angle that can be used to ensure synchronization in an analogous way to the coupling between active power and power angle used by Grid-Supporting VSMs. A new synchronization

system, called Reactive Power Synchronization (RPS), is proposed to take advantage of this coupling. Simulation and experimental results are presented to show how this system allows a VSC to synchronize to the grid without relying on frequency measurement systems such as PLLs.

Based on the RPS system, a solution for the black-start of WECSs is proposed. This solution is intended to support the Power System Restoration through the establishment of islanded Microgrids with black-start capabilities. A case study where two WECSs connected in parallel are operated following a black out is presented. The solution includes a novel droop regulation between active power and voltage in order to share the local loads among multiple WECSs. The proposed RPS allows both WECSs to synchronize with each other and with the grid. In case one of the WECSs is not able to supply its share of the load, it is automatically supplied by the remaining WECSs and all the units remain in synchronism.

The proposed solutions have been validated with experimental results of a grid connected VSC under the proposed RPS and a complete Full-Converter WECS operating in islanded mode.

7.2 Original contributions

The main original contributions of this Thesis are:

- **Demonstration of the dynamic coupling between reactive power and power angle through the model of a grid-connected VSC:** The presented model shows that reactive power can be used as a synchronizing mechanism. Most of the previous studies on synchronous operation of VSCs were based on the quasi-static relationships of active power with power angle and reactive power with voltage magnitude while the ones that presented a dynamic model did not focus on the relation between reactive power and power angle.

- **Novel synchronizing algorithm for VSCs based on the regulation of reactive power:** The presented algorithm shares one of the most promising features of power/frequency droops and Virtual Synchronous Machines: avoiding the use of a PLL and providing a synchronizing torque. Moreover, with the proposed system, the active power regulation scheme of the VSC remains unchanged. The proposed control system includes internal current regulation loops that avoid overcurrents in the VSC, solving one of the main drawbacks of VSM control systems. The proposal has been validated by experimental results of a grid-connected VSC.

- **Novel solution for damping low-frequency oscillations:** Based on the dynamic coupling between reactive power and power angle, a new damping mechanism is proposed where the quadrature component of a VSC current, which it is proportional to reactive power, is used to damp low frequency oscillations through variations of the VSC voltage quadrature component, which it is proportional to the VSC voltage phase.

- **Solution for the black-start of full-converter WECSs:** This Thesis proposes a control system designed to perform a black start in a wind farm, without relying on any additional systems. For black start, WECSs must be able to regulate the local frequency and voltage, in contrast with their most common operation mode in which they are controlled to extract the maximum power available from the wind. Generation and demand must be balanced so WECSs must extract from the wind only the power demanded by the loads. The proposed solution includes the control of the WECS pitch angle and the generator side (GSC) and line side (LSC) power converters. The LSC includes the proposed RPS control that allows the synchronization of multiple WECSs. The WECSs active power is controlled through a droop control that uses a relation between voltage and active power in order to share the load between WECSs. The pitch angle is regulated to ensure that the WECSs extracts from the wind only the power demanded by the loads. The GSC regulates the DC-link voltage, ensuring the transmission of the power required by the LSC. Another important feature is that the proposed control system allows a hot-swapping to a grid-connected mode.

- **Analysis of the emulated inertial response provided by solutions both with and without the use of a PLL:** Solutions with both PLL and SG-based synchronizing mechanisms have been reported to emulate the inertial response of SGs. In order to study the effect of the synchronization system on the resulting emulated inertial response, representative solutions of both Grid-Tied and Grid-Supporting VSM control systems have been modeled and implemented with equivalent emulated inertia characteristics in a dynamic simulation. Results show the contribution of a BESS, controlled under the different VSM implementations, to the inertia support of an isolated MG following a load variation. Differences emerge when the analysis is performed for the first moments following a load disturbance. For the PLL-based solutions, the initial dynamics are dominated by the low-level current control, resulting in fast under-damped oscillations. The effect of the derivative component is small, as the results for the VI and Droop implementations are very close. On the other hand, Grid-Supporting systems present a slower response, defined by the emulated swing equation, resulting in a higher amount of energy exchanged but also on a higher sensitivity of the MG stability to the emulated inertia requirements.

7.3 Publications

- A. P. Asensio, S. A. Gómez, J. L. Rodriguez-Amenedo, M.A. Cardiel-Alvarez, “Reactive Power Synchronization Method for Voltage Sourced Converters,” IEEE Transactions On Sustainable Energy, 2019. *In review.*

- A. P. Asensio, S. A. Gómez, J. L. Rodriguez-Amenedo, M.A. Cardiel-Alvarez, “Distributed Fre-

quency Control for Black Start of Full-Converter Wind Turbines," IEEE Transactions On Power Systems, 2019. *In review.*

- A. P. Asensio, S. A. Gómez, J. L. Rodriguez-Amenedo, M. G. Plaza, J. E. G. Carrasco, and J. M. A. M. De Las Morenas, "A Voltage and Frequency Control Strategy for Stand-Alone Full Converter Wind Energy Conversion Systems," Energies, vol. 11, no. 3, p. 474, 2018.

- A. P. Asensio, S. A. Gomez, J. L. Rodriguez Amenedo, M. G. Plaza and M. Prodanovic, "Real-time operation of a centralized Energy Management System for an islanded Microgrid," The Renewable Energy & Power Quality Journal, vol. 1, no. 16, 2018.

- A. P. Asensio, M. G. Plaza, S. A. Gomez, J. L. Rodriguez Amenedo, J. E.-G. Carrasco and J. Alonso-Martinez, "Isolated operation of wind energy system in critical micro-grid," The Renewable Energy & Power Quality Journal, vol. 1, no. 15, 2017.

- A. P. Asensio, S. A. Gomez, J. L. Rodriguez Amenedo, J. Alonso-Martinez, M. G. Plaza, and J. E.-G. Carrasco, "Master of power: A power plant controller and energy management system concept," in 2017 IEEE PES Innovative Smart Grid Technologies Conference - Latin America (ISGT Latin America), 2017, vol. 2017–Janua, pp. 1–6.

7.4 Funding

This Thesis has been supported by the Autonomous Community of Madrid under the PRICAM project (S2013-ICE-2933).

Appendix A

Description of the set-up used to obtain experimental results.

Contents

A.1 Grid-connected Voltage Sourced Converter. 99
A.2 Isolated wind turbine system. 101

For this Thesis, two different test benchs have been developed with the support of the Power Control Group (GSP) of the Electrical Engineering department of Universidad Carlos III de Madrid. These test benchs have been used to obtain the experimentals results presented throughout the Thesis.

Section A.1 describes the set-up of a grid-connected VSC that was used to validate the proposed RPS presented in Chapter 5 while Section A.2 describes the isolated wind turbine emulator used to validate the control system presented in Section 6.2.

A.1 Grid-connected Voltage Sourced Converter.

The diagram of the experimental set-up used to obtain the real-time results is depicted in Fig. A.1. This set-up consists of a commercial three-phase two-level VSC (BGRID) with a rated power of 300kW and a switching frequency of 3.35kHz equal to the sampling frequency, which includes a 0.2mH/200μF LC filter. An overview picture of the set-up is presented in Fig. A.2.

The inverter is fed by a three-phase diode rectifier composed of three SEMIKRON SKKD46 mono-phase diode branches, in order to provide a dc bus voltage of around 550 V, which gives enough head-room to connect the inverter to a 400-V grid through a 230/400-V DY isolation transformer. A picture of these elements is shown in Fig. A.3.

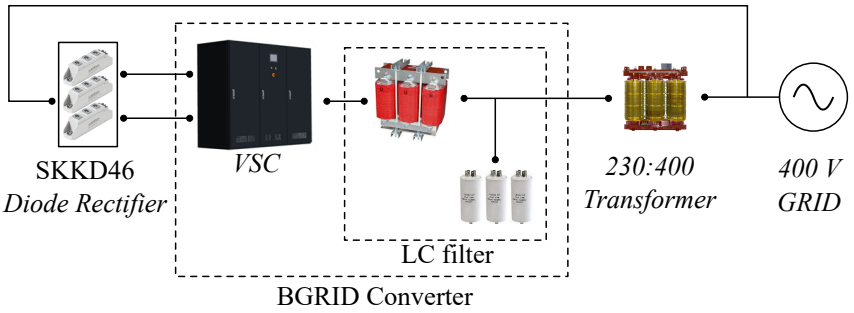

Figure A.1: Schematic diagram of the set-up configuration used in the real-time experiments

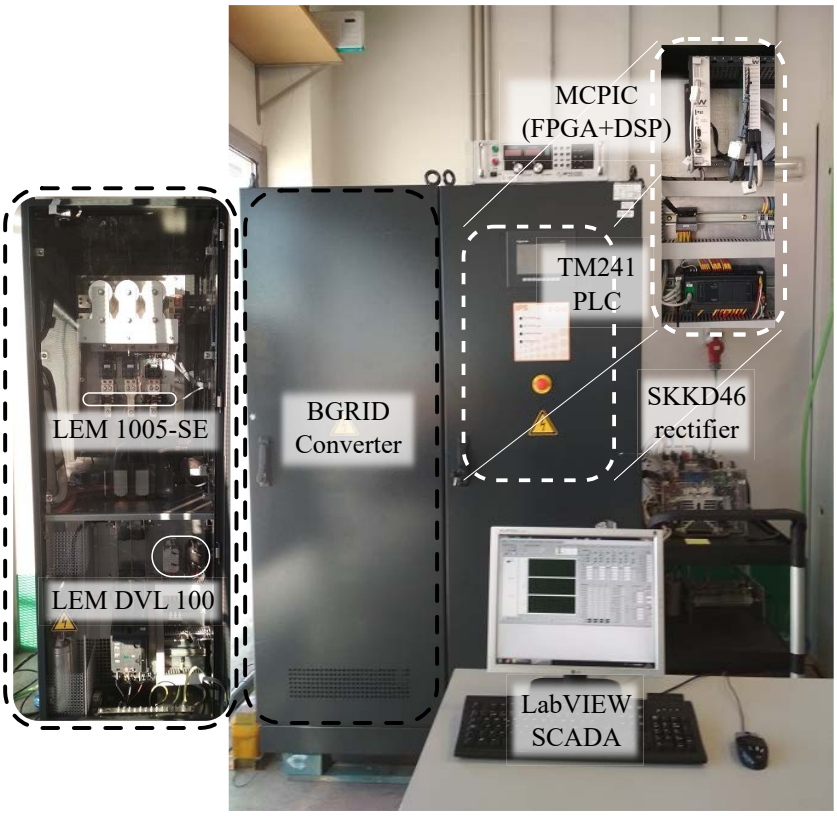

Figure A.2: Overview of the set-up used in the real-time experiments.

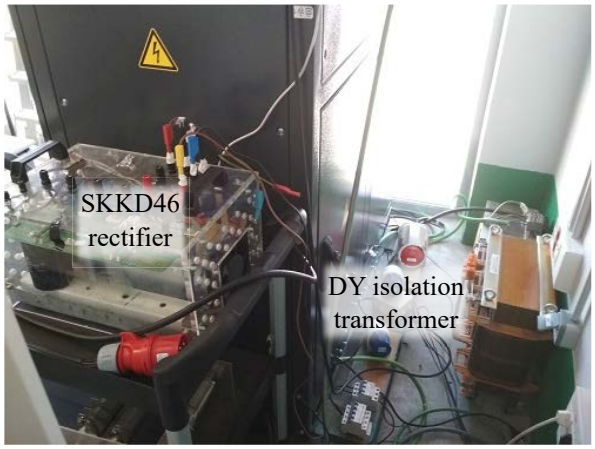

Figure A.3: Picture of the diode rectifier and transformer used in the real-time experiments.

The presented results have been obtained with dedicated measuring instruments that are included in the BGRID converter presented in Fig. A.2. The hardware components used for measurement were:

- 2 LEM DVL 100 voltage transducers (1000V) for measuring the converter output voltage. Line voltages v_{ab} and v_{ab}, as defined in Fig. 5.1 of Chapter 5, were measured.
- 2 LEM 1005-SE current transformers (1000A) for measuring the converter output currents. Line currents i_a and i_c, as defined in Fig. 5.1 of Chapter 5, were measured.

The rest of the represented variables were calculated from these measurements. The analogue to digital conversion was performed by the FPGA of the MCPIC control board, which is a commercial solution by WYNNERTECH. Input signals are low-pass filtered at 10KHz.

Finally, the digital measurements of the control board are transmitted through an ethernet UDP communication at the controller sampling time (298 μs) to a dedicated SCADA software developed in the LabVIEW environment (version 2014, Copyright 1986-2014, National Instruments). The LabVIEW environment includes the possibility to save the data in .csv format, which was used to obtain the data used for the presented results. A capture of the control interface used to obtain the data is shown in Fig. A.4 for an active power step.

Another capture with instantaneous values is shown in Fig. A.5. This figure shows the same current harmonic components that are present in the experimental results of Fig. 5.12.

A.2 Isolated wind turbine system.

This appendix describes in more detail the WT emulation system used for the real-time implementation of the control system presented in Section 6.2.

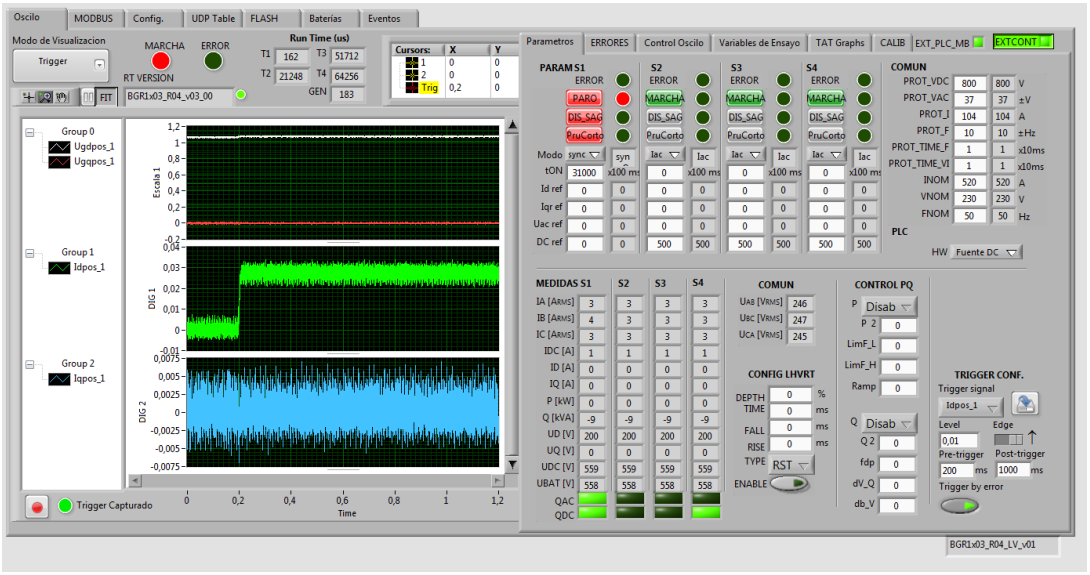

Figure A.4: Capture of the Human Machine Interface (HMI) used in the real-time experiments for an active power step.

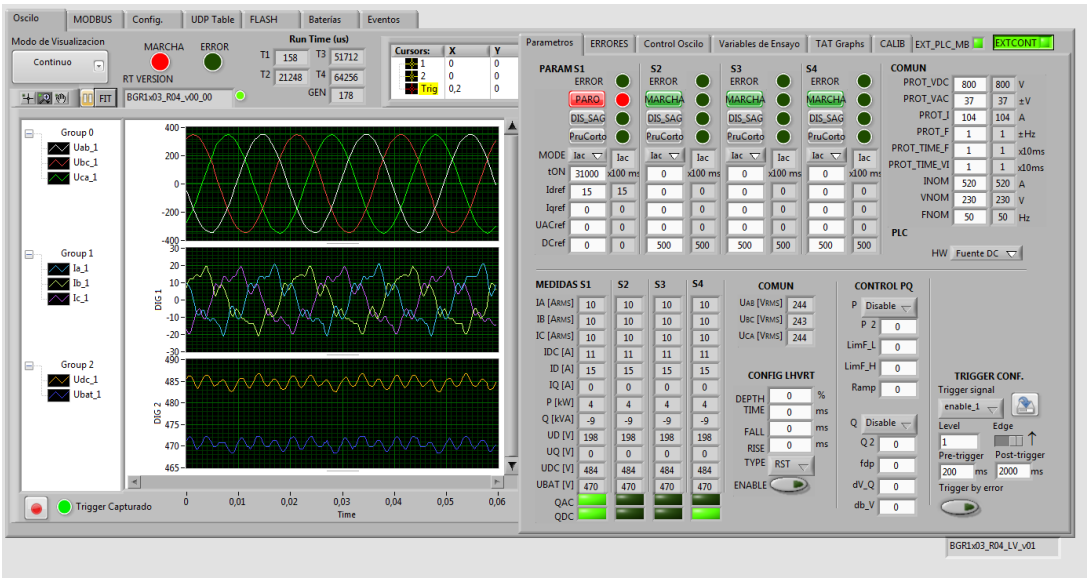

Figure A.5: Capture of the Human Machine Interface (HMI) used in the real-time experiments with instantaneous values.

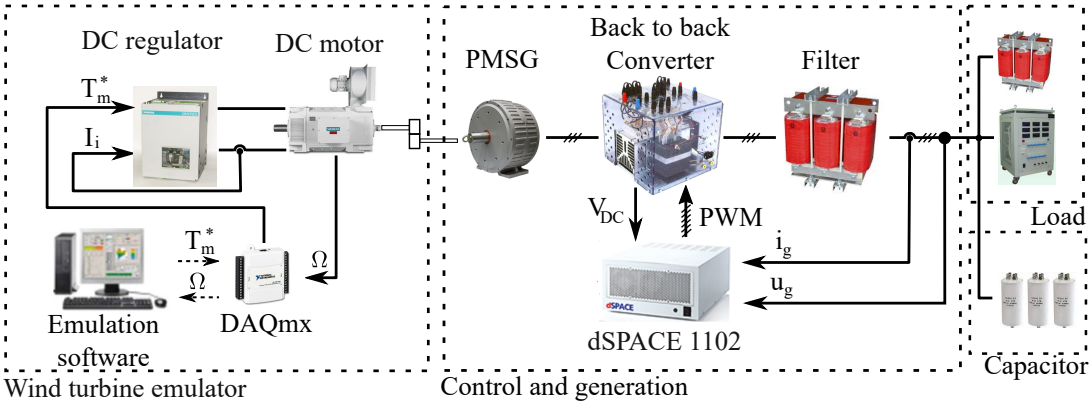

Figure A.6: Test bench used for real-time experiments of the isolated Full-Converter system. PWM: pulse-width modulation.

WT emulation is based on a DC electrical drive that applies the emulated WT torque to the mechanical axis of the PMSG. An schematic diagram is shown in Fig. A.6. The load could not be emulated as a constant power source, as in the simlated results presented in Section 6.2; instead a resistor and a reactance were used.

The emulation system uses both hardware and software elements. Hardware includes:

- SIMOREG 6RA23s driver (Figure A.7a), to regulate de DC motor.
- DAQmx USB-6009 model DAC (Digital to Analog Converter), from National Instruments, to provide the analogue torque reference (Figure A.7a).
- SEMIKRON SEMITEACH Power Converter stack, including a three phase inverter, composed of three SKM 50 GB 123 D dual IGBT modules, and an SKKD45 three phase diode rectifier (Figure A.7b).
- 1GG5 SIEMENS DC motor (Figure A.7c)
- Bornay INCLIN 3000 PMSG (Figure A.7d).

The digital torque reference for the DC motor driver is generated from a LabVIEW (version 2014, Copyright 1986-2014, National Instruments) program, running on a PC with a sample time of 100 ms, which is considered sufficient to simulate the WT dynamics. A capture of the software Human-Machine Interface (HMI) is presented in Figure A.8.

The LabVIEW software was used to obtain the measurements of the WT data such as pitch angle and rotational speed. For electrical dalta, a Chauvin Arnoux C.A 8335 Power Analyzer, as shown in Figure A.9, was used.

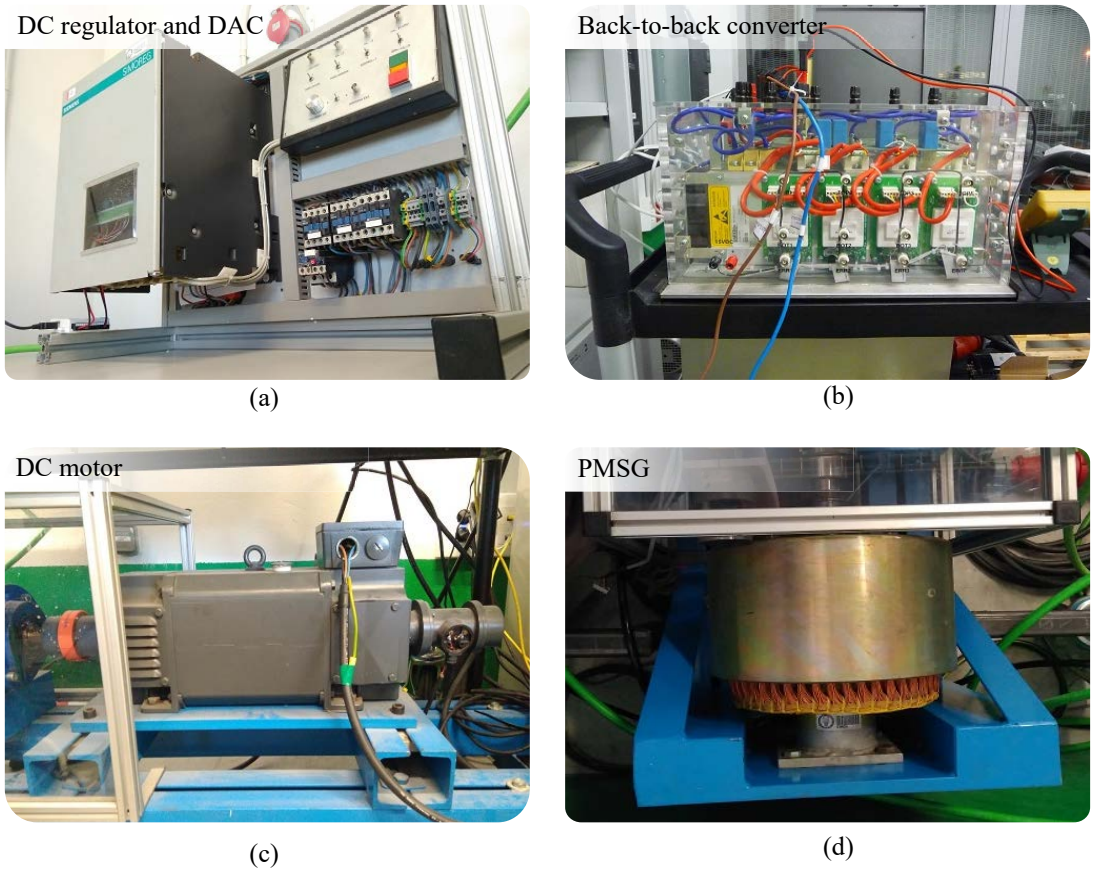

Figure A.7: Pictures of the elements used for the Wind Turbine emulator including (a) the DC motor driver, (b) the back-to-back converter, (c) the DC motor and (d) the Permanent Magnet Synchronous Generator (PMSG).

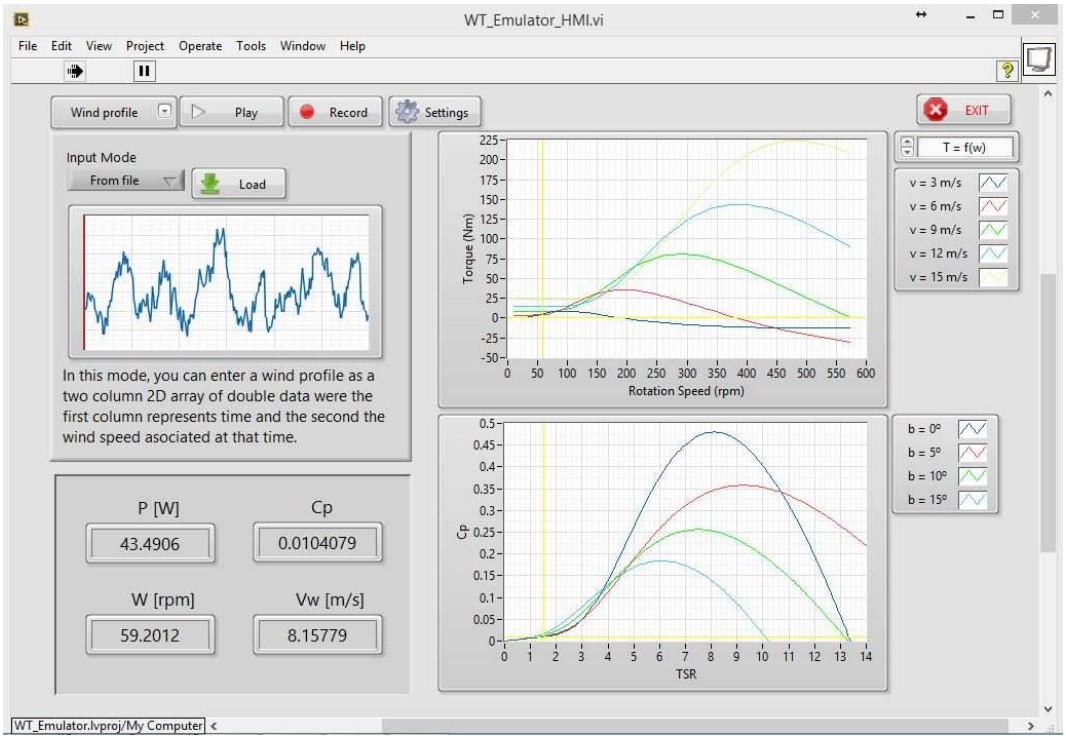

Figure A.8: Capture of the Human-Machine Interface (HMI) of the LabVIEW software used for the Wind Turbine emulator.

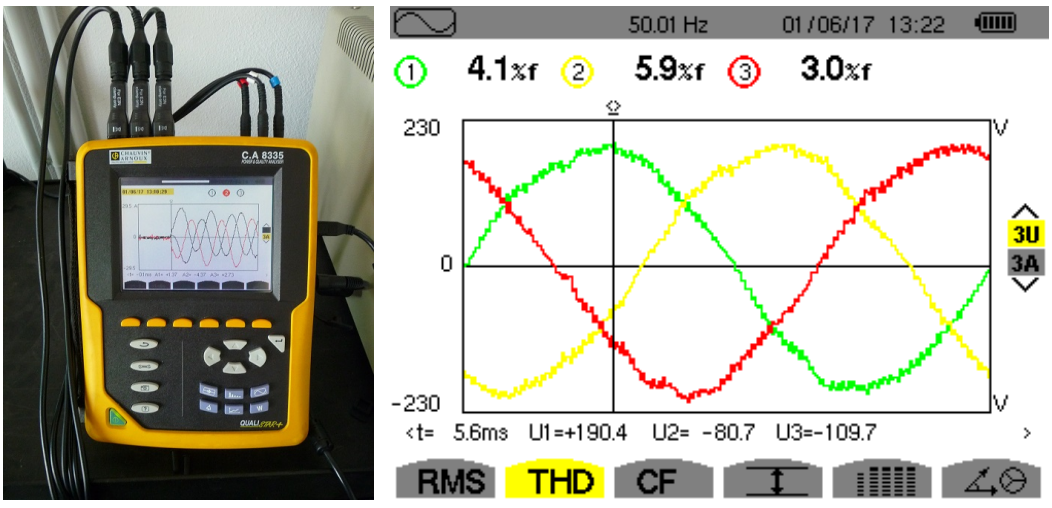

(a) (b)

Figure A.9: Power Analyzer used for electrical measurements of the Wind Turbine emulator including (a) a picture of the Power Analyzer and (b) results of the voltage measured during the tests.

Bibliography

[1] M. G. L. Prabha Kundur, Neal J. Balu, *Power system stability and control*. McGraw-hill New York, 1994, vol. 7.

[2] J. K. Kaldellis and D. Zafirakis, "The wind energy (r)evolution: A short review of a long history," *Renewable Energy*, vol. 36, no. 7, pp. 1887–1901, jul 2011.

[3] Y. Amirnaser and I. Reza, *Voltage-Sourced Converters in Power Systems : Modeling, Control, and Applications*. John Wiley & Sons, 2010.

[4] H. Lund and B. V. Mathiesen, "Energy system analysis of 100% renewable energy systems-The case of Denmark in years 2030 and 2050," *Energy*, vol. 34, no. 5, pp. 524–531, 2009.

[5] R. Lasseter, A. Akhil, C. Marnay, J. Stephens, J. Dagle, R. Guttromson, A. Sakis Meliopoulous, R. Yinger, and J. Eto, "The CERTS MicroGrid Concept, white paper on Integration of Distributed Energy Resources," *California Energy Commission, Office of Power Technologies-US Department of Energy, LBNL-50829,*, 2002.

[6] G. Pepermans, J. Driesen, D. Haeseldonckx, R. Belmans, and W. D'haeseleer, "Distributed generation: definition, benefits and issues," *Energy Policy*, vol. 33, no. 6, pp. 787–798, apr 2005.

[7] IEEE Standard Conformance, *IEEE Standard Conformance Test Procedure for Equipment Interconnecting Distributed Resources with Electric Power Systems*. Institute of Electrical and Electronics Engineers, 2005, no. July.

[8] D. T. Ton and M. A. Smith, "The U.S. Department of Energy's Microgrid Initiative," *Electricity Journal*, vol. 25, no. 8, pp. 84–94, oct 2012.

[9] A. Hirsch, Y. Parag, and J. Guerrero, "Microgrids: A review of technologies, key drivers, and outstanding issues," *Renewable and Sustainable Energy Reviews*, vol. 90, pp. 402–411, jul 2018.

[10] H. Konishi, "A consideration of stable operating power limits in VSC-HVDC systems," in *Seventh International Conference on AC and DC Transmission*, vol. 2001, 2001, pp. 102–106.

[11] D. Dong, B. Wen, D. Boroyevich, P. Mattavelli, and Y. Xue, "Analysis of phase-locked loop low-frequency stability in three-phase grid-connected power converters considering impedance interactions," *IEEE Transactions on Industrial Electronics*, vol. 62, no. 1, pp. 310–321, 2015.

[12] National Grid, "Performance of Phase-Locked Loop Based Converters," National Grid, Tech. Rep., 2017.

[13] J. Ma, Y. Qiu, Y. Li, W. Zhang, Z. Song, and J. S. Thorp, "Research on the impact of DFIG virtual inertia control on power system small-signal stability considering the phase-locked loop," pp. 2094–2105, 2017.

[14] National Grid, "Black Start from Distributed Sources," National Grid, Tech. Rep., 2017.

[15] L. Zhang, L. Harnefors, and H. P. Nee, "Power-synchronization control of grid-connected voltage-source converters," *IEEE Transactions on Power Systems*, vol. 25, no. 2, pp. 809–820, 2010.

[16] M. Yu, A. J. Roscoe, C. D. Booth, A. Dyśko, R. Ierna, J. Zhu, and H. Urdal, "Use of an inertia-less Virtual Synchronous Machine within future power networks with high penetrations of converters," in *19th Power Systems Computation Conference, PSCC 2016*, jun 2016, pp. 1–7.

[17] P. Asmus, "Microgrids, Virtual Power Plants and Our Distributed Energy Future," *Electricity Journal*, vol. 23, no. 10, pp. 72–82, 2010.

[18] F. Martin-Martínez, A. Sánchez-Miralles, and M. Rivier, "A literature review of Microgrids: A functional layer based classification," *Renewable and Sustainable Energy Reviews*, vol. 62, pp. 1133–1153, 2016.

[19] IEC, "IEC 62116:2014: Utility-interconnected photovoltaic inverters - Test procedure of islanding prevention measures," IEC, Tech. Rep., 2014.

[20] Institute of Electrical and Electronics Engineers, "IEEE Standard for Interconnection and Interoperability of Distributed Energy Resources with Associated Electric Power Systems Interfaces," *IEEE Std 1547-2018 (Revision of IEEE Std 1547-2003)*, pp. 1–138, 2018.

[21] R. Lasseter, "MicroGrids," in *2002 IEEE Power Engineering Society Winter Meeting. Conference Proceedings (Cat. No.02CH37309)*, vol. 1, 2002, pp. 305–308.

[22] F. M. A.-S. Magdi S. Mahmoud, *Control and optimization of distributed generation systems*. Springer, 2015.

[23] P. Lombardi, M. Powalko, and K. Rudion, "Optimal operation of a virtual power plant," in *2009 IEEE Power and Energy Society General Meeting, PES '09*. IEEE, 2009, pp. 1–6.

[24] D. E. Olivares, A. Mehrizi-Sani, A. H. Etemadi, C. A. Cañizares, R. Iravani, M. Kazerani, A. H. Hajimiragha, O. Gomis-Bellmunt, M. Saeedifard, R. Palma-Behnke, G. A. Jiménez-Estévez, and N. D. Hatziargyriou, "Trends in microgrid control," *IEEE Transactions on Smart Grid*, vol. 5, no. 4, pp. 1905–1919, 2014.

[25] S. Parhizi, H. Lotfi, A. Khodaei, and S. Bahramirad, "State of the art in research on microgrids: A review," *IEEE Access*, vol. 3, pp. 890–925, 2015.

[26] P. Piagi and R. Lasseter, "Autonomous control of microgrids," in *2006 IEEE Power Engineering Society General Meeting*, 2006, p. 8 pp.

[27] H. Bevrani, B. Francois, and T. Ise, *Microgrid dynamics and control*. John Wiley & Sons, 2017.

[28] E. Solutions, C. Gee, and P. Manager, "CERTS Microgrid Demonstration with Large scale Energy Storage & Renewable Generation," *ieeexplore.ieee.org*, no. November, 2010.

[29] R. Lasseter, A. Abbas, C. Marnay, J. Stevens, J. Dagle, R. Guttromson, A. S. Meliopoulos, R. Yinger, and J. Eto, "Integration of Distributed Energy Resources: The CERTS Microgrid Concept California Energy Commission," *P500-03 F*, vol. 89, 2003.

[30] L. Mariam, M. Basu, and M. F. Conlon, "Microgrid: Architecture, policy and future trends," *Renewable and Sustainable Energy Reviews*, vol. 64, pp. 477–489, 2016.

[31] O. Palizban, K. Kauhaniemi, and J. M. Guerrero, "Microgrids in active network management - Part I: Hierarchical control, energy storage, virtual power plants, and market participation," *Renewable and Sustainable Energy Reviews*, vol. 36, pp. 428–439, 2014.

[32] J. M. Guerrero, J. C. Vasquez, J. Matas, L. G. de Vicuna, and M. Castilla, "A1 - Hierarchical Control of Droop-Controlled AC and DC Microgrids—A General Approach Toward Standardization," *IEEE Transactions on Industrial Electronics*, vol. 58, no. 1, pp. 158–172, 2011.

[33] F. Katiraei, R. Iravani, N. Hatziargyriou, and A. Dimeas, "Microgrids management," *IEEE Power and Energy Magazine*, vol. 6, no. 3, pp. 54–65, 2008.

[34] J. K. Gruber, F. Huerta, P. Matatagui, and M. Prodanović, "Advanced building energy management based on a two-stage receding horizon optimization," *Applied Energy*, vol. 160, pp. 194–205, 2015.

[35] D. Ton and J. Reilly, "Microgrid Controller Initiatives: An Overview of R&D by the U.S. Department of Energy," *IEEE Power and Energy Magazine*, vol. 15, no. 4, pp. 24–31, jul 2017.

[36] G. Joos, J. Reilly, W. Bower, and R. Neal, "The need for standardization," *IEEE Power and Energy Magazine*, vol. 15, no. 4, pp. 32–40, jul 2017.

[37] R. Lasseter, A. Akhil, C. Marnay, J. Stephens, J. Dagle, R. Guttromson, A. S. Meliopoulous, R. Yinger, and J. Eto, "Consortium for Electric Reliability Technology Solutions White Paper on Integration of Distributed Energy Resources The CERTS MicroGrid Concept," *Program, Transmission Reliability Systems, Energy Program, Integration Interest, Public Commission, California Energy*, no. April, pp. 1–29, 2002.

[38] R. Firestone and C. Marnay, "Energy Manager Design for Microgrids - LBNL No. 54447," *Contract*, no. 150, p. 58, 2005.

[39] J. Moreno, M. E. Ortúzar, and J. W. Dixon, "Energy-management system for a hybrid electric vehicle, using ultracapacitors and neural networks," *IEEE Transactions on Industrial Electronics*, vol. 53, no. 2, pp. 614–623, 2006.

[40] D. Weisser, "On the economics of electricity consumption in small island developing states: A role for renewable energy technologies?" *Energy Policy*, vol. 32, no. 1, pp. 127–140, jan 2004.

[41] S. A. Papathanassiou and N. G. Boulaxis, "Power limitations and energy yield evaluation for wind farms operating in island systems," *Renewable Energy*, vol. 31, no. 4, pp. 457–479, apr 2006.

[42] D. Linden and T. Reddy, *Handbook of batteries*. McGraw-Hill Companies, Inc., New York2002,(1.3-1.17, 7.10-7.11, 22.12-22.13), 1995, vol. 36, no. 4.

[43] J. Fang, Y. Tang, H. Li, and X. Li, "A Battery/Ultracapacitor Hybrid Energy Storage System for Implementing the Power Management of Virtual Synchronous Generators," *IEEE Transactions on Power Electronics*, vol. 33, no. 4, pp. 2820–2824, apr 2018.

[44] W.-G. Früh, "Optimising the use of a battery in a wind-diesel-battery hybrid island grid using power prediction and day-ahead optimisation," *International Conference on Renewable Energies and Power Quality (ICREPQ'16)*, vol. 14, no. 14, 2016.

[45] H. Kanchev, D. Lu, F. Colas, V. Lazarov, and B. Francois, "Energy management and operational planning of a microgrid with a PV-based active generator for smart grid applications," *IEEE Transactions on Industrial Electronics*, vol. 58, no. 10, pp. 4583–4592, 2011.

[46] F. Katiraei, M. R. Iravani, and P. W. Lehn, "Micro-grid autonomous operation during and subsequent to islanding process," *IEEE Transactions on Power Delivery*, vol. 20, no. 1, pp. 248–257, jan 2005.

[47] S. Hong, T.; Fan, "Probabilistic electric load forecasting: A tutorial review," *International Journal of Forecasting*, vol. 32, no. 3, pp. 914–938, 2016.

[48] Y. Kabalci, "A survey on smart metering and smart grid communication," *Renewable and Sustainable Energy Reviews*, vol. 57, no. Supplement C, pp. 302–318, may 2016.

[49] a. Oudalov and D. Chartouni, "Value analysis of battery energy storage applications in power systems," in *Power Systems ...* . IEEE, 2006, pp. 2206–2211.

[50] L. Xiangjun, H. Dong, and L. Xiaokang, "Battery Energy Storage Station (BESS)-Based Smoothing Control of Photovoltaic (PV) and Wind Power Generation Fluctuations," *IEEE Transactions on Sustainable Energy*, vol. 4, no. 2, pp. 464–473, 2013.

[51] U. Focken, M. Lange, K. Mönnich, H. Waldl, H. Beyer, and A. Luig, "A statistical analysis of the reduction of the wind power prediction error by spatial smoothing effects," *Journal of Wind Engineering and Industrial Aerodynamics*, vol. 90, no. July 2001, pp. 231–246, 2002.

[52] T. H.-J. T.-J. Kim, K. Brancik, D. Dickinson, A. Perrig, B. Sinopoli, Y. Mo, and H. Lee, "Cyber–Physical Security of a Smart Grid Infrastructure," *Proceedings of the IEEE*, vol. 100, no. 1, pp. 195–209, 2012.

[53] M. H. Rehmani, M. Reisslein, A. Rachedi, M. Erol-Kantarci, and M. Radenkovic, "Integrating Renewable Energy Resources Into the Smart Grid: Recent Developments in Information and Communication Technologies," *IEEE Transactions on Industrial Informatics*, vol. 14, no. 7, pp. 2814–2825, jul 2018.

[54] H. Farhangi, "The path of the smart grid," *IEEE Power and Energy Magazine*, vol. 8, no. 1, pp. 18–28, 2010.

[55] S. Rusitschka, K. Eger, and C. Gerdes, "Smart Grid Data Cloud: A Model for Utilizing Cloud Computing in the Smart Grid Domain," in *2010 First IEEE International Conference on Smart Grid Communications*. IEEE, oct 2010, pp. 483–488.

[56] National Grid, "Operability Strategy Report," National Grid ESO, Tech. Rep. November, 2018.

[57] J. Rocabert, A. Luna, F. Blaabjerg, and P. Rodríguez, "Control of power converters in AC microgrids," *IEEE Transactions on Power Electronics*, vol. 27, no. 11, pp. 4734–4749, 2012.

[58] J. Beerten, S. Cole, and R. Belmans, "Modeling of multi-terminal vsc hvdc systems with distributed dc voltage control," *IEEE Transactions on Power Systems*, vol. 29, no. 1, pp. 34–42, 2014.

[59] R. Peña, J. Clare, and G. Asher, "A doubly fed induction generator using back-to-back PWM converters supplying an isolated load from a variable speed wind turbine," *Electric Power Applications, IEE . . .*, vol. I, no. 5, pp. 380–387, 1996.

[60] A. P. Asensio, S. A. Gómez, J. L. Rodriguez-Amenedo, M. G. Plaza, J. E. G. Carrasco, and J. M. A. M. De Las Morenas, "A voltage and frequency control strategy for stand-alone full converter wind energy conversion systems," *Energies*, vol. 11, no. 3, p. 474, 2018.

[61] N. Mendis, K. M. Muttaqi, and S. Perera, "Management of battery-supercapacitor hybrid energy storage and synchronous condenser for isolated operation of PMSG based variable-speed wind turbine generating systems," *IEEE Transactions on Smart Grid*, vol. 5, no. 2, pp. 944–953, 2014.

[62] G. Martínez-Lucas, J. Sarasúa, and J. Sánchez-Fernández, "Frequency Regulation of a Hybrid Wind–Hydro Power Plant in an Isolated Power System," *Energies*, vol. 11, no. 1, p. 239, jan 2018.

[63] S. A. Daniel and N. AmmasaiGounden, "A novel hybrid isolated generating system based on PV fed inverter-assisted wind-driven induction generators," *IEEE Transactions on Energy Conversion*, vol. 19, no. 2, pp. 416–422, jun 2004.

[64] F. P. Demello and C. Concordia, "Concepts of Synchronous Machine Stability as Affected by Excitation Control," in *IEEE Transactions on Power Apparatus and Systems*, vol. PAS-88, no. 4. Citeseer, 1969, pp. 316–329.

[65] Q. C. Zhong, "Robust droop controller for accurate proportional load sharing among inverters operated in parallel," *IEEE Transactions on Industrial Electronics*, vol. 60, no. 4, pp. 1281–1290, 2013.

[66] M. C. Chandorkar, D. M. Divan, and R. Adapa, "Control of parallel connected inverters in standalone ac supply systems," *IEEE Transactions on Industry Applications*, vol. 29, no. 1, pp. 136–143, 1993.

[67] J. W. Simpson-Porco, F. Dörfler, and F. Bullo, "Synchronization and power sharing for droop-controlled inverters in islanded microgrids," *Automatica*, vol. 49, no. 9, pp. 2603–2611, 2013.

[68] S. D'Arco and J. A. Suul, "Equivalence of virtual synchronous machines and frequency-droops for converter-based Microgrids," *IEEE Transactions on Smart Grid*, vol. 5, no. 1, pp. 394–395, 2014.

[69] E. Barklund, N. Pogaku, M. Prodanovic, C. Hernandez-Aramburo, and T. C. Green, "Energy management in autonomous microgrid using stability-constrained droop control of inverters," *IEEE Transactions on Power Electronics*, vol. 23, no. 5, pp. 2346–2352, 2008.

[70] J. Liu, Y. Miura, and T. Ise, "Comparison of Dynamic Characteristics between Virtual Synchronous Generator and Droop Control in Inverter-Based Distributed Generators," *IEEE Transactions on Power Electronics*, vol. 31, no. 5, pp. 3600–3611, may 2016.

[71] Q. C. Zhong, "Virtual Synchronous Machines: A unified interface for grid integration," *IEEE Power Electronics Magazine*, vol. 3, no. 4, pp. 18–27, 2016.

[72] Y. Ma, W. Cao, L. Yang, F. F. Wang, and L. M. Tolbert, "Virtual Synchronous Generator Control of Full Converter Wind Turbines with Short-Term Energy Storage," *IEEE Transactions on Industrial Electronics*, vol. 64, no. 11, pp. 8821–8831, nov 2017.

[73] J. A. Suul, S. D'Arco, and G. Guidi, "Virtual Synchronous Machine-Based Control of a Single-Phase Bi-Directional Battery Charger for Providing Vehicle-to-Grid Services," *IEEE Transactions on Industry Applications*, vol. 52, no. 4, pp. 3234–3244, jul 2016.

[74] L. Zhang, L. Harnefors, and H. P. Nee, "Interconnection of two very weak AC systems by VSC-HVDC links using power-synchronization control," *IEEE Transactions on Power Systems*, vol. 26, no. 1, pp. 344–355, 2011.

[75] H. P. Beck and R. Hesse, "Virtual synchronous machine," in *2007 9th International Conference on Electrical Power Quality and Utilisation, EPQU*. IEEE, 2007, pp. 1–6.

[76] U. Tamrakar, D. Shrestha, M. Maharjan, B. Bhattarai, T. Hansen, and R. Tonkoski, "Virtual Inertia: Current Trends and Future Directions," *Applied Sciences*, vol. 7, no. 7, p. 654, 2017.

[77] J. Svensson, "Synchronisation methods for grid-connected voltage source converters," *IEE Proceedings - Generation, Transmission and Distribution*, vol. 148, no. 3, p. 229, 2001.

[78] F. Blaabjerg, R. Teodorescu, M. Liserre, and A. V. Timbus, "Overview of control and grid synchronization for distributed power generation systems," *IEEE Transactions on Industrial Electronics*, vol. 53, no. 5, pp. 1398–1409, 2006.

[79] H. Han, X. Hou, J. Yang, J. Wu, M. Su, and J. M. Guerrero, "Review of power sharing control strategies for islanding operation of AC microgrids," *IEEE Transactions on Smart Grid*, vol. 7, no. 1, pp. 200–215, jan 2016.

[80] M. Marwali and a. Keyhani, "Control of distributed generation systems-Part I: Voltages and currents control," *IEEE Transactions on Power Electronics*, vol. 19, no. 6, pp. 1541–1550, 2004.

[81] K. De Brabandere, B. Bolsens, J. Van den Keybus, A. Woyte, J. Driesen, and R. Belmans, "A Voltage and Frequency Droop Control Method for Parallel Inverters," *IEEE Transactions on Power Electronics*, vol. 22, no. 4, pp. 1107–1115, jul 2007.

[82] J. M. Guerrero, M. Chandorkar, T. L. Lee, and P. C. Loh, "Advanced control architectures for intelligent microgrids. Part I : Decentralized and hierarchical control," *IEEE Transactions on Industrial Electronics*, vol. 60, no. 4, pp. 1254–1262, apr 2013.

[83] M. Ashabani, F. D. Freijedo, S. Golestan, and J. M. Guerrero, "Inducverters: PLL-Less Converters With Auto-Synchronization and Emulated Inertia Capability," *IEEE Transactions on Smart Grid*, vol. 7, no. 3, pp. 1660–1674, 2016.

[84] Q. C. Zhong and G. Weiss, "Synchronverters: Inverters that mimic synchronous generators," *IEEE Transactions on Industrial Electronics*, vol. 58, no. 4, pp. 1259–1267, 2011.

[85] Q. C. Zhong, P. L. Nguyen, Z. Ma, and W. Sheng, "Self-synchronized synchronverters: Inverters without a dedicated synchronization unit," *IEEE Transactions on Power Electronics*, vol. 29, no. 2, pp. 617–630, 2014.

[86] S. D'Arco and J. A. Suul, "Virtual synchronous machines - Classification of implementations and analysis of equivalence to droop controllers for microgrids," in *2013 IEEE Grenoble Conference PowerTech, POWERTECH 2013*. IEEE, 2013, pp. 1–7.

[87] D. Kottick, M. Blau, and D. Edelstein, "Battery Energy Storage for Frequency Regulation in an Island Power System," *IEEE Transactions on Energy Conversion*, vol. 8, no. 3, pp. 455–459, 1993.

[88] K. Visscher and S. De Haan, "Virtual synchronous machines (VSG'S) for frequency stabilisation in future grids with a significant share of decentralized generation," *CIRED Seminar 2008: SmartGrids for Distribution*, pp. 82–82, 2008.

[89] J. Morren, S. W. de Haan, W. L. Kling, and J. A. Ferreira, "Wind turbines emulating inertia and supporting primary frequency control," *IEEE Transactions on Power Systems*, vol. 21, no. 1, pp. 433–434, 2006.

[90] J. Mauricio, A. Marano, A. Gomez-Exposito, and J. Martinez Ramos, "Frequency Regulation Contribution Through Variable-Speed Wind Energy Conversion Systems," *IEEE Transactions on Power Systems*, vol. 24, no. 1, pp. 173–180, feb 2009.

[91] P. K. Keung, P. Li, H. Banakar, and B. T. Ooi, "Kinetic energy of wind-turbine generators for system frequency support," *IEEE Transactions on Power Systems*, vol. 24, no. 1, pp. 279–287, 2009.

[92] A. Teninge, C. Jecu, D. Roye, S. Bacha, J. Duval, and R. Belhomme, "Contribution to frequency control through wind turbine inertial energy storage," *IET Renewable Power Generation*, vol. 3, no. 3, pp. 358–370, 2009.

[93] N. R. Ullah, T. Thiringer, and D. Karlsson, "Temporary primary frequency control support by variable speed wind turbines - Potential and applications," *IEEE Transactions on Power Systems*, vol. 23, no. 2, pp. 601–612, 2008.

[94] L. Ruttledge and D. Flynn, "Emulated inertial response from wind turbines: Gain scheduling and resource coordination," *IEEE Transactions on Power Systems*, vol. 31, no. 5, pp. 3747–3755, 2016.

[95] Y.-z. Sun, Z.-s. Zhang, G.-j. Li, and J. Lin, "Review on frequency control of power systems with wind power penetration," in *2010 International Conference on Power System Technology*. IEEE, 2010, pp. 1–8.

[96] J. Ma, Y. Qiu, Y. Li, W. Zhang, Z. Song, and J. S. Thorp, "Research on the impact of DFIG virtual inertia control on power system small-signal stability considering the phase-locked loop," *IEEE Transactions on Power Systems*, vol. 32, no. 3, pp. 2094–2105, may 2017.

[97] R. Aouini, B. Marinescu, K. Ben Kilani, and M. Elleuch, "Synchronverter-Based Emulation and Control of HVDC Transmission," *IEEE Transactions on Power Systems*, vol. 31, no. 1, pp. 278–286, 2016.

[98] V. Knap, R. Sinha, M. Swierczynski, D.-I. Stroe, and S. Chaudhary, "Grid inertial response with Lithium-ion battery energy storage systems," in *2014 IEEE 23rd International Symposium on Industrial Electronics (ISIE)*, vol. 2014-July, no. July. IEEE, 2014, pp. 1817–1822.

[99] K. C. Divya and J. Østergaard, "Battery energy storage technology for power systems-An overview," *Electric Power Systems Research*, vol. 79, no. 4, pp. 511–520, apr 2009.

[100] A. Oudalov, D. Chartouni, and C. Ohler, "Optimizing a Battery Energy Storage System for Primary Frequency Control," *IEEE Transactions on Power Systems*, vol. 22, no. 3, pp. 1259–1266, aug 2007.

[101] S. K. Chung, "A phase tracking system for three phase utility interface inverters," *IEEE Transactions on Power Electronics*, vol. 15, no. 3, pp. 431–438, 2000.

[102] J. Roldán-Pérez, M. Prodanovic, and A. Rodríguez-Cabero, "Detailed discrete-time implementation of a battery-supported synchronverter for weak grids," in *Proceedings IECON 2017 - 43rd Annual Conference of the IEEE Industrial Electronics Society*, vol. 2017-Janua. IEEE, 2017, pp. 1083–1088.

[103] H. Wu, X. Ruan, D. Yang, X. Chen, W. Zhao, Z. Lv, and Q. C. Zhong, "Small-Signal Modeling and Parameters Design for Virtual Synchronous Generators," *IEEE Transactions on Industrial Electronics*, vol. 63, no. 7, pp. 4292–4303, 2016.

[104] C. Pradhan, C. N. Bhende, and A. K. Samanta, "Adaptive virtual inertia-based frequency regulation in wind power systems," *Renewable Energy*, vol. 115, pp. 558–574, jan 2018.

[105] G. Delille, B. François, and G. Malarange, "Dynamic frequency control support by energy storage to reduce the impact of wind and solar generation on isolated power system's inertia," *IEEE Transactions on Sustainable Energy*, vol. 3, no. 4, pp. 931–939, oct 2012.

[106] Á. Ortega and F. Milano, "Comparison of different PLL implementations for frequency estimation and control," in *Harmonics and Quality of Power (ICHQP), 2018 18th International Conference on*. IEEE, 2018, pp. 1–6.

[107] J. Van De Vyver, J. D. De Kooning, B. Meersman, L. Vandevelde, and T. L. Vandoorn, "Droop Control as an Alternative Inertial Response Strategy for the Synthetic Inertia on Wind Turbines," *IEEE Transactions on Power Systems*, vol. 31, no. 2, pp. 1129–1138, 2016.

[108] M. F. M. Arani and E. F. El-Saadany, "Implementing virtual inertia in DFIG-based wind power generation," *IEEE Transactions on Power Systems*, vol. 28, no. 2, pp. 1373–1384, 2013.

[109] F. P. Demello, R. J. Koessler, J. Agee, P. M. Anderson, J. H. Doudna, J. H. Fish, P. A. L. Hamm, P. Kundur, D. C. Lee, G. J. Rogers, and C. Taylor, "Hydraulic-Turbine and Turbine Control-Models for System Dynamic Studies," *Ieee Transactions on Power Systems*, vol. 7, no. 1, pp. 167–179, 1992.

[110] H. Kodama, T. Sugiyama, Y. Morimoto, Y. Oya, K. Okuno, N. Inoue, A. Sagara, and N. Noda, *Thermal annealing effects on chemical states of deuterium implanted into boron coating film*. McGraw-hill New York, 2003, vol. 313-316, no. SUPPL.

[111] H. Hanaoka, M. Nagai, and M. Yanagisawa, "Development of a novel parallel redundant UPS," *The 25th International Telecommunications Energy Conference, 2003. INTELEC '03.*, pp. 493–498, 2003.

[112] C. K. Sao and P. W. Lehn, "Control and power management of converter fed microgrids," *IEEE Transactions on Power Systems*, vol. 23, no. 3, pp. 1088–1098, 2008.

[113] J. M. Guerrero, N. Berbel, J. Matas, J. L. Sosa, J. Cruz, and A. Alentorn, "Decentralized Control for Parallel Operation of Distributed Generation," *IEEE Transactions on Industrial Electronics*, vol. 54, no. 2, pp. 1–10, 2007.

[114] E. A. A. Coelho, P. C. Cortizo, and P. F. D. Garcia, "Small-signal stability for parallel-connected inverters in stand-alone ac supply systems," *IEEE Transactions on Industry Applications*, vol. 38, no. 2, pp. 533–542, mar 2002.

[115] N. Pogaku, M. Prodanović, and T. C. Green, "Modeling, analysis and testing of autonomous operation of an inverter-based microgrid," *IEEE Transactions on Power Electronics*, vol. 22, no. 2, pp. 613–625, mar 2007.

[116] J. Roldan-Perez, E. J. Bueno, R. Pena-Alzola, and A. Rodriguez-Cabero, "All-Pass-Filter-Based Active Damping for VSCs With LCL Filters Connected to Weak Grids," *IEEE Transactions on Power Electronics*, vol. 33, no. 11, pp. 9890–9901, nov 2018.

[117] F. O. Resende, N. J. Gil, and J. A. Lopes, "Service restoration on distribution systems using Multi-MicroGrids," *European Transactions on Electrical Power*, vol. 21, no. 2, pp. 1327–1342, mar 2011.

[118] W. Teng, H. Wang, and Y. Jia, "Construction and control strategy research of black start unit containing wind farm," in *IEEE Region 10 Annual International Conference, Proceedings/TENCON*, vol. 2016-Janua. IEEE, nov 2016, pp. 1–5.

[119] B. Singh and G. K. Kasal, "Voltage and frequency controller for a three-phase four-wire autonomous wind energy conversion system," *IEEE Transactions on Energy Conversion*, vol. 23, no. 2, pp. 509–518, jun 2008.

[120] M. Lotfy, T. Senjyu, M. Farahat, A. Abdel-Gawad, and A. Yona, "A Frequency Control Approach for Hybrid Power System Using Multi-Objective Optimization," *Energies*, vol. 10, no. 1, p. 80, jan 2017.

[121] R. Cárdenas, R. Peña, J. Proboste, G. Asher, and J. Clare, "MRAS observer for sensorless control of standalone doubly fed induction generators," *IEEE Transactions on Energy Conversion*, vol. 20, no. 4, pp. 710–718, 2005.

[122] R. Peña, R. Cárdenas, E. Escobar, J. Clare, and P. Wheeler, "Control system for unbalanced operation of stand-alone doubly fed induction generators," *IEEE Transactions on Energy Conversion*, vol. 22, no. 2, pp. 544–545, 2007.

[123] S. Arnaltes, J. L. Rodriguez-Amenedo, and M. E. Montilla-DJesus, "Control of variable speed wind turbines with doubly fed asynchronous generators for stand-alone applications," *Energies*, vol. 11, no. 1, p. 26, dec 2018.

[124] Z. C. &. H. Li, "Overview of different wind generator systems and their comparisons," *IET Renewable Power Generation*, vol. 2, no. 2, pp. 123–138, 2008.

[125] Z. Alnasir and M. Kazerani, "An analytical literature review of stand-alone wind energy conversion systems from generator viewpoint," *Renewable and Sustainable Energy Reviews*, vol. 28, pp. 597–615, dec 2013.

[126] G. K. Kasal and B. Singh, "Voltage and frequency controllers for an asynchronous generator-based isolated wind energy conversion system," *IEEE Transactions on Energy Conversion*, vol. 26, no. 2, pp. 402–416, jun 2011.

[127] R. Teodorescu and F. Blaabjerg, "Flexible control of small wind turbines with grid failure detection operating in stand-alone and grid-connected mode," *IEEE Transactions on Power Electronics*, vol. 19, no. 5, pp. 1323–1332, sep 2004.

[128] M. E. Haque, K. M. Muttaqi, and M. Negnevitsky, "Control of a stand alone variable speed wind turbine with a permanent magnet synchronous generator," in *2008 IEEE Power and Energy Society General Meeting - Conversion and Delivery of Electrical Energy in the 21st Century*, jul 2008, pp. 1–9.

[129] C. N. Bhende, S. Mishra, and S. G. Malla, "Permanent magnet synchronous generator-based standalone wind energy supply system," *IEEE Transactions on Sustainable Energy*, vol. 2, no. 4, pp. 361–373, 2011.

[130] Z. Alnasir and M. Kazerani, "A small-scale standalone wind energy conversion system featuring SCIG, CSI and a novel storage integration scheme," *Renewable Energy*, vol. 89, pp. 360–370, apr 2016.

[131] M. F. Elmorshedy, S. M. Allam, A. I. Shobair, and E. M. Rashad, "Voltage and frequency control of a stand-alone wind-energy conversion system based on PMSG," in *2015 4th International Conference on Electric Power and Energy Conversion Systems, EPECS 2015*, Sharjah, UAE, nov 2015, pp. 1–6.

[132] V. Akhmatov, "Variable-Speed Wind Turbines with Doubly-Fed Induction Generators, Part I: Modelling in Dynamic Simulation Tools," *Wind Engineering*, vol. 26, no. 2, pp. 85–108, 2002.

[133] S. Cole, J. Beerten, and R. Belmans, "Generalized dynamic VSC MTDC model for power system stability studies," *IEEE Transactions on Power Systems*, vol. 25, no. 3, pp. 1655–1662, 2010.

[134] A. Yazdani and R. Iravani, "A unified dynamic model and control for the voltage-sourced converter under unbalanced grid conditions," *IEEE Transactions on Power Delivery*, vol. 21, no. 3, pp. 1620–1629, 2006.

[135] L. Xu, B. R. Andersen, and P. Cartwright, "VSC transmission operating under unbalanced AC conditions - Analysis and control design," *IEEE Transactions on Power Delivery*, vol. 20, no. 1, pp. 427–434, 2005.

[136] C. Du and E. Agneholm, "Investigation of frequency/AC voltage control for inverter station of VSC-HVDC," in *IECON Proceedings (Industrial Electronics Conference)*. IEEE, 2006, pp. 1810–1815.

[137] G. Abad, J. López, M. A. Rodríguez, L. Marroyo, and G. Iwanski, *Doubly Fed Induction Machine: Modeling and Control for Wind Energy Generation*. John Wiley & Sons, 2011.

[138] M. Chinchilla, S. Arnaltes, and J. C. Burgos, "Control of permanent-magnet generators applied to variable-speed wind-energy systems connected to the grid," *IEEE Transactions on Energy Conversion*, vol. 21, no. 1, pp. 130–135, mar 2006.

[139] M. Chinchilla, S. Amaltes, and J. Rodriguez-Amenedo, "Laboratory set-up for wind turbine emulation," in *2004 IEEE International Conference on Industrial Technology, 2004. IEEE ICIT '04.*, vol. 1, dec 2004, pp. 553–557.